EXPERIMENTAL INVESTIGATION OF PARABOLIC DISH SOLAR COLLECTOR USING NANOFLUIDS FOR STEAM COOKING

Shifera Dereje Ayane

A Thesis Submitted to the Department of Mechanical Engineering
School of Mechanical, Chemical and Materials Science and Engineering
Presented in Partial Fulfillment of the Required for the Degree of Master's in Thermal Engineering

Office of Graduate Studies

Adama Science and Technology University

March, 2022

Adama, Ethiopia

EXPERIMENTAL INVESTIGATION OF PARABOLIC DISH SOLAR COLLECTOR USING NANOFLUIDS FOR STEAM COOKING

Shifera Dereje Ayane

Advisor: Dr. Addisu Bekele

A Thesis Submitted to the Department of Mechanical Engineering
School of Mechanical, Chemical and Materials Science and Engineering
Presented in Partial Fulfillment of the Degree of Master's in Thermal Engineering

Office of Graduate Studies

Adama Science and Technology University

March, 2022

Adama, Ethiopia

Declaration and Recommendation

Declaration

I hereby declare that this Master Thesis entitled "Experimental Investigation of Parabolic Dish Solar Collector using Nanofluids for Steam Cooking" is my original work. That is, it has not been submitted for the award of any academic degree, diploma or certificate in any other university. All sources of materials that are used for this thesis have been duly acknowledged through citation

____________________	_________________	_________________
Candidate	Signature	Date

Recommendation

I the advisor of this thesis, hereby certify that I have read the revised version of the thesis entitled "Experimental Investigation of Parabolic Dish Solar Collector using Nanofluids for Steam Cooking" prepared under my guidance by Shifera Dereje submitted in partial fulfillment of the requirements for the degree of Mater's of Science in Thermal Engineering.

Therefore, I recommend the submission of revised version of the thesis to the department following the applicable procedures.

_________________________ ______________________ _______________

Advisor Signature Date

Approval Page

I, the advisors of the thesis entitled "Experimental Investigation of Parabolic Dish Solar Collector using Nanofluids for Steam Cooking'' developed by Shifera Dereje, hereby certify that the recommendation and suggestions made by the board of examiners are appropriately incorporated into the final version of the thesis.

Advisor	Signature	Date

We, the undersigned, members of the Board of Examiners of the thesis by Shifera Dereje have read and evaluated the thesis entitled "Experimental Investigation of Parabolic Dish Solar Collector using Nanofluids for Steam Cooking'' and examined the candidate during open defense. This is, therefore, to certify that the thesis is accepted for partial fulfillment of the requirement of the degree of Master of Science in Thermal Engineering.

Chairperson	Signature	Date
Internal Examiner	Signature	Date
External Examiner	Signature	Date

Finally, approval and acceptance of the thesis is contingent upon submission of its final copy to the Office of Postgraduate Studies (OPGS) through the Department Graduate Council (DGC) and School Graduate Committee (SGC).

Department Head	Signature	Date
School Dean	Signature	Date
Office of Postgraduate Studies, Dean	Signature	Date

ACKNOWLEDGMENT

First and for most, I want to thank the Almighty God who is at my side, gives me patient, strength, courage and wisdom to complete this thesis. Next, I would like to express my deepest thanks to my advisor Dr. Addisu Bekele for his guidance, intellectual support, invaluable advice throughout this thesis. I extend my deep gratitude to Adama Science and Technology University for giving me this scholarship and for its willingness in providing and supporting me financially. I also like to express my special thanks go to the lab assistants of Thermal Aerospace engineering, Automotive Engineering and manufacturing Engineering. I would like to thanks all my best friends for their encouragement, suggestion, and assistance, and gave a worthy comment on my work and through the process of researching. My heartfelt and deepest gratitude goes to all of my family who was always on my side persistently throughout my entire academic life.

Table of Contents

LIST OF TABLES

LIST OF FIGURES

ABBREVIATIONS AND ACRONYMS

CVD	Chemical Vapor Deposition
DW	Distilled Water
ECOMSC	Eastern and Central Oromia Meteorological Service Center (ECOMSC)
EG	Ethylene Glycol
HTF	Heat Transfer Fluid
LHS	Latent Heat Storage
NTU	Number of Transfer Unit
PDSC	Parabolic Dish Solar Collector
PCM	Phase Change Material
PV/T	Photovoltaic Thermal system
SC	Solar Collector
SDC	Solar dish concentrators
SHT	Sensible Heat Storage
SEM	Scanning Electron Microscope,
SFPC	Solar Flat Plate Collector
TEM	Transmission Electron Microscope
XRD	X-ray diffraction

GREEK SYMBOLS

ρ	Density (kg/m^3)
μ	Viscosity (Ns/m^2)
α_s	Solar altitude angle (°)
δ	Declination angle (°)
θ	Incidence angle (°)
θ_f	melt fraction
θ_z	Zenith angle (°)
γ_s	Solar azimuth angle (°)
$\emptyset$	Latitude angle (°)
$\emptyset_r$	Rim angle (°)
φ	Volume fraction of nanoparticles in nanofluid (%)
ω	Solar hour angle (°)
ω_s	Sunset hour angle (°)
η_{opt}	Optical efficiency
η_{th}	Thermal efficiency

NOMENCLATURES

A Area (m^2)

C Heat capacity rate (kj/kg K)

D Diameter (m)

De Dean Number

f Focal length (m)

f_c Friction factor

H Global daily radiation ($W/_{m^2}$)

h Convective heat transfer coefficient ($W/_{m^2K}$)

I Global hourly radiation ($W/_{m^2}$)

K Thermal conductivity (W/mK)

L Length (m)

m Mass (kg)

$\dot{m}$ Mass flow rate ($kg/_{s}$)

Nu Nusselt number

$\dot{Q}$ Heat transfer rate (W)

ΔP Pressure drop (Pa)

Re Reynolds number

T Temperature (K)

U Overall heat transfer coefficient (W/m^2K)

Z Elevation above sea level (m)

SUBSCRIPT

ap	Aperture	p	Pipe
ave	Average	r	Receiver
bf	Base fluid	rad	Radiation
B	Beam	s	Shell
c	Cold	sur	Surface
D	Diffuse	t	Tube
amb	Ambient	u	Useful
conv	Convective		
cond	Conduction		
eff	Effective		
fm	Mean fluid		
h	Hot		
i	Inner		
in	Inlet		
ins	Insulation		
max	Maximum		
min	Minimum		
nf	Nanofluid		
o	Outer		
out	Outlet		

ABSTRACT

Renewable energy sources play an important role in heating applications. Among the renewable sources of energy, solar energy is considered the most abundant and viable option for thermal energy applications. Cooking is one of the most essential human activities in everyday life. The energy demand for cooking is fulfilled by conventional energy sources like biofuels, fossil fuels and electricity. Environmental degradation, harmful gas emissions, and the increase in prices of fuel and electricity are the main driving forces behind the need for more effective utilization of renewable energy. Parabolic dish solar collector is a device collects solar radiation and converts into thermal energy to the fluid. To improve the performance of a collector a high heat transfer fluid is used. Sol-gel and precipitation methods are used to synthesis aluminum oxide and zinc oxide nanoparticles, respectively. In this study, nanofluids are used to enhance the heat transfer due to their high thermal conductivity compared with the base fluid. Two-step and single-step methods are techniques for the preparation of nanofluid. In this thesis, a two-step method was used. The performance analysis of parabolic dish solar collector with and without nanofluids was studied. The result obtained showed that the collector efficiency for 1% of volume fraction of nanoparticles for aluminum oxide and Zinc oxide as HTF is 69.13% and 65.5% respectively. Similarly, the thermal efficiency of the collector for a volume fraction of 2% of Al_2O_3 *and ZnO nanofluids was 71.63% and 67.99% respectively. The efficiency of parabolic dish solar collector using water as working fluid obtained was obtained 61.6%. The outlet temperature for volume fraction 1% for aluminum oxide and zinc oxide nanofluid as HTF is 456 and 452 K* respectively. *Similarly, the outlet temperature for a volume fraction of 2% of aluminum oxide and zinc oxide nanofluid was 459.6 and 454.7 K respectively. The maximum average outlet temperature of the water as a working fluid was 439.4 K. No-load test established the cooking ability of the cooker, water boiling test and actual load test is performed. The actual load was pasta and the time taken to cook was 33 min. The experimental result of Latent heat storage using* $MgCl_2.6H_2O$ *showed that time it takes and amount of sensible, latent and total energy stored/released during the charging/discharging processes are found to be 125 min, 1.92, 1.436 and 3.35 MJ and 161 min, 1.57, 1.35 and 2.92 MJ respectively. From the result obtained the aluminum oxide nanofluids have good heat transfer than zinc oxide. The performance test revealed that the maximum amount of the first figure of merits (F1) obtained was 0.31 K* m^2/W *and the second figure of merits(F2) for the cooker was evaluated from the water boiling test and found to be 0.42 K* m^2/W.

Keywords

Solar collector, Parabolic Dish, Nanoparticles, Nanofluid, Cooking, Phase change material

CHAPTER ONE

INTRODUCTION

1.1 Background works

Maxwell initiated the efforts to enhance inherently poor thermal conductivity of fluids by adding solid particles in base fluids. Earlier studies used millimeter or micrometer solid particles, which led to problems such as rapid settling of solid particles, clogging, surface abrasion & high-pressure drop, limiting their practical applications. Nanoparticles have good potential to overcome these problems.

(Choi, 1995) came up with the novel concept of nanoparticles by making use of particles sizes in the range of 1 to 100 nm.

Thermal system is a complex assembly of coupled components, showing a common structured behavior interacting to a common goal. The thermal systems devices are refrigeration systems, air -conditioning systems, solar thermal systems, heat exchanger etc.

Many industrial processes such as thermal power plant, heating or cooling processes, and chemical processes the base fluids such as water, ethylene glycol, and heat transfer oil are used as working fluid. However, these base fluids have relatively low thermal conductivity and thus heat exchange rates in thermal engineering devices are low. To minimize this problem nanoparticles are added to common fluids to improve the thermal conductivity of the base fluid. The suspension of nano-sized particles in a conventional base fluid is called a nanofluid. Choi first used the term ‘‘nanofluid’’ in 1995. Nanofluids, compared to suspensions with particles size of millimeter-or-micrometer, show better stability, rheological properties, and considerably higher thermal conductivities.

In recent years, many researchers have studied the effects of nanofluids on the enhancement of heat transfer in thermal engineering devices, both experimentally and theoretically. Researchers have also investigated a variety of preparation methods, characteristics, and different models used for the calculation of thermos physical properties of nanofluids such as thermal conductivity, viscosity, density, specific heat capacity (Li et al., 2009, Lee et al., 2010, Ghadimi et al., 2011, Ramesh et al.,2011, Khanafer et al., 2011, Trisaksri et al., 2007).

Recently, the use of solar energy has had a remarkable edge. The perceived shortage of fossil fuels as well as environmental considerations will constrain the use of fossil fuels in the future. Therefore, researchers are motivated to find alternative sources of energy. This has become even more popular as the price of fossil fuels continues to rise. The earth receives in just about 1 h more energy from the sun than that consumed by the entire world for 1 year. Most solar energy applications are financially viable while small systems for individual use require just a few kilowatts of power (Özerinç et al., 2010).

It is important to apply solar energy to a wide range of applications and provide solutions through the modification of the energy proportion, improving energy stability, increasing energy sustainability, and enhancing system efficiency (Mekhilef et al., 2011). The solar cooking system is one of the applications of solar thermal systems at which solar energy is used to heat, cook or pasteurize drink and other food materials. Solar cookers can generally be divided into two: direct and indirect type cookers. The first type of solar cooker uses solar radiation directly in the cooking process whereas indirect cookers use solar radiation to heat up the heat transfer fluid (HTF), which transports this heat to the place of food processing

There are different techniques for the synthesis of nanoparticles such as sol-gel, precipitation, chemical vapor deposition (CVD), spinning, pyrolysis, and biosynthesis methods are commonly used. In this thesis aluminum oxide and zinc oxide nanoparticles are synthesized using sol-gel and precipitation methods, respectively. To prepare nanofluids one step and two-step methods are used and for this thesis two-step method is used. In this study parabolic dish solar collector for indirect cooking was studied. Nanofluids are used as heat transfer fluid for indirect cooking in this study.

1.2 Statement of the Problem

In Ethiopia, various domestic applications, social services, higher institutions, hospitals, hotels, and industries need hot water in large volume for multi-purposes. The sources of energy for these hot water supplies are either electricity or fossil fuels. Due to our dependency on imported fossil fuels and their cost it is important to look for alternative and renewable source of energy. Solar energy is one of the best alternative renewable energy sources that can be used for steam generation. Parabolic dish solar collector is a device convert the sun radiation into thermal energy to heat water. There are two methods for solar cooking. These are direct and indirect cooking. In Ethiopia climate condition many researchers conduct the experimental investigation of indirect cooking. (Asfafaw et al., 2015) conducted experimental investigation on Solar cookers with latent heat storage for intensive cooking application.the thermal efficience obtained was 23%. In order to overcome the low, the thermal efficiency of the indirect solar cooking system use of high heat transfer rate fluid is used. To improve the performance of the indirect solar cooker nanofluids are used as heat transfer.

1.3. Objective

1.3.1. General Objective

To study the performance analysis of parabolic dish solar collector using nanofluids to generate steam used for cooking.

1.3.2. Specific Objectives

The specific objectives of this thesis are

- To design, fabricate and test of parabolic dish solar collector.
- To synthesis nanoparticles and experimentally test the effect of nanofluids on the performance of parabolic dish solar collector.
- To study effect of phase change material on performance of the collector during indirect cooking.

1.4 Benefits and Beneficiaries

The benefits that can be obtained from this project work are

- High efficiency of parabolic dish solar collector for steam generation system can be obtained.
- The nanofluids that have good thermo-physical properties are used to improve the efficiency of the solar collector.
- Reduce the cost for cooking.
- The system can be used for various applications.

The beneficiaries of this thesis work are

- Use for domestic cooking.
- Food and beverage industries.
- Large industries use steam in the processes.
- Higher institutions use steam for cooking.
- A hotel requires steam water for cooking and cleaning.
- In thermal power plant steam can be used for electric generation.

1.5 Scope and Limitation of the Study

In this study the nanofluids preparation and characterization of nanoparticles was done. XRD (X-ray diffraction) was used for characterization of nanoparticles. The prototype of parabolic dish solar collector with cooking units was done. The performance of parabolic dish solar collector with and without nanofluids was studied. The present work includes collecting of metrological solar energy data of Adama city input for design and analysis of the proposed solar collector system. This study automatic tracking mechanism is not studied.

CHAPTER TWO

LITERATURE REVIEW

2.1 Solar Thermal Energy

Now a day many researchers are working on thermal systems performance improvement. Among the renewable energy sources, solar energy is considered as the most abundant and a viable option for thermal energy applications. (Thirugnanasambandam et al., 2010) highlighted, the total annual solar radiation falling on the earth is more than 7500 times of the world's total annual primary energy consumption. The annual solar radiations are reaching on the earth's surface, approximately 3.4×10^6 EJ, is an order of magnitude greater than all the estimated non-renewable energy resources, including fossil fuels and nuclear.

(Panwar et al., 2011) studied solar cookers provide many advantages, including fuel economy, reduction in greenhouse gas emission, firewood utilization saving, lower cost and high durability, compared with other source of energy. However, in many parts of the world, especially in developing countries wood and fossil fuel-based cooking energy resources still predominate with the highest share of global energy consumption in the residential sector. This situation creates serious ecological problems, such as deforestation, economical and health problems are also consequences of firewood use. Currently, renewable energy sources supply about 14% of the total world energy demand, and their potential will play an important role in the world's future. Solar cooking technology began with the invention of the first solar box cooker by a French–Swiss physicist named Horace de Saussure; his work was introduced in 1767. A solar cooker converts solar energy into heat, which is used to cook food kept in the cooking utensil. Solar cookers also enable some significant processes such as pasteurization and sterilization. Different types of solar cookers have been designed and developed around the world in the past and are still being improved by scientists and researchers. Therefore, the classification of solar cookers is a complicated task. In the present review, solar cookers are classified into three main categories based on the type of collector and temperature order: box-type cookers, concentrating-type cookers and non-focusing type cookers. Within these three, main categories are included cookers with direct or indirect heat-transferring modes, cookers with or without storage, and cookers with tracking or non-tracking systems (Mathusivagami et al., 2010).

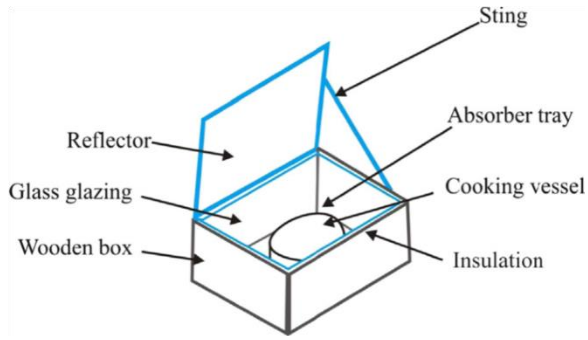

Figure 2.1 Components of a box solar cooker (Yettuo et al., 2014).

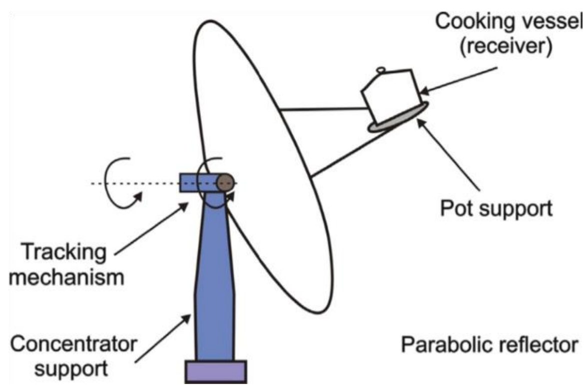

Figure 2.2 Components of a parabolic solar cooker (Yettuo et al., 2014).

Direct-type solar cookers use solar radiation directly in the cooking process, while the indirect cookers use a heat transfer fluid to transfer the heat from the collector to the cooking unit. The thermal energy storage option must be provided with solar cookers in order to allow late evening/night cooking and overcome the limitations of solar cookers during off-sunshine hours. Sometimes, these cookers are equipped with one- or two axis tracking systems to follow the sun.

(Shubham et al., 2017) they conduct experimental investigation to study the performance of the concentrator water circulated as heat transfer fluid. The system is fabricated with highly reflective aluminum foil sheet material. They used four parabolic dishes mounted on a stand kept helical coil at focal point of all four dishes. They obtained that the temperature of steam in the range of 120 to 160℃.

(Fareed et al., 2012) studied on portable parabolic dish solar concentrator and they designed and fabricated solar dish concentrator with aperture diameters of 1.6 m for water heating application and they were achieved steam. They fabricated dish with galvanized steel, and its interior surface is covered by a reflecting layer with reflectivity up to 76 %, and a receiver located at the focal point. Water temperature increased up to 80℃ , and the system efficiency increased by 30% at mid noon time.

(Ibrahim et al., 2012) works on the design and development of a parabolic dish solar water heater for domestic hot water application. He found that the parabolic dish water heater is gives 40 liters of hot water per day. Initially he expected that the thermal efficiencies of 50% by his design but finally he obtained thermal efficiencies of 52 - 56%.

(Eswaramoorthy et al., 2013) conducted an experiment on small scale solar parabolic dish thermoelectric generator. They fabricated solar parabolic dish collector using satellite dish antenna fitted with polished aluminum sheet as concentrator surface. The concentrated solar radiation and water-cooled heat sink was the driving potential to generate electricity; they studied various operating parameters like receiver plate temperature, power output and conversion efficiency with respect to solar radiation. From the experiment it was found that the receiver plate temperature was significantly affecting the power output. Parabolic dish solar thermal cooker was designed and constructed by (Ibrahim et al.,2012)

(El Ouederni et al., 2009) conducted experimental to measure temperature distribution on the receiver. They obtained that the temperature in the center reaches a value which is about 400℃.So that, a good quality of industrial high temperature equipment's, can be obtained using this technology of solar energy concentration. By using this solar collector, they can extract eventually 27 % of direct solar energy and convert it into thermal energy that can be used directly for several purposes such as water heating, electricity generation using Stirling engine, vapor production, etc.

(Sakhare et al., 2014) used line focus concentrator with a copper tube in the form of helical coil receiver mounted at focal point. They investigated the performance of the concentrator experimentally with the water circulated as heat transfer fluid. They fabricated the system with highly reflective aluminum foil sheet. They placed experimental setup in open, and the tests were carried out. The results they obtained were encouraging to provide the data for developing steam generation for rural application. The concentrated heat was absorbed by a copper tube which was made up of coil in a curved shape (22cm diameter and length with 15 no of turns) and it was fixed on solar trace path in which, it eliminates tracking the sun in the east west direction and optimal tracking of the sun in the north-south to obtain maximum solar energy. The experimental results were taken on summer and cloud free days. The test results were measured 215℃ with solar steam conversion efficiency is 60-70% measured.

(Parthipan et al., 2015) design of solar parabolic dish concentrator for low cost solar water heating system. In this work a small-scale aluminum cylindrical solar receiver with spherical cavity was installed at the focal point of the dish. Receiver efficiencies were shown in terms of mass flow rate, receiver spherical diameter, maximum receiver surface temperature and inlet temperature of the working fluid. An overall solar to heat efficiency between 45 and 70 % is attainable for the solar collector using the open cavity receiver.

(Badran et al., 2010) designed, built and tested a portable solar water heater. They built parabolic dish solar collector with aperture diameter of 150 cm to concentrate solar radiation. The surface of the dish was covered with reflective aluminum foil which was used to concentrate solar energy on a cooking pot in one mode of operation. This technique was operated in two ways: one with bare pot and the other with the pot being covered with glazing by putting it inside a glass box. The device was also used in another mode of operation to heat water for domestic use by placing a specially designed solar collector in the focus.

Figure 2.3 The device in the water heating mode (Badran et al., 2010).

They were found that, when the device was operated in the bare cooker mode, a 7 kg of water at 20℃ was brought to a boil in 1 h. Putting the pot inside the glass box reduced the time required for boiling to 40 min and the cooking power was increased by 27.5%. In the collector mode, the device was able to heat 30 kg of water from 20 to 50℃ in 2½ h. The highest efficiency obtained for this mode was 77% and the slope of the efficiency curve was 10.63 W/m^2°C.

(Yaseen et al., 2015) studied a parabolic dish concentrates performance the incoming solar radiation to a point. An insulated cavity containing tubes or some other heat transfer device, is placed at this point absorbing the concentrated radiation and transferring it to a gas. Parabolic dishes must be tracked about two axes.

(Joshua, 2009) studied the design, construction and testing of a parabolic dish solar steam generator. Using concentrating collector, heat from the sun is concentrated on a black absorber located at the focus point of the reflector in which water is heated to a very high temperature to form steam. It also describes the sun tracking system unit by manual tilting of the lever at the base of the parabolic dish to capture solar energy. The whole arrangement is mounted on a hinged frame supported with a slotted lever for tilting the parabolic dish reflector to different angles so that the sun is always directed to the collector at different period of the day. On the average sunny and cloud free days, the test results gave high temperature above 200℃.

(Yaseen *et al.,* 2018) developed two solar dish concentrators (SDC) with diameter of 2 m were designed for water heating purpose. This study was applied on solar steam water heater. Both of the dishes coated with thick layer of steel (galvanized), while its interior surface covered with a reflector layer.

Figure 2.5 Parabolic dish concentrator for water heating purpose (Yaseen et al., 2018).

The first dish interior surface covered with a layer of reflectivity up to 80 %, whereas the second one covered by a piece of mirrors with a reflectivity of 95%. The receivers have been fixed in the focal position of both dishes. The measurement of temperature and solar power for both types have been documented and recorded. They obtained that an optical energy for the 1^{st} dish is 1909 W, the final energy is 1551 W, and the optical efficiency is 61 %, while the optical energy for the 2^{nd} dish is 1607.68 W, the final energy is 1853 W, and the optical efficiency is 73 %.

(Lifang *et al*., 2011) developed of large parabolic dish concentrator for oil heating. The dish mirror was formed from several optimal-shaped thin flat metal petals with highly reflective surfaces. The result showed that the concentrator reaches maximum temperature of 680 ℃.

(Asfafaw *et al*., 2014) the second experimental study was a solar thermal stove which generates steam by concentrating suns ray using a parabolic dish on the receiver. The steam flows through a pipe to the injera baking stove and condenses by transferring heat to the baking pan which is placed on the steel plate that is in contact with steam. They conclude from the study that baking injera using indirect steam in a temperature range from 135 to 160 °C.

The indicated temperature was less than the literature or experimental values obtained earlier by other researchers or developers working on an injera baking stove. The thermal efficiency they obtained from the experimental investigation was 23%.

Figure 2.6 Solar thermal injera baking stove (Asfafaw *et al*., 2014).

2.2 Parabolic Dish Solar Receiver

(Yaseen et al., 2015) the receiver of a solar dish system is the interface between the concentrator and the heats point. It has two functions: First, it absorbs a large part or the radiation reflected by the collector and converts it into heat.

Second, it transfers the heat to the working gas of the heat engine. Important requirements for the receiver are, thus, high absorption rates and good heat transfer characteristics. In general, two types of receiver geometries could be used with parabolic dish collectors: external receivers and cavity receivers. External receivers are usually spherical and absorb radiation coming from different directions. In case of cavity receivers the radiation passes through aperture.

(Evangelos et al., 2019) investigated on five different cavity receivers under different operating temperature and the selection of the most appropriate designs. The cavity receivers have the following shapes: cylindrical, rectangular, spherical, conical and cylindrical-conical. The optimization of the cavity receiver is done to obtain the best design which increases the thermal efficiency of the solar collector.

The optimization variables are different for every design and they regard the cavity length, the cone angle and the distance from the concentrator base. From investigation they obtained that, the best design is the cylindrical-conical shape, while the conical and the spherical are the next choices.

(Manav et al., 2015) presented Design, fabrication and analysis of helical coil receiver with varying pitch for solar parabolic dish concentrator. In this study they reported that the parabolic dish with aperture diameter of 1.4 m and fabricated using galvanized steel and its interior surface covered with reflective surface of ionized aluminum with a reflectivity of 92.5 %. The system is equipped with a helical coil receiver fabricated using copper metal positioned at the focal point. The working fluid is water. The research was focused on the temperature variations achieved from changes in the geometry of the helical receiver. This paper reveals the temperature variations achieved with a bare tube helical receiver with zero pitch and with black coated helical receiver with non-zero pitch and capped. The maximum attainable temperature with non-zero pitch helical receiver coated with black paint and capped was approximately 43 % higher than that of bare tube helical receiver with zero pitch.

(Azzouri et al., 2017) examined experimentally a cylindrical cavity receiver with the absorber tubes to be inside the insulation layer. They found that the maximum thermal efficiency of their design is 75 %.

(Karimi et al., 2018) found that thermal performance of the cylindrical receiver (without the optical losses) can reach up to 90 % for a receiver aperture diameter at 0.2 m while the concentrator has a diameter of 2.88 m.

(Mawire and Taole, 2014) studied experimentally a homemade parabolic dish concentrator with a cylindrical receiver. They found that the thermal efficiency is up to 40%and the exergy efficiency by up to 10 %.

(Wang et al., 2013) studied a cylindrical receiver with a modified back surface. Their work is optical and they found maximum optical efficiency at 72%. This value is 7.67% higher than the optical efficiency of the conventional cylindrical cavity receiver with 10% dead space.

(Loni et al., 2016) optimized a cylindrical receiver for application in an Organic Rankine Cycle. They found that the optimum depth of the cavity is equal to the cavity diameter. They stated that the optimum concentration ratio is around 32 and the receiver efficiency reaches 90%.

(Soltani et al., 2019) performed and optimization work about a cylindrical cavity receiver. They found that the receiver position has to be at the 90 % of the focal distance, while its length has to be 1.5–2 times greater than the aperture diameter. The maximum thermal efficiency of the system was about 78 %.

2.3 Nanofluids

(Taylor et al., 2012) compared a nanofluid-based concentrating solar thermal concentrator system with a conventional one. They obtained that the use of nanofluid in the receiver improves the efficiency of the system by 5-10%. They also concluded graphite/therminol VP-1 nanofluids with a volume fraction of 0.001 % or less could be beneficial for 10-100 MWe power plant. They estimated that the use of nanofluid in solar thermal power towers with a capacity of 100MWe in Tucson and Arizona could generate $3.5 million per year.

(Agabalaie**,** 2017) study the effect of nanofluids on a parabolic solar collector. He put the comparison of temperature, thermal efficiency and outlet average temperature for a conventional parabolic collector and a collector with nanofluids (water-silver and silver-copper). The obtained results of the simulations demonstrated under the similar working conditions the thermal efficiency increased from 27.8 to 95.2% for water and nanofluids, respectively.

(Harikesh et al., 2017) conducted an experiment to study the performance of parabolic dish solar collector with nanofluid as working fluid. They used diameter of collector 1180 mm with the depth of 310 mm and evaluate the performance of collector with and without nanofluid. From an experiment they obtained that outlet temperature of fluid with and without nanofluid is 90 and 85 ℃ respectively . The efficiency of collector is found to be higher by about 10 % when nanofluid are used.

(Abid et al., 2015) conduct comparative study on the performance assessment of parabolic dish (PD) and parabolic trough (PT) solar thermal power plant using nanofluids and molten salts. They used four different nanofluids aluminum oxide (Al_2O_3) and ferric oxide (Fe_2O_3) nanofluids and LiCl-RbCl and $NaNO_3$-KNO_3 molten salts. The results obtained showed that the outlet temperature of parabolic dish solar collector is higher as compared to parabolic trough solar collector under identical operating conditions. The outlet temperature of PD and PT solar collectors is noticed to increase from 480.9 to 689.7 K and 468.9 to 624.7 K, respectively. The overall performance of PD solar collector is observed to be higher upon using nanofluids as the solar absorbers.

(Rajendran et al., 2018) conduct experimental studies on the effect of enhancement of thermal conductivity of SiC +Water nanofluid. They used a step dish concentrator with five parts. They finally found 76 % exergy efficiency enhancement for flow rate 0.5 l/min.

(Delfani et al., 2014) conducted numerical investigation of nanofluid-based solar collectors. They solved radiative heat transfer and energy equations numerically. They found that the efficiency improvement of about 0.8 % is obtained by adding 0.02 g/l carbon nano horns (h=5 mm) to the base fluid (water) compare to a typical flat-plate collector. This increase is 9 and 17 % for 0.05 g/l carbon nano horns and collector heights 3 and 5 mm, respectively.

(Sahi and Alrazzaq, 2017) conducted experimental and numerical heat transfer of SFPC by using nanofluid. They use Al_2O_3 nanoparticles with three different volume fraction (0.2,0.4 and 0.6 %) for enhancement of working fluid. The numerical CFD-Model did by using interfaces between laminar flow and heat transfer by COMSOL version 5.2a. The maximum temperature difference found between inlet and outlet is 15.3 °C, at Nanofluid for the volume fraction of 0.6 %.

(Yousefi et al., 2012) conducted experimentally investigated on the effects of Al_2O_3/water nanofluid on the efficiency of a flat-plate solar collector. They examined the effects of two different weight fractions of the nanofluid, including 0.2 and 0.4 %, where the diameter of particles was 15 nm. The result obtained that the efficiency of the solar collector with 0.2 % volume fraction nanofluid is greater than that with water by 28.3 %. Also, they obtained that the efficiency of 0.2 % weight fraction nanofluid is higher compared to 0.4 % weight fraction.

(Qinbo et al., 2015) conducted an experimental investigation on the efficiency of SFPC with nanofluids. Cu-H_2O nanofluids with different mass fraction and size prepared through two-step method. Accordingly, the result obtained that the highest temperature and heat gain of water in the nanofluid 25 nm, 1.1 wt % tank can increase up to 12.24 and 24.52 % compared with water tank, respectively.

(Reza et al., 2016) conduct an experiment study to see the effect of nanofluid on heat transfer in closed cycle system in shell and tube heat exchangers at Isfahan power plant. The study investigated the effect of distilled-water/ silver nanofluid (with a size of 0.01, 0.025, 0.05, and 0.075 %) on heat transfer in a closed cooling system of one of the electrical energy generation units at Isfahan power plant. The authors come with nanofluid increased heat transfer coefficient by 16 %. The pressure drops of nanofluid, however, has no significant change compared with the pressure drop of pure water.

(Ebrahimnia et al., 2016) conducts an experimental and numerical investigation of nanofluids heat transfer characteristics for potential application in solar heat exchangers. The thermal conductivity and dynamic viscosity of the prepared nanofluids haven measured and modeled at different temperatures and nanoparticle concentrations. The results indicated that the maximum enhancement of the heat transfer coefficient at a lower concentration of 2.3 vol.% to be 21 %.

(Vandaarkuzhali and Elansezhian, 2014) studied the performance evaluation of air conditioning using nanofluids. An experimental measurement performed for three types of Nano-fluids namely (CuO, ZnO, and Al_2O_3) was analyzed. Simulation was shown that for the same geometric characteristics of the system performance increased from 12 to 18 % by the application of Nano-fluid as a fluid in vapor compression cycle (VCS).

(Harsh et al., 2018) studied the heat transfer characteristics of nanofluids in an automotive radiator. This study presented an experimental study on heat transfer using Nano-fluid as coolants in engines. Particles having a diameter in the range 10^{-3} to 10^{-6} m have low thermal conductivities and cause clogging in the flow section along with significant friction and are highly unstable in solution. The nanoparticles used in this experiment are CuO and TiO_2 having a particle size less than 80 nm. The result shows that there is an improvement of 24.5 % in the overall heat transfer coefficient and there was an increase of 13.9 % in the heat transfer rate compared to the base fluid (80:20 Water: ethylene glycol EG solution).

(Miqdam et al., 2018) performed a numerical study on the effect of operating nanofluids of the photovoltaic thermal system (PV/T) on the convective heat transfer. The heat transfer coefficient for different nanofluids was higher than the conventional ones by 3.9 % for SiO_2, 2.67 % for CuO and 4.42 % for Al_2O_3. The pressure drops higher than the numerical ones the reduction was 0.487% for CuO nanofluid and nanofluid it was 2.55 % for Al_2O_3.

2.4 Thermal Energy Storage Systems

One of the major drawbacks of a solar cooker is its inability to cook during off sunshine hours or cloudy periods. In order to overcome this problem, solar systems should be integrated with energy storage systems. Generally, energy storage systems can be classified as mechanical, chemical, biological, magnetic and thermal energy storage systems (Kumaresan, 2012).

Among those energy storage systems, thermal energy storage systems get more attention due to its ability to meet the society's needs for more efficient, environmentally friendly energy use in cooking, building heating and cooling, aerospace power, and other utility applications. From all the types of thermal energy storage systems, sensible heat storage (SHS) and latent heat storage (LHS) systems are the most common in storing solar energy for solar cooking applications. (Ashish, 2019) classified thermal energy storage system as latent and sensible

The literature showed that the performance of indirect SC relies intently upon the type of the HTF that flows through the absorber tube to absorb solar energy. (Saini et al., 2016) examined the performance of a solar cooker with PCM storage and equipped with parabolic trough collector. The solar radiation was concentrated on the receiver tube and the accumulated thermal energy was exchanged to the SC by natural circulation of HTF. Engine oil and water were utilized as working fluids, while acetanilide was utilized as PCM. Cooking process was done with various nourishments and with varying amount of food.

The SC was capable of cooking food two times a day. The night cooking was observed to be faster in respect to noon cooking. By utilizing engine oil as a HTF, the amount of thermal energy absorbed by PCM was improved by about 19.45 to 30.38 % in comparison with water, which demonstrates that the performance of SC with PCM using various HTFs was independent on the thermal properties of these fluids.

(Rai and Srivastava, 2019) tested the performance of box-type SC with PCM (paraffin wax) filled into cooking pot of two different encapsulation materials (aluminum and steel); to evaluate the cooking process during daytime and evening periods. The results demonstrated that the maximum water temperature in PCM filled aluminum pot was about 9 % higher than that with PCM filled steel pot (80 °C), which indicates the suitability of PCM filled aluminum pots for daytime cooking. It was also revealed that the water temperature in PCM filled steel pots was maintained above 95 °C for more than 3 h as compared to PCM filled aluminum pots during evening period, indicating the preference of steel pots for late evening cooking. The results of daytime and evening cooking can be explained as the high thermal conductivity of aluminum (237 W/m °C) heats the pot faster during the evening, while low thermal conductivity of steel (45 W/m °C) keeps the pot hot for a longer duration during daytime.

(Gabisa and Aman, 2016) presented an experimental study on using eutectic PCM ($NaNO_3/KNO_3$) for solar cooking where an electric heater was used to simulated the solar radiation. The experiments were carried out on two Ethiopian local meals; shiro wet and potato meal. It was revealed that about 2.38 kWh heat was needed to cook the two meals for family of 5 members during lunch and dinner. The results showed that the PCM could store the required heat in 50 min and provide it to the two meals for 4.5 h.

(Kumaresan et al., 2016) experimentally studied the performance of an indirect SC integrated with PCM. The prototype comprises of a PCM storage tank, a cooking pot and a positive displacement pump. Therminol 55 was utilized as the HTF while D-Mannitol was utilized as the PCM. During the experiments, the peak temperature was 152 °C inside a span of 15 min which is nearly lower than the time consumed by a traditional LPG oven in stewing mode. A heat balance for the designed cooking system was set up to record for the heat input and the circulation design. They observed that the storage system was capable of conveying thermal energy to the cooking pot at a steady rate for more time. The PCM could also increase the heat for cooking by 10.2 %. However, the piping circuit heat loss was found to be 54.3 %. Thus, the authors recommended to positioning all the segments nearer to the cooking unit in order to reduce such losses.

At present, energy shortage is faced around the world with the quick economic growth. A number of studies are focused on the high effective regenerated green energy. Hence, the development of novel materials which can store and release energy becomes an important means of energy conservation. As the most typical representative, phase change materials (PCMs) have variety of interesting advantages as energy storage materials, such as large heat fusion, stable temperature and properties, abundance reserves (Dutil et al., 2011). Materials as PCMs on hydrated salts, paraffin waxes, fatty acids and eutectics of organic and non-organic compounds were studied during the last 40 years.

Hydrated salts become a type of attractive PCMs due to their high volumetric storage density, relatively high thermal conductivity and moderate costs (Demirbas, 2006).

(Essen et al., 2009) investigated four salt hydrates including $MgSO_4 \cdot 7H_2O$, $Al_2(SO_4)_3 \cdot 18H_2O$, $CaCl_2 \cdot 2H_2O$ and $MgCl_2 \cdot 6H_2O$ on their potential for compact seasonal heat storage in built environment, and the reaction temperatures of which can be reached by a medium temperature solar collector, as the results showed that $MgCl_2 \cdot 6H_2O$ is the most promising salt hydrate of the four selected salts. Based on the above research, (Zondag et al., 2010) who used TGA equipment to measure $MgCl_2 \cdot 6H_2O$ samples in order to verify the performance of $MgCl_2 \cdot 6H_2O$, and the results showed that the dehydration of hexahydrate started at about 323 K and the formation of monohydrate started at about 393 K. Those results indicated that the dehydration temperature of $MgCl_2 \cdot 6H_2O$ occurs in a range of solar thermal collectors, and it also showed that the dehydration of $MgCl_2 \cdot 6H_2O$ and subsequent hydration at 12 mbar vapor pressure give the reactor bed a good temperature rise of 20 K.

2.5 Thermo physical properties of nanofluids

Thermo physical properties of the nanofluids are quite essential to estimate their heat transfer behavior. It is extremely important in the control for the industrial and energy saving perspectives.

Nanoparticles have great potential to improve the thermo-physical properties compared to conventional particles fluids suspension, millimeter and micrometer sized particles. In the last decade, nanofluids have gained significant attention due to its enhancement of thermal properties.

Experimental studies show that thermal conductivity of nanofluids depends on many factors such as particle volume fraction, particle material, particle size, particle shape, base fluid material, and temperature.

Many studies showed that the thermal conductivity as well as viscosity both increases by use of nanofluid compared to base fluid. So far, various theoretical and experimental studies have been conducted and various correlations have been proposed for thermal conductivity, Specific heat, density and dynamic viscosity of nanofluids.

2.5.1 Thermal Conductivity

A wide range of experimental and theoretical studies were conducted in the literature to model thermal conductivity of nanofluids. The existing results were generally based on the definition of the effective thermal conductivity of a two-component mixture. The (Maxwell, 1881) model was one the first models proposed for solid–liquid mixture with relatively large particles. It was based on the solution of heat conduction equation through a stationary random suspension of spheres. The effective thermal conductivity is given by (Eq.2.1)

$$k_{eff} = \frac{k_p + 2k_{bf} + 2\varphi(k_p - k_{bf})}{k_p + 2k_{bf} - \varphi(k_p - k_{bf})} k_{bf} \qquad (2.1)$$

Where: k_p- Thermal conductivity of the particles,

k_{eff}- effective thermal conductivity of nanofluid, k_{bf} is the base fluid thermal conductivity, and φ is the volume fraction of the suspended particles.

The experimental studies show that the thermal conductivity of nanofluids increases with decreasing particle size. This is theoretically supported by two mechanisms of thermal conductivity enhancement; Brownian motion of nanoparticles and liquid layering around nanoparticles (Ozerinc et al., 2010).

2.5.2 Viscosity

Many researchers model the effective viscosity of nanofluid as a function of volume fraction. The effective viscosity of a suspension of solids particles in terms of volume fraction (volume concentration lower than 5 %) is calculated using the phenomenological hydrodynamic equations (Eq.2.2) (Einstein, 1956)

$$\mu_{eff} = (1 + 2.5\varphi)\mu_{bf} \qquad (2.2)$$

Where: $\mu_{eff}$the effective viscosity of Nano-fluid is, μ_{bf} is the base fluid viscosity, and φ is the volume fraction of the suspended particles.

(Brinkman, 1952) presented that a viscosity correlation (Eq.2.3) that extended Einstein's equation to suspensions with moderate particle volume fraction, typically less than 4 %.

$$\mu_{eff} = \mu_{bf} \frac{1}{(1-\varphi)^{2.5}} \qquad (2.3)$$

The effect of Brownian motion on the effective viscosity in a suspension of rigid spherical particles was studied by (Batchelor, 1977). For isotropic structure of suspension, the effective viscosity is given by (Eq.2.4):

$$\mu_{eff} = (1 + 2.5\varphi + 6.2\varphi^2)\mu_{bf} \qquad (2.4)$$

2.5.3 Specific Heat and Density

The specific heat and density of two phase mixture of nanofluid as function particle volume fraction and individual properties is estimated as equation 2.5 and 2.6 (Pak and Cho, 1998), (Xuan and Roetzel, 2000)

$$\rho_{eff} = (1-\varphi)\rho_{bf} + \varphi\rho_p \quad (2.5)$$

$$(\rho C_p)_{eff} = (1-\varphi)(\rho C_p)_{bf} + \varphi(\rho C_p)_p \quad (2.6)$$

Where: ρ_{eff} – Effective density of nanofluid

ρ_{bf} – Density of base fluid

ρ_p – Density of particles

Table 2.1 Shows the some of the common thermal properties of nanoparticles (Evangelos et al., 2018).

Nanoparticles	Density (kg/m^3)	Specific heat (J/kg K)	Thermal Conductivity (W/m K)
Al_2O_3	3880	773	36
CuO	6350	535	69
Fe_2O_3	5180	670	80.4
SiO_2	2220	754	1.4
TiO_2	4175	692	8.4
ZnO	5600	514	29

2.6 The Factor Affecting Performance Improvement of Nanoparticles on Heat Transfer Enhancement

2.6.1 Effect of Particle Volume Fraction

Particle volume fraction is a parameter that has been investigated in almost all of the experimental studies and most of the results are generally in agreement qualitatively. Most of the research reports show that an increasing in particle volume fraction increase the thermal conductivity of nanofluid and the relation found is, in general, linear. There are many studies on the effect of particle volume fraction on the thermal conductivity of nanofluids.

(Ji et al., 2020) measured the thermal conductivity of SiO_2 - DW and SiO_2 - EG nanofluids at different volume fractions, and found that the thermal conductivity of nanofluids improved with the increase of the volume fraction of nanoparticles.

(Moosavi et al., 2010) measured the relationship between thermal conductivity and volume fraction of ZnO nanofluids, and they found that with the volume fraction of ZnO - EG and ZnO - DW increased to 3.0 %, the thermal conductivity improved by 10.5 and 7.2% respectively. According to the current experimental results, it can be agreed that the thermal conductivity of nanofluids depends on the volume fraction of nanoparticles

(Masuda et al., 1993) conducted experiment to measure the thermal conductivity of water based nanofluids such as of Al_2O_3, SiO_2 and TiO_2 nanoparticles. The thermal conductivity enhancement up to 32.4 % was observed for 4.3 % volume fraction of Al_2O_3 nanoparticles (Lee et al., 1999). studied the thermal conductivity of water as well as ethylene glycol (EG) based nanofluids consisting of Al_2O_3 (38.5 nm) and CuO (23.6 nm) nanoparticles. From the studies they found that 20 % enhancement of thermal conductivity was observed for 4 % of volume fraction of CuO/EG nanofluid. Later (Wang et al., 1999) repeated the measurement on the same type of nanofluids based on EG and water with Al_2O_3 (28 nm) and CuO (23 nm) nanoparticles. The measurements carried out by these groups showed that for water and ethylene glycol-based nanofluids, thermal conductivity ratio showed a linear relationship with particle volume fraction and the lines representing this relation were found to be coincident.

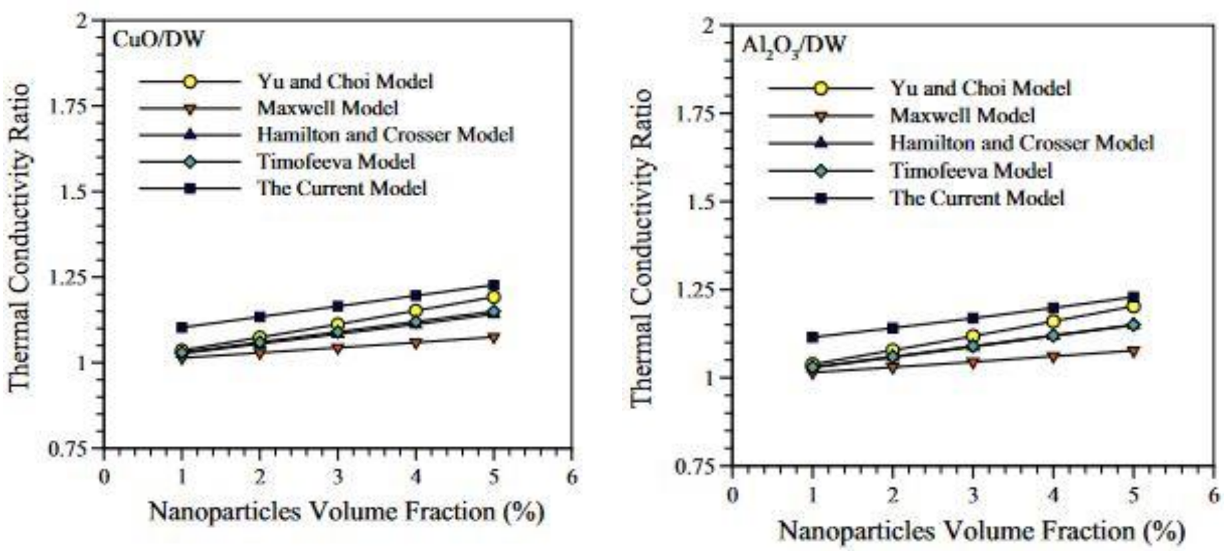

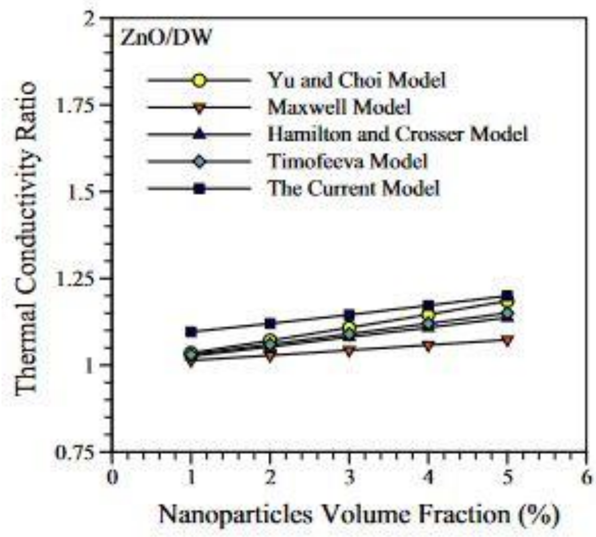

Figure 2.7 Thermal conductivity ratio as a function of nanoparticle volume fraction of different model and different nanoparticles types (Alawi et al., 2017).

2.6.2 Effect of Base Fluid

According to the conventional effective medium theory (Maxwell, 1873), as the base fluid thermal conductivity decreases, the effective thermal conductivity of a nanofluid increases. Most of the experimental reports agree with the theoretical values given by this conventional mean field model. (Wang *et al.*, 1999) results obtained on the thermal conductivity of suspensions of Al_2O_3 and CuO nanoparticles in several base fluids such as water, ethylene glycol, vacuum pump oil and engine oil, the highest thermal conductivity ratio was observed when ethylene glycol was used as the base fluid. EG has comparatively low thermal conductivity compared to other base fluids. Engine oil showed somewhat lower thermal conductivity ratios than Ethylene Glycol.

Water and pump oil showed even smaller ratios respectively. However, CuO/EG as well as CuO/water nanofluids showed exactly same thermal conductivity enhancements at the same volume fraction of the nanoparticles. The theoretical analysis made by (Hasselmann and Johnson, 1987) have shown that the effective thermal conductivity of fluid-particle mixtures were nearly independent of base fluid thermal conductivity.

2.6.3 Effect of Particle Size

There are many studies reported in literature regarding the dependence of nanoparticle size on effective thermal conductivity of nanofluids. (Chopkar *et al.*, 2008) also study on the effect of particle size on effective thermal conductivity of nanofluids. From the study they found that effective thermal conductivity of nanofluids increases with decreasing particle size.

Also, the results of (Eastman *et al.*, 2001) and (Lee *et al.*, 1999) support the conclusion drawn by (Chopkar *et al.*, 2008) on the particle size effect on the effective thermal conductivity of nanofluids.

(Aklilu and Woldeyohannes, 2013) Study on the effect of particle size on effective thermal conductivity of nanofluids and they obtained that thermal conductivity of nanofluid increase with decrease particle size as shown in figure below.

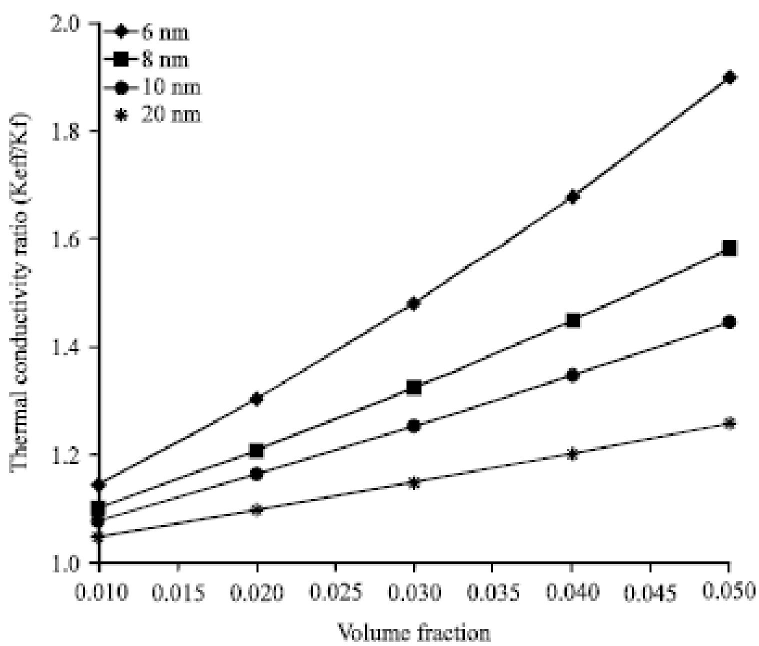

Figure 2.8 Effect of nanoparticles size on the effective thermal conductivity for Al_2O_3 -water Nanofluid. (Aklilu and Woldeyohannes, 2013).

2.6.4 Effect of Particle Shape

For experimentation, spherical as well as cylindrical shaped nanoparticles are commonly used for preparation of nanofluid. The cylindrical particles have larger aspect ratio (length to diameter ratio) than spherical particles (Xie *et al.*, 2002a). Measured the thermal conductivity of water and EG base fluid with SiC nanoparticles consisting of both cylindrical and spherical shapes.

From experimental result they obtained that water based nanofluids, the cylindrical shaped nanoparticles suspensions had higher thermal conductivity enhancement of about 22.9 % than the spherical particles for the same volume fraction (4.2 %). The theoretical study based on Hamilton-Crosser model (1962) is found that there is a good agreement with this comparatively higher enhancement for cylindrical particle suspensions.

(Murshed et al., 2005) conducted experimental investigation and they founded that TiO_2 nanoparticles in water the rod-shaped particles (32.8 %) higher enhancement than spherical particles (29.7 %) at volume fraction of 5 %.

2.7 Summary of Literature Review

Different experimental and theoretical result obtain in literature showed that use of nanofluids as working fluid in solar collector increase the outlet temperature of the base fluid and improve the efficiency of collector however, has no insignificant change compared with the pressure drop of pure water. From many experimental studies the thermal conductivity of nanofluids depends on many factors such as volume fraction of particles, particle size, and particle shapes, temperature and particles material.

2.8 Research Gap

Currently many researchers are working on solar collectors for different applications. In Ethiopia climate conditions many researchers study parabolic dish solar collectors for heating water, steam generation and cooking. Asfafaw et al., 2015) Solar cookers with latent heat storage for intensive cooking application and obtained that the thermal efficiency of the collector was 23 %. To improve the thermal efficiency of the indirect solar cooker nanofluids were used as HTF to generate steam.

CHAPTER THREE

MATERIALS AND METHODS

3.1 Introduction

To accomplish this thesis the different methodologies are carried out. The solar radiation data is collected from Eastern and Central Oromia Meteorological Service Center (ECOMSC). From the meteorology data sunshine hour duration, mean temperature, wind speed, altitude and latitude are collected and global, beam, and diffuse solar radiation are not available in metrology Angstrom correlation is used to estimate it. In this section the preliminary design used to construct the parabolic dish solar collector for each part is discussed. The nanoparticles are synthesized in materials science and engineering laboratory. Solgel and precipitation methods are used to synthesize Aluminum oxide and zinc oxide nanoparticles respectively. Nanofluid is prepared by using two step method where ultrasonic machine was used to disperse the base fluid (water) with the nanoparticles. The best suitable materials used for solar collector are selected according to their properties. The software used for this work are Catia V5, MATLAB and Microsoft excel.

3.2 Materials and Methods

This section contains the materials used to construct the parabolic dish solar collector and to prepare nanofluids. The best suitable materials used to construct the solar collector and prepare nanofluids are selected according to the appropriate properties. The following materials are used for experimental work.

Table 3.1 Materials used for construction solar collector and receiver.

No	Materials
1	Satellite dish
2	Mirror (high reflectivity)
3	Copper tube
4	Stainless pipe
5	Gate valves
6	Angle iron metal

Table 3.2 Materials use for preparation nanofluids.

S. No.	Materials
1	$Al(NO_3)_3$
2	$Zn\ (NO_3)_2 \cdot 6H_2O$
3	NaOH
4	Citric Acid
5	Ethylene Glycol
6	Ethanol
7	Distilled water

3.2.1 Overall Process

The overall process of the thesis is described by a flow diagram below;

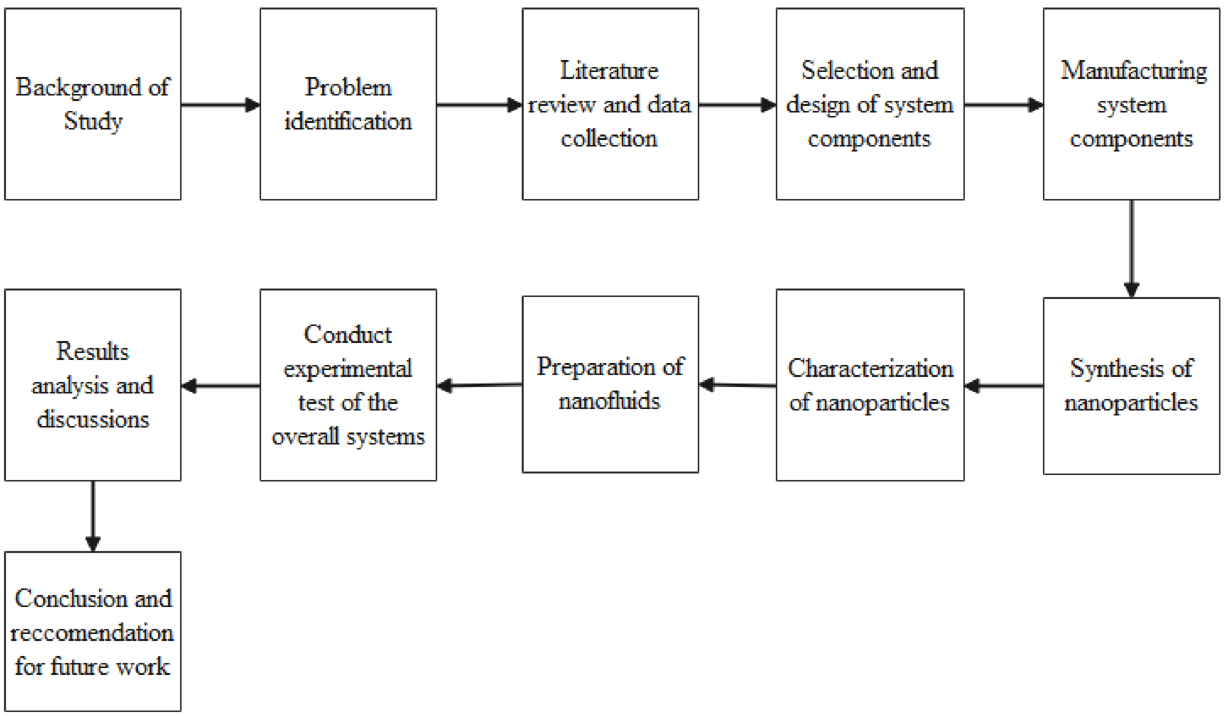

Figure 3.1 General process layout of the thesis.

3.3 Experimental Setup of Parabolic Dish Solar Collector

To conduct the experiment the following setup is used for performance analysis of parabolic dish solar collector with nanofluids and water as heat transfer fluid. In this setup the working fluid is heated at focal point of parabolic dish solar collector. After the working fluid is heated at receiver(absorber) the steam is leave the absorber used for cooking.

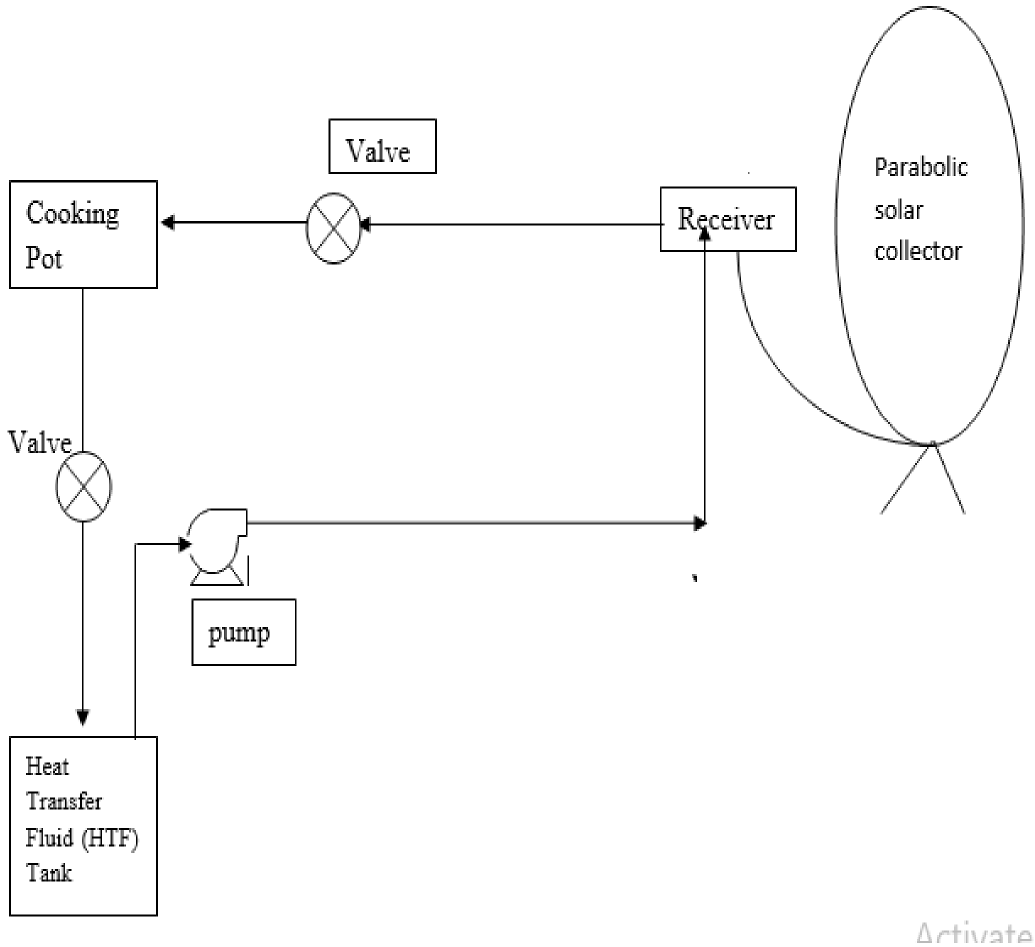

Figure.3.2 Schematic diagram of experimental setup of the system.

CHAPTER FOUR

SOLAR RADIATION POTENTIAL

4.1 Introduction

Ethiopia has an annual mean average solar radiation of about 5.2 kWh/m^2, and the range of 4 – 6 kWh/m^2 with average sun light length of more than 10 hours per day throughout the year and has high potential of solar irradiation (UNCC, 2002). Adama city has high solar radiation potential through the year.

4.2 Estimation of Solar Radiation

Solar radiation data is necessary for any solar conversion device design and to determine the level of solar radiation at given location and the amount of energy actually available at various orientations of the collector.

According to (Duffie et al., 2013) the most common measurements of solar radiation is a total solar radiation on a horizontal surface, often referred to as global radiation on the surface. However, there are different methods to predict the amount of solar radiation reaching the Earth's surface at a given location. Attempts have therefore been made to develop empirical relations for estimating radiation from weather data: temperature, humidity, sunshine hour, cloudiness and precipitation, which are actually easier to measure and are available in meteorology. Sunshine duration is the length of time that the ground surface is irradiated by direct solar radiation and used to characterize the climate of location, Adama city has a latitude 8.53°N, longitude of 39.28°E and an elevation of 1648 m above sea level. The data obtained from Eastern and Central Oromia Meteorological Service Center (ECOMSC) is sunshine hour and the global solar radiation is estimated by Angstrom correlation.

4.3 Sun–Earth Angles

The sun –earth angles are defined as follows.

Latitude Angle (ϕ):

Latitude angle is the angle made between the radial line joining the observer (location) with the center of the Earth, and its projection on the equatorial plane. For an observer in the northern hemisphere, latitude is positive, whereas for the southern hemisphere it is negative (Tiwari et al., 2016).

Declination (δ):

Declination is defined as the angle between the line joining the centers of the Sun and the Earth, which also determines the direction of the direct rays coming from the Sun and their projection on the equatorial plane (Tiwari et al., 2016).

Its value in degrees for n, average number of the days in the month (Table 4.1) is given by the Cooper's equation:

$$\delta = 23.45 \sin\left[360 \frac{284+n}{365}\right] \quad (4.1)$$

Table 4.1 Recommended average days for months and values of n by months.

Months	n for ith Day of Month	For average Day of month		
		Date	N	δ
January	i	17	17	-20.9
February	31+i	16	47	-13
March	59+i	16	75	-2.4
April	90+i	15	105	9.4
May	120+i	15	135	18.8
June	151+i	11	162	23.1
July	181+i	17	198	21.2
August	212+i	16	228	13.5
September	243+i	15	258	2.2
October	273+i	15	288	-9.6
November	304+i	14	318	-18.9
December	334+i	10	344	-23

Sunset Hour Angle

The sunset hour angle in degree, ωs can be calculated by using equation (4.2) and the values for each month of the year are tabulated in Table 4.2 for the study location.

$$\omega_s = \cos^{-1}(-\tan \emptyset \times \tan \delta) \quad (4.2)$$

Table 4.2 Sunset hour angle of the location

Sunset Hour Angle $\boldsymbol{\omega_s}$											
Jan	**Feb**	**Mar**	**Apr**	**May**	**Jun**	**Jul**	**Aug**	**Sep**	**Oct**	**Nov**	**Dec**
86.71	88.01	89.64	91.42	92.92	93.66	93.33	92.06	90.32	88.54	87.05	86.35

Sunshine hour (N)

Sunshine hour is total duration in hours of the Sun's movement from sunrise to sunset. It is defined in terms of the hour angle as (Tiwari et al., 2016)

$$N_s = \frac{2}{15}\omega_s \tag{4.3}$$

Here 1 h = 15°.

Solar Hour angle ($\boldsymbol{\omega}$)

Solar hour angle is the angular displacement of the sun east or west of the local meridian due to rotation of the earth on its axis at 15° per hour (morning negative and afternoon positive) it is given by equation (4.4) (Duffie and Beckman, 2013).

$$\omega = (Solar\ time - 12) \times 15° \tag{4.4}$$

Zenith Angle (θz)

Zenit angle is the angle between the vertical and the line to the sun or the angle of incidence of beam radiation on a horizontal surface It is given by equation (4.5) (Tiwari *et al.*, 2016).

$$\cos\theta_z = \cos\emptyset\cos\delta\cos\omega + \sin\emptyset\sin\delta \tag{4.5}$$

Where, φ is Latitude angle;$-90° \leq \varphi \leq +90°$

δ is solar declination angle;$-23.45° \leq \delta \leq +23.45°$

Solar Azimuth Angle ($\boldsymbol{\gamma_s}$)

Solar azimuth angle is the angular displacement from south of the projection of beam radiation on the horizontal plane. Displacements east of south are negative and west of south are positive.

Solar Altitude Angle ($\boldsymbol{\alpha_s}$)

Solar altitude angle is the angle between the horizontal and the line to the sun, that is, the complement of the zenith angle.

Angle of incidence ($\boldsymbol{\theta}$)

Is the angle between the beam radiation on a surface and the normal to that surface (Tiwari *et al.*, 2016).

$$\cos\theta = \cos\delta\cos\omega\,(\cos\varphi\cos\beta + \sin\varphi\sin\beta + \sin\delta\,(\sin\varphi\cos\beta - \cos\varphi\cos\beta) \qquad (4.6)$$

Solar Constant

The solar constant I_{sc} is the rate at which energy is received from the sun on a unit area perpendicular to the rays of the sun, at the mean distance of the earth from the sun outside the atmosphere (Tiwari *et al.*, 2016).

$$I_{sc} = 1367\, {W}/{m^2}$$

4.4 Extraterrestrial Radiation

Extraterrestrial radiation is the radiation incident on the outer atmosphere of the earth. At any point in time, the solar radiation incident on a horizontal plane outside of the atmosphere and it is given by equation (4.7) (Duffie and Beckman, 2013).

$$I_{ext} = I_{sc}(1 + 0.033\cos\frac{360n}{365})\cos\theta_z \qquad (4.7)$$

Where: I_{sc} is the solar constant,1367${W}/{m^2}$

I_{ext} is the extraterrestrial radiation on a horizontal surface

n is day of the year, 1 for January first

Extraterrestrial solar radiation that would fall on a horizontal surface at the location is given by:

$$I_o = I_{ext}\cos\theta_z$$

Where θ_z is zenith angle

$$\cos\theta_z = \cos\emptyset\cos\delta\cos\omega + \sin\emptyset\sin\delta \qquad (4.8)$$

Therefore I_o becomes

$$I_o = I_{sc}[1 + 0.033\cos\left(\frac{360n}{365}\right)]\,[\cos\delta\cos\emptyset\cos\omega + \sin\emptyset\sin\delta] \qquad (4.9)$$

Daily extraterrestrial radiation on a horizontal surface, Ho can be obtained by integrating equation (4.9) over the period of sunrise to sunset.

$$H_o = I_{sc}\frac{24\times3600}{\pi}\left[1 + 0.033\cos\frac{360n}{365}\right]\left[\cos\emptyset\cos\delta\sin\omega_s + \frac{\pi\omega_s}{180}\sin\emptyset\sin\delta\right] \qquad (4.10)$$

4.4.1 Beam Radiation

Beam radiation is solar radiation received from the sun without having been dispersed by the atmosphere. It is also often referred to as direct solar radiation.

4.4.2 Diffuse Radiation

The solar radiation received from the sun after its direction has been changed by scattering by the atmosphere. Diffuse radiation is referred to in some meteorological literature as sky radiation or solar sky radiation.

4.4.3 Global Solar Radiation

Global solar radiation is the total solar radiation falling onto horizontal surface of the earth. It is the sum of the beam and the diffuse solar radiation on the surface.

One of the simplest, which also gives the smallest percentage error for the estimation of the global solar radiation from sunshine hour data, is the well-known Angstrom correlation, which can be given by Equation (4.11) (Tiwari *et al*., 2016).

$$\frac{H}{H_o} = a + b\frac{n_s}{N_s} \qquad (4.11)$$

In addition, a and b are regression coefficients depend on the location and expressed as a function of latitude and sunshine hours respectively as following.

Regression Coefficients

$$a = -0.309 + 0.539 cos\phi - 0.0693 * z + 0.290\frac{n_s}{N_s}$$

$$b = 1.449 - 0.553 cos\phi - 0.694\frac{n_s}{N_s}$$

Where: H = hourly global solar radiation on a horizontal surface (KWh/m2)

Ho = extraterrestrial solar radiation on a horizontal surface (KWh/m2)

n_s= sunshine hour of the day,

N_s = the maximum possible daily hours of bright sunshine

Z= elevation above sea level (1648 m)

$\emptyset$= latitude of the location (8.53°)

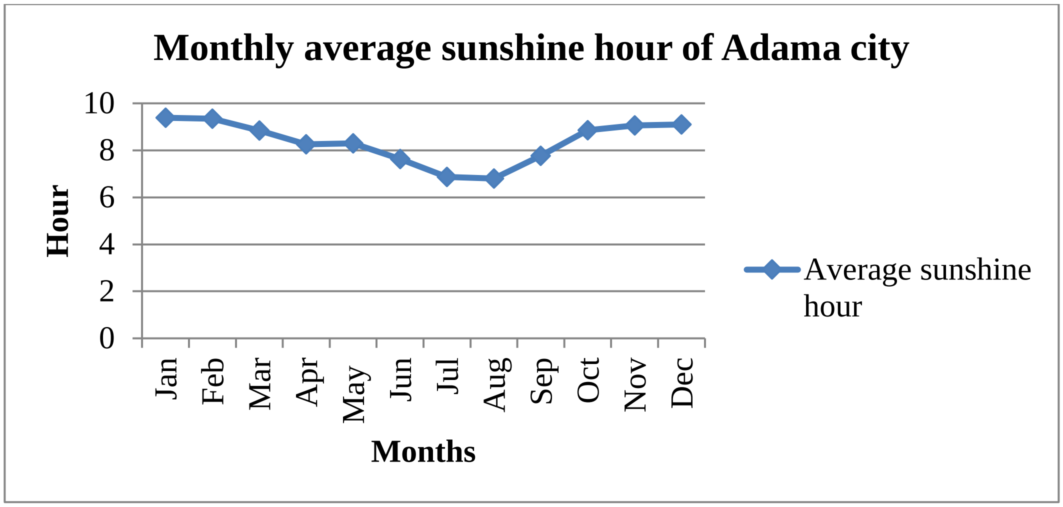

Figure 4.2 Monthly average sunshine hour of Adama city.

4.5 Estimation of Monthly Average Daily Global, Beam and Diffuse Radiation on a Horizontal Surface

4.5.1 Global Monthly Average Daily Radiation

To estimate the average daily global radiation the Angstrom model is used. The Angstrom correlation related to the amount of sunshine by a single linear relation (Tiwari *et al.*, 2016).

$$\frac{\bar{H}}{\bar{H}_o} = a + b\frac{\bar{n}_s}{\bar{N}_s} \tag{4.12}$$

$$a = -0.110 + 0.235\cos\emptyset + 0.323 \times \left(\frac{n_s}{N_s}\right)$$

$$b = 1.449 - 0.533cos\emptyset - 0.694 \times \left(\frac{n_s}{N_s}\right)$$

Where: $\bar{H}$ is the monthly average daily radiation on horizontal surface (global radiation)

$\bar{H}_o$-Monthly average radiation outside of the atmosphere for the same location.

a,b-empirical constant(values are obtained by regression).

$\bar{n}_s$-Monthly average daily hours of bright sunshine.

$\bar{N}_s$-Monthly average of the maximum possible daily hours of bright sunshine.

n-mean day of the month

4.5.2 Estimation of Diffuse Monthly Average Daily Radiation

Diffuse solar radiation is the solar radiation received from the sun after its direction has been changed by scattering the atmosphere. The monthly average daily diffuse solar radiation on a horizontal surface can be determined from the monthly average daily global radiation and the number of bright sunshine hours (Tiwari *et al.*, 2016).

$$\bar{H}_D = \bar{H}(0.931 - 0.814\frac{\bar{n}_s}{\bar{N}_s}) \quad (4.13)$$

Where: $\bar{H}_D$ - Monthly average daily diffuse radiation

4.5.3 Beam Monthly Average Daily Radiation

Beam (direct) solar radiation is solar radiation which reaching the earth surface without scattering in the atmosphere. Monthly average daily beam radiation on a horizontal surface is the difference between global and diffuse monthly daily average radiation

$$\bar{H}_B = \bar{H} - \bar{H}_D \quad (4.14)$$

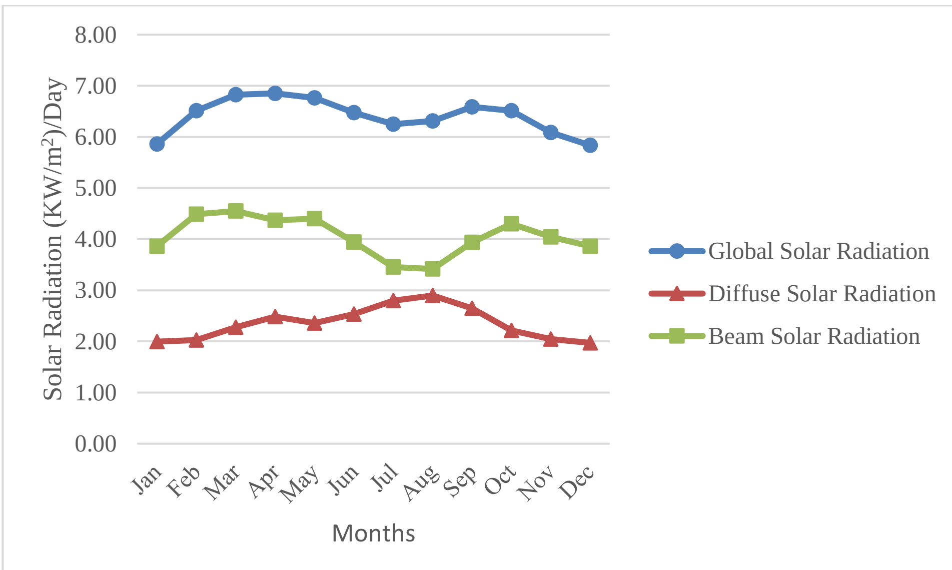

Figure 4.3 Monthly average daily global, diffuse and beam solar radiation on a horizontal surface.

4.6 Prediction of Monthly Average Hourly Global, Beam and Diffuse Radiation on a Horizontal Surface

The monthly average hourly global and diffuse radiation on a horizontal surface can be calculated from the knowledge of the monthly average daily global and diffuse radiation on a ground level.

4.6.1 Global Hourly Solar Radiation Estimation

Estimation of monthly average hourly global radiation on a horizontal surface is given by equation (4.15) (Tiwari *et al.*, 2016).

$$\bar{I} = \frac{\bar{H}\pi}{24}(a_1 + b_1 \cos\omega)\frac{\cos\omega - \cos\omega_s}{\sin\omega_s - \frac{\pi\omega_s \cos\omega_s}{180}} \quad (4.15)$$

Where: $\bar{I}$ –Monthly average hourly global radiation

a_1 and b_1 are regression constant

$a_1 = 0.409 + 0.5016\sin(\omega_s - 60)$

$b_1 = 0.6609 - 0.4767\sin(\omega_s - 60)$

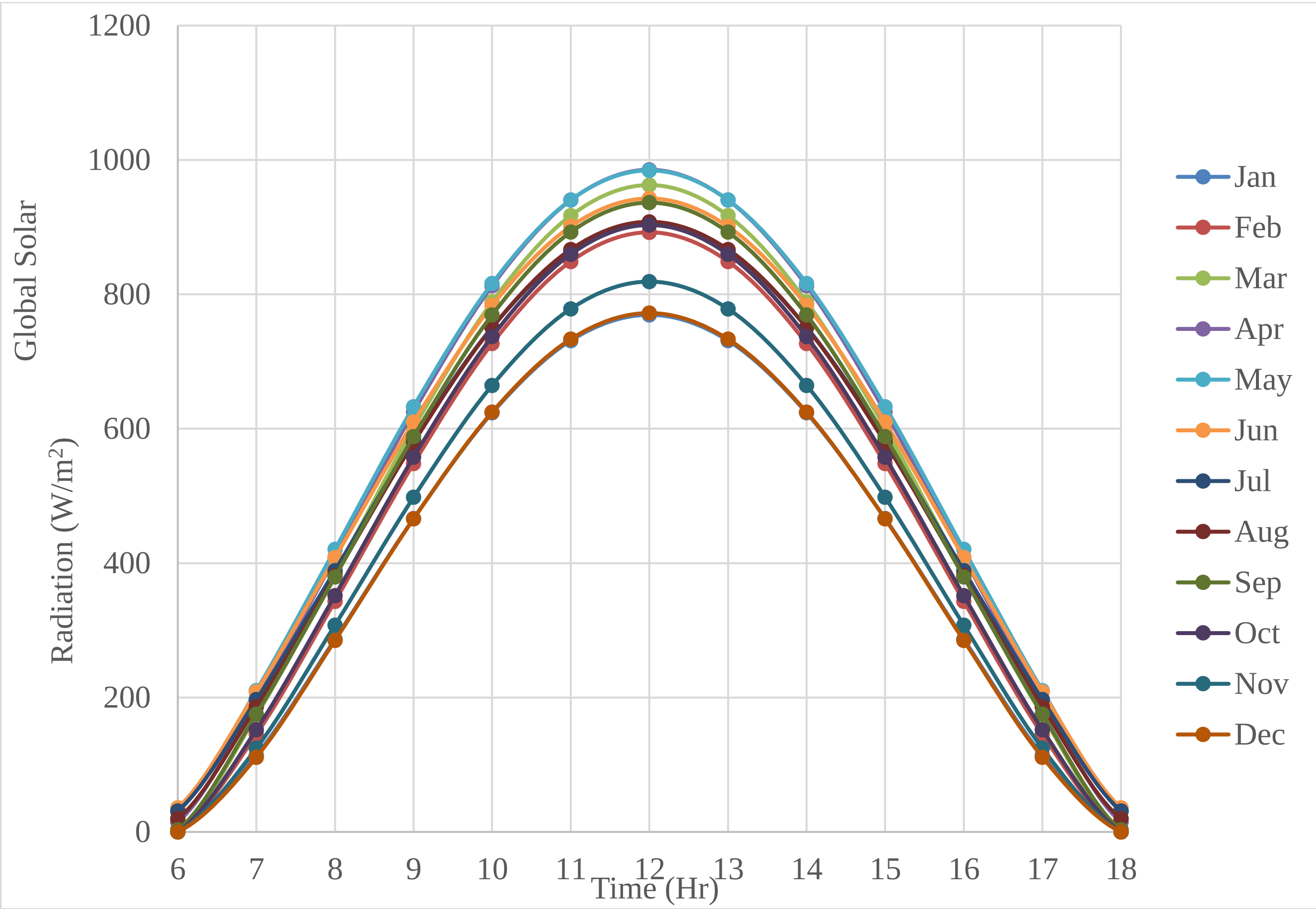

Figure 4.4 Monthly average hourly global radiation on horizontal surface.

4.6.2 Diffuse Hourly Solar Radiation Estimation

Estimation of monthly average hourly diffuse radiation on horizontal surface (ID) is given by equation 4.16 (Tiwari *et al.*, 2016)

$$\bar{I}_D = \frac{\bar{H}_D \pi}{24} \frac{\cos\omega - \cos\omega_s}{\sin\omega_s - \frac{\pi\omega_s \cos\omega_s}{180}} \qquad (4.16)$$

Where: $\bar{I}_D$ - Monthly average hourly diffuse radiation

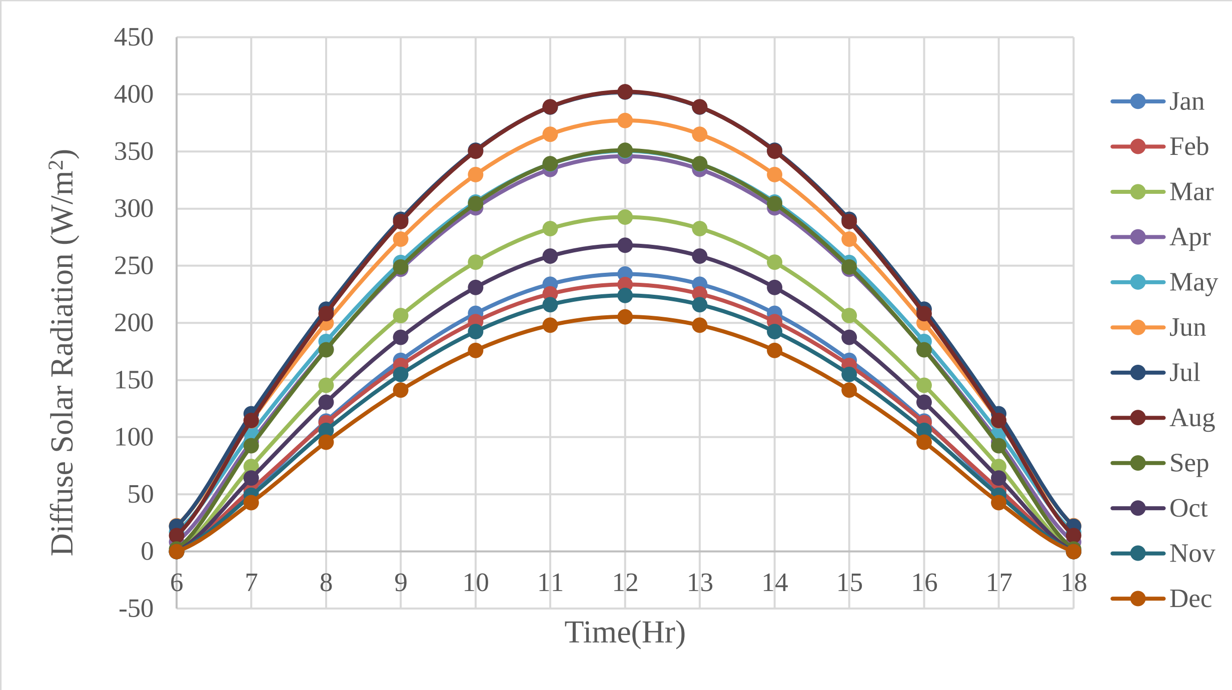

Figure 4.5 Monthly average hourly diffuse solar radiation on horizontal surface

4.6.3 Estimation of Beam Hourly Solar Radiation

Estimation of monthly average hourly beam radiation on horizontal surface is given by

$$\bar{I}_B = \bar{I} - \bar{I}_D \qquad (3.17)$$

Where: $\bar{I}_b$- Monthly average hourly beam radiation

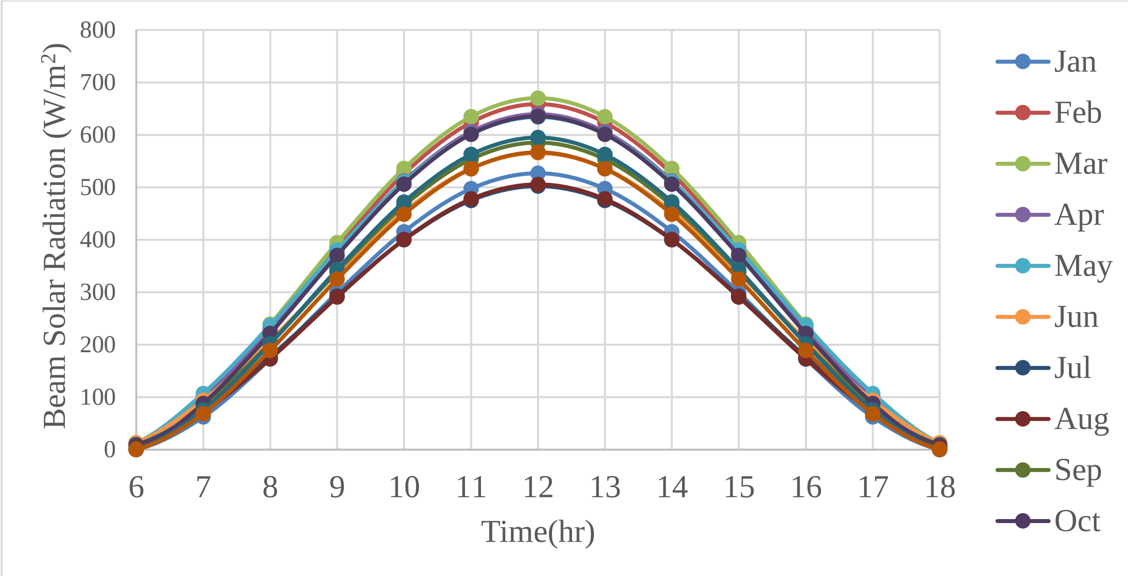

Figure 4.6 Monthly average hourly beam solar radiation

4.7 Meteorological Data of Average Ambient Temperature and Wind Speed of Adama City

Figure 4.7 shows the average temperature and wind speed of Adama city for seven years.

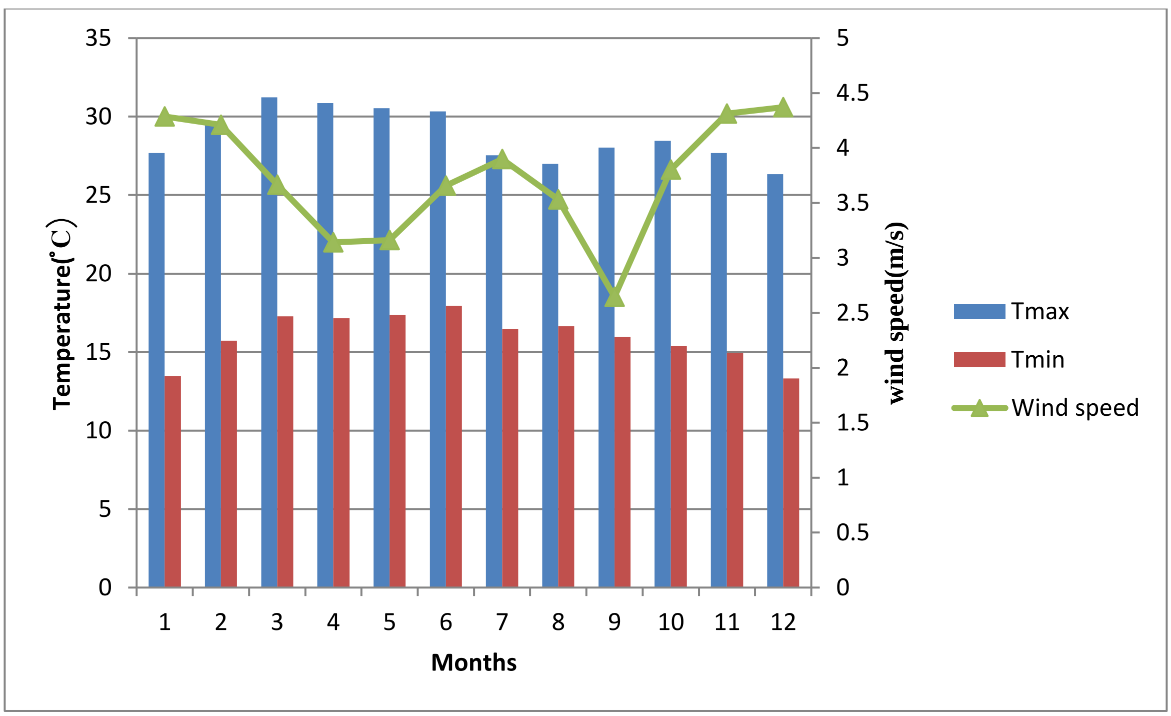

Figure 4.7 Meteorological data of average ambient temperature and wind speed.

CHAPTER FIVE

THEORETICAL FORMULATION OF PARABOLIC DISH SOLAR COLLECTOR AND LHS UNIT

5.1 Introduction

In this section the theoretical design of PDSC and thermal storage unit that can used for indirect solar cooking system. The design, sizing, selection and specifications for both the PDSC parameters and the thermal energy storage unit are presented in detail. Selection of PCM and HTF and sizing of LHS unit is also addressed.

5.2 Design of Parabolic Dish Solar Collector

The parabolic dish solar collector collects energy from the solar irradiation and converts into heat energy that is used to heat the fluid. A receiver absorbs the heat reflected from the collector and heats the fluids in the absorber. The following parameters are taken in to consideration to design of parabolic dish solar collector.

- Available solar radiation
- Diameter of the parabolic dish collector
- Diameter of receiver (absorber)
- Focal point parabolic dish collector
- Aperture area of collector
- Area of receiver
- Height of parabolic dish
- Concentration ratio
- Rim angle
- The working fluid

a) Concentrating Solar Collector

The word collector will be applied for both the receiver and concentrator. The receiver is the component of the system where the radiation is absorbed and converted to heat. The concentrator, or optical system, is the part of the collector that directs the sun radiation onto the receiver.

b) Collector Configurations

Many concentrator types are used to direct a heat flux on the receiver. They can be 2 dimensional (trough) to focus on a ‘‘line’’ or 3 dimensional to focus on a ‘‘point.’’ Receivers can be concave, flat, or convex. In general, concentrators are effective only for beam radiation. It is evident also that the angle of incidence of the beam radiation on the concentrator is important and that sun-tracking will be required for these collectors. A variety of orienting mechanisms have been designed to move focusing collectors so that the incident beam radiation will be reflected on the receiver (Duffie and Beckman, 2013).

c) Concentration Ratio

The concentration ratio is a ratio of aperture area of a collector to the receiver area. Also, a flux concentration ratio is the ratio of the average energy flux on the receiver to that on the aperture. There can be substantial variations in energy fluxes over the surface of a receiver. A local flux concentration ratio can be defined as the ratio of the flux at any element on the receiver to that on the aperture, which will vary across the receiver.

The area concentration ratio can be given as

$$CR = \frac{A_{ap}}{A_r} \quad (5.1)$$

$$A_{ap} = \pi \times D_a^2/4 \quad (5.2)$$

Where, A_{ap} is aperture area, A_r is receiver area

5.3 Sizing Analysis of Parabolic Dish

To calculate the parabola equation, mathematical analysis can be performed to find the values that satisfy the design criteria, like diameter, aperture angle and concentration ratio. Figure 5.1 shows geometry of the solar collector parabolic dish.

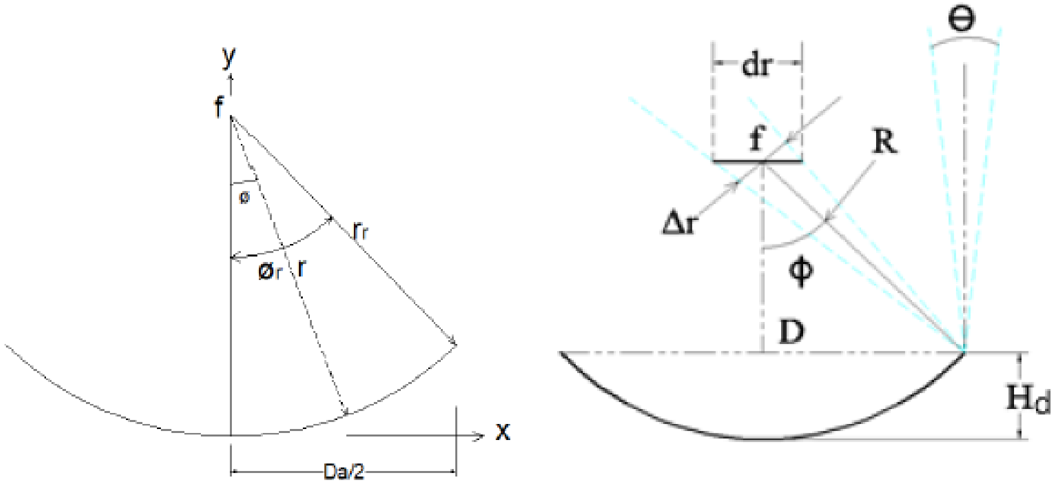

Figure 5.1 Geometry and dimension of the solar collector parabolic dish (Dejene, 2020).

Table 5.1 Geometric Specification of parabolic dish.

S. No.	Description	Value
1	Height	0.296 m
2	Rim angle	66.8 °
3	Focal point	0.68 m
4	Aperture area	2.54 m^2

5.3.1 Geometric Sizing of Parabolic Dish

Under this topic, the geometric analysis of the parabolic solar collector can be determined. All the required parameters are calculated as in the following equations. From the parabola geometry as shown in Figure 5.1, the rim angle is calculated as

$$\tan(\emptyset_r) = \frac{\frac{D_{ap}}{2}}{f-h_d} \tag{5.3}$$

From the parabolic equation the height of dish is derived as follows.

The height of parabolic h_d is found from the equation of parabola. From definition of parabola any point M(x,y) on the parabola is equidistance from the focus and the directrix. Then the distance FM=MD from figure (5.2) this means.

$$\sqrt{(x-0)^2+(y-f)^2}=\sqrt{(x-x)^2+(y-(-f))^2} \tag{5.3 a}$$

Squaring both side and expand

$$x^2 + y^2 + f^2 - 2yf = y^2 + f^2 + 2yf \qquad (5.3\text{ b})$$

Then rearranging

$$y=\frac{x^2}{4f} \qquad (5.3\text{ c})$$

When, x=$D_{ap}/2$,y=h_d (5.3 d)

Then the height of parabolic becomes

$$h_d = \frac{(D_{ap}/2)^2}{4f} = \frac{(D_{ap})^2}{16f} \qquad (5.4)$$

From equation 5.4 the focal point(f) becomes

$$f = \frac{(D_{ap})^2}{16h_d} \qquad (5.5)$$

From equation 5.5 the focal point of dish is 0.68 m.

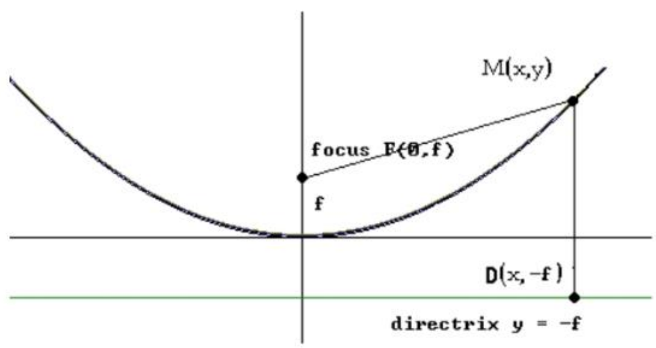

Figure 5.2 Parabola geometry

Substituting equation (5.4) in to equation (5.3) and the rim angle is written as

$$\emptyset_r = \tan^{-1}\left(\frac{D_{ap}/_2}{f-h_d}\right) = \tan^{-1}\left(\frac{D_{ap}/_2}{f-\frac{D_{ap}^2}{16f}}\right) \qquad (5.6)$$

Where: D_{ap} the diameter of the aperture.

From equation 5.6 the rim angle of parabolic dish is 66.8 °.

5.4 Geometry Analysis of Receiver

5.4.1 Conical Cavity Tube Receiver of Parabolic Dish Solar Collector

The receiver of a solar dish system is the interface between the concentrator and the heats point. The sun radiation from solar collector is collected at point called receiver (absorber) of solar collector and heat the fluid at focal point. In generally there are two types of absorbers; external and cavity absorber.

i) External Absorber

An external absorber is essentially a flat plate. The reflected radiation strikes on the plate and heats the surface. External absorbers are extremely simple and cheap but have many inefficiencies. External absorbers are directly exposed to ambient air and at high temperatures convection losses can be extreme (John, 2009).

ii) Cavity Absorber

In cavity absorber solar radiation is reflected by the concentrator through an opening, referred to as the receiver aperture, and collected on the absorber surface. Now a day most modern receivers are used this type absorber. Cavity absorbers are more expensive and complicated than external absorbers, but are much more efficient. If any radiation reflects off the absorber surface it was reflected onto another part of the absorber. In this way, the absorber has an increased chance of absorbing radiation each time light strikes its surface (John, 2009). In this study cavity receiver is selected due to it is more efficiency compared to other type receiver. Conical coil tube receiver is used in this study.

5.4.2 Absorber/Receiver Area

This is the total area that receives the concentrated solar beam radiation. This area delivers the useful thermal energy to the system. The surface area exposed to solar radiation of conical tube is calculated as (Jayachandraiah and Praveen, 2016)

$$A_r = \pi \times d_o \times L \qquad (5.7)$$

Area of a conical tube is calculated using equation (5.7).

Where: L is total the receiver tube (Eterafi et al., 2021).

$$L = \frac{\pi w(d_o + w)}{4 d_o \sin(\frac{\theta}{2})} \quad (5.8)$$

Where: w the aperture diameter of cavity

The area of conical cavity tube is estimated using equation (5.7) is 0.097 m^2.

5.5 Heat Transfer Analysis of Receiver of Parabolic Dish Solar Collector

The heat transfer coefficient (h) of the flow can be calculated according to the following formula:

$$h = \frac{\dot{Q}_u}{A_{coil}(T_r - T_{fm})} \quad (5.9)$$

Where: T_r Receiver temperature

The mean fluid temperature (T_{fm}) is calculated as:

$$T_{fm} = \frac{T_{in} + T_{out}}{2} \quad (5.10)$$

The Nusselt number (N_u) of the flow is calculated as follow

$$N_u = \frac{h \times D_{coil,in}}{k} \quad (5.11)$$

The theoretical value of the Nusselt, which is used only for validation reasons, is estimated using the model of Dittus-Boelter equation.

$$N_u = 0.023 \times R_e^{0.8} \times P_r^{0.4} \quad (5.12)$$

5.6 Heat Loss Analysis over the Receiver

There are different heat transfers lost from the receiver these are conduction, convection, and radiation heat lost.

5.6.1 Conduction Heat Loss

The conduction heat loss through the cavity insulation was modelled by considering the conduction mechanism through the insulation medium, as well as the convection mechanism present on the outside of the receiver cavity. This is evident in the thermal resistance (R_{total}) presented in Eq. (5.13) (Jonathan et al., 2020).

$$\dot{Q}_{cond,loss} = \frac{T_{sur} - T_{amb}}{R_{total}} = \frac{T_{sur} - T_{amb}}{\frac{t_{ins}}{k_{ins} A_{ins,in}} + \frac{1}{h A_{ins,out}}} \quad (5.13)$$

Where: T_{sur} −Surface Temperature

T_{amb} − Ambient Temperature

t_{ins} −Insulation thickness

A_{ins} −Insulation Area

k_{ins} −Insulation thermal conductivity

h − Convection heat transfer coefficient, W/m^2·K

5.6.2 Convection and Radiation Heat Loss

Convection heat losses occur from the absorber surface directly exposed to the moving stream of air. Radiation heat loss through the receiver aperture is described by operating temperatures only slightly above ambient and becomes dominant for collectors operating at higher temperatures. The convective and radiation heat loss from absorber is estimated as follows.

$$\dot{Q}_{loss} = A_r U_L (T_{rm} - T_{amb}) \quad (5.14)$$

Where: U_L is the mean coefficient of heat losses,

T_{rm} mean receiver temperature

The mean coefficient of heat losses is calculated using equation (5.15)

$$U_L = \left[\frac{1}{h_c + h_r}\right]^{-1} \quad (5.15)$$

Where: h_c and h_r correspond to the convection coefficient and radiation coefficient, respectively.

To calculate the convection coefficient, we consider the thermal conductivity of air (k_{air}) the receiver diameter (D_{out}), and the Nusselt number (Nu), which must be calculated from the Reynolds number (Re).

For Reynolds numbers comprised between 0.1 and 1000, the Nusselt number is given by equation (5.16).

$$N_u = 0.4 + 0.54Re^{0.52} \qquad (5.16)$$

for Re numbers comprised between 1000 and 50,000, the Nusselt number is given by equation (5.17)

$$N_u = 0.30Re^{0.6} \qquad (5.17)$$

$$Re = \frac{V_{air} \times D_{out}}{\vartheta_{air}} \qquad (5.18)$$

Where: $\vartheta_{air}$is the kinematic viscosity of air

V_{air} is the average velocity of air

$$\vartheta_{air} = \frac{Dynamic\ viscosity\ of\ air}{Density\ of\ air} = \frac{0.00001983\,{}^{N\times s}/_{m^2}}{1.2\,{}^{kg}/_{m^3}} = 1.652 \times 10^{-5}\,{}^{m^2}/_{s}$$

Then Reynolds number from equation 5.18 is 35400.9

Then the Nusselt number from equation 5.17 becomes

$$N_u = 0.30Re^{0.6} = 0.3 \times 35400.9^{0.6} = 160.89$$

Convective heat transfer coefficient air is given by equation (5.19)

$$h_c = \frac{k_{air}}{D_{out}} \times N_u \qquad (5.19)$$

The convective heat transfer coefficient from equation (5.19) is 21.45 W/m^{2}K.

The radiation heat transfer coefficient is calculated using equation (5.20)

$$h_r = 4\sigma\varepsilon T_{air}^3 \qquad (5.20)$$

where: $\varepsilon -$ Emissivity factor

$\sigma -$ Stefan-Boltzmann Constant (${}^{W}/_{m^2K^4}$)

$T_{air} -$ Temperature of the air (K).

Using equation (5.20) radiation heat transfer coefficient is 0.044 W/m^{2}K.
From equation (5.15) the mean heat loss coefficient(U_L) is 21.45 W/m^{2}K.

Then from equation (5.14) heat loss from the receiver is 260.3 W by neglecting conduction heat loss due to the surface being well insulated.

5.7 Pipe Line Design

The pipework in a solar system must be able to withstand circulating fluid at high temperatures without corroding. For cold water galvanized iron pipe is used. The copper tube is used for steam side fluid.

5.7.1 Pipe Loss Analysis

The heat loss from the pipe line through conduction, convection and radiation is computed using eq. (5.21). Where, thermal conductivity and thickness of polystyrene foam insulation are 0.023 W/mK and 0.05 m respectively.

$$\dot{Q}_{loss} = \frac{2\pi kL}{ln(\frac{D_o+2t}{D_i})}\left[T_p - T_{amb}\right] + A_p\sigma\varepsilon\left[{T_p}^4 - {T_{amb}}^4\right] + hA_p[T_p - T_{amb}] \tag{5.21}$$

Where: k is thermal conductivity of polystyrene foam (W/m K).
Tp is Temperature of pipe (K).
Ap is Area of pipe (m^2).
$h-$ convective heat transfer coefficient of air (W/m^{2}K)
$T_{amb}-$ Ambient temperature (K).
$\varepsilon-$ Emissivity of the insulator
D_o and D_i- Outer and inner diameter of the pipe (m).

5.8 Required Pumping Power

In order circulate the HTF through the system, it must be equipped with a pumping system that can overcome the pressure drop throughout the whole system which is specified by ΔP. The pumping power is calculated using equation (5.30).

$$P = \frac{\dot{m}}{\rho} \times \Delta P \tag{5.30}$$

5.9 Pressure Drop in System

Pressure drop in the collector is the sum of pressure drop in the receiver, pipe and fittings and bending's.

5.9.1 Pressure Drop in the Receiver

The Reynolds number (Re) for the tubular coil is calculated as:

$$R_e = \frac{4\times\dot{m}}{\pi\times D_{coil}\times\mu} \qquad (5.22)$$

Using equation (5.22) the Reynolds number (Re) is 1011.31 and flow is laminar flow. The Reynolds number calculated using high viscosity fluid and nanofluid have higher viscosity compared to a water.

Conical cavity tube friction factor

The friction factor of the flow (*fc*) can be calculated as follows

Laminar friction factor:

$$f_c = \frac{64}{Re} \qquad (5.23)$$

From equation (5.23) the friction factor is 0.063.

The pressure drop in coil tube is calculated as

$$\Delta P_t = \frac{2 f_c \rho L u^2}{di} \qquad (5.24)$$

Where: u is velocity (u) inside the coil is calculated as

$$u = \frac{\dot{m}}{\rho\times\left(\frac{\pi\times D_{coil,in}^2}{4}\right)} \qquad (5.25)$$

From equation (5.24) the pressure drop in the receiver coil is 440.85 Pa.

5.9.2 Pressure Drop in Pipe

The pressure drop in the pipe is estimated using the following equation.

Calculation of the pressure drop equation is based on the Darcy-weisbach equation is

$$\Delta P = f_c \frac{L}{D} \frac{\rho V^2}{2} \tag{5.26}$$

Where D is pipe diameter

f_c is friction factor

V is fluid velocity

L is pipe length

First check the type of by calculating Reynolds number.

The Reynolds number is calculated using the following equation.

$$R_e = \frac{\rho V D}{\mu} \tag{5.27}$$

From equation (5.27) the Reynolds number in the tube is 786.2 and the flow is laminar flow.

The friction factor is representing the loss of pressure of a fluid in a pipe due to the interactions in between the fluid and pipe. The Darcy friction factor can be calculated using equation

$$f_c = \frac{64}{R_e} \tag{5.28}$$

Using equation (5.26) the pressure drop in tube side was estimate as 48.74 Pa.

5.9.3 Pressure Drop in Connections Fitting and Bending's in the Whole System

The length of total connecting tubes is 6.7m 12.7 mm diameter with 4 right angle bending's. Thus, the pressure drop developed can be estimated by assuming uniform flow inside the pipes;

$$\Delta P_{con} = f_c \rho \frac{V^2}{d_i} L + K_f \frac{\rho V^2}{2} \tag{5.29}$$

Where Kf is pressure loss factor

V is the average velocity in the tube upstream fittings

For right angle bend, laminar flow Kf= 0.9

From equation (5.30) the pressure drops in connections fitting and bendings is 15.55 Pa.

Total pressure drop in the system =$\Delta P_{rec} + \Delta P_t + \Delta P_{con}$ =505.14 Pa

Allowance factor of 1.5 is given for reliability of the pump ΔP_{tot} = 758.1 Pa

Total specific work Y = $\frac{\Delta P_{tot}}{\rho}$ = 0.737 m^2/s^2

Total dynamic head TDH =$\frac{Y}{g}$= 0.075 m

Total volume flow rate $\dot{Q}$= $8.34x10^{-6}$ m^3/s = 0.03 m^3/hr

Therefore, a proper pump with requirement of head more than 0.075 m and flow rate 0.03 m^3/hr can perform the required pumping effect. In the market the least power of pump (centrifugal) available is 0.5hp.

Table 5.2 specification of selected pump

Pump specification		Motor specification	
Flow rate	35 l/min	Frequency	50 Hz
Shaft power	0.37 kw	Voltage	220 V
Lift distance	8 m	Current	2.5 A

5.10 Thermal and Optical Analysis of Parabolic Dish Solar Collector

5.10.1 Thermal Analysis of PDSC

In this section appropriate expressions are derived for the collector thermal efficiency, useful heat energy and the available solar irradiation. The useful energy delivered from a concentrator is given by:

$$\dot{Q}_u = I_b \eta_{th} A_{ap} = \dot{m} C_p (T_{out} - T_{in}) \quad (5.31)$$

Using equation 5.31 the useful energy is 683 W.

Aperture area of parabolic dish solar collector is estimated from equation (5.31).

$$A_{ap} = \frac{\dot{Q}_u}{I_b \eta_{th}} \quad (5.32)$$

From equation (5.32) the area aperture is 2.54 m^2

The thermal efficiency of the collector (η_{th}) is the ratio of the useful heat production to the available solar irradiation and mathematical written as

$$\eta_{th} = \frac{\dot{Q}_u}{Q_s} \quad (5.33)$$

The average hourly beam radiation estimated is 536.77 W/m^2

The available solar irradiation on the collector aperture (Qs) is calculated as the product of the dish aperture area (A_{ap}) and the direct solar beam radiation (Ib).

$$Q_s = A_{ap} I_b \quad (5.34)$$

The available solar radiation on the aperture collector is 1356.9W.

Where: $\dot{Q}_u$ Useful energy absorbed by the fluid

Q_s is available solar irradiation on the collector aperture

A_a is area of aperture area of concentrator

I_b is solar beam radiation

η_{th} is the thermal efficiency of the collector

5.10.2 Energy Absorbed by Receiver

The energy absorbed by receiver is calculated as the sum ofthe useful heat delivered by a solar collector system and direct or indirect heat losses from the receiver.

$$\dot{Q}_r = \dot{Q}_u + \dot{Q}_{loss} \quad (5.35)$$

Where: $\dot{Q}_r$ heat absorbed by receiver

The heat loss from the receiver is calculated using equation (5.14).

The receiver efficiency η_r is defined as the ratio of the useful energy delivered to the energy falling on the receiver.

$$\eta_r = \frac{\dot{Q}_u}{\dot{Q}_r} \quad (5.36)$$

From equation (5.36) obtained was 72.4%.

5.10.3 Optical Analysis

The optical efficiency (η_{opt}) is calculated as the ratio of the absorbed solar irradiation from the absorber (Q_{abs}) to the incident solar irradiation (Q_s) (Evangelos et al., 2019).

$$\eta_{opt} = \frac{Q_{abs}}{Q_s} \quad (5.37)$$

The optical efficiency of most parabolic solar concentrators lies between 0.6 and 0.7 (Ibrahim, 2013). Taking the average value, $\eta_o = 0.65$

5.11 Synthesis of Nanoparticles

In general, to synthesis nanoparticles, two methods are used. These are bottom-up and top-down methods.

Bottom-up method

The bottom-up or constructive method is the build-up of material from atoms to clusters to nanoparticles. The most commonly used bottom-up methods for synthesis nanoparticles are chemical vapour deposition (CVD), Sol-gel, spinning, (CVD), pyrolysis and biosynthesis method (Saravanakumar et al., 2017).

Top-down Method

Top-down or destructive method is the minimizing of a bulk material into nanoparticles. To synthesis nanoparticles the most widely used top-down methods are mechanical milling, nanolithography, laser ablation, sputtering and thermal decomposition method (Saravanakumar et al., 2017).

In this thesis bottom -up method is used to synthesis of nanoparticles. Under bottom-up chemical method sol-gel was used to synthesis nanoparticles.

Sol-gel Method

Sol-gel process involve the conversion of a solution system from a liquid’’sol’’ into a solid ‘’gel’’phase. The starting materials used in the preparation of the ‘’sol’’are usually inorganic, metal salt or organic compound such as metal oxides.

Sol-gel method is the most preferred bottom-up method due to its simplicity and as most of the nanoparticles can be synthesized from this method. It is a wet-chemical process containing a chemical solution acting as a precursor for an integrated system of discrete particles. Metal oxides and chlorides are the typically used precursors in sol-gel process (Saravanakumar et al., 2017).

To synthesis nanoparticles the following equipment are used

- ❖ Magnetic stirrer
- ❖ Centrifuge
- ❖ Oven
- ❖ Furnace
- ❖ Mortar (for grinding the powder)

i) Magnetic Stirrer

A magnetic stirrer is a device widely used in laboratories and consists of a rotating magnet or a stationary electromagnet that creates a rotating magnetic field. This device is used to make a stir bar, immerse in a liquid, quickly spin, or stirring or mixing a solution (Loos, 2015).

Figure 5.3 Magnetic stirrer (Loos, 2015)

ii) Centrifuge

A centrifuge is a device that uses centrifugal force to separate various components of a fluid. This is achieved by spinning the fluid at high speed within a container, thereby separating fluids of different densities or liquids from solids. In synthesis of nanoparticles used to separate solid particles and liquid.

iii) Oven

An oven is a device that used to dry the solid power. Ovens contain a hollow chamber and provide a means of heating the chamber in a controlled way.

iv) Furnace

The furnace is a device used to increase the crystallinity of particles and remove the impurity present on the surface. Calcination temperature utilized to prepared material converted one phase to other.

5.11.1 Synthesis of Aluminum Oxide Nanoparticles

In this thesis, sol gel method is used to synthesize aluminum oxide nanoparticles. The raw materials are used to synthesize of aluminum oxide are aluminum nitrate (($Al(NO_3)_3.9H_2O$) distilled water (DW), citric acid ($C_6H_8O_7$), ethylene glycol and ethanol (C2H5OH). Initially 0.1mol of aluminum nitrate and 30 mL ethylene glycol was gradually added to the aqueous alcoholic solution including 100 mL of DW and 100 mL of ethanol, and then it is placed on a hot plate (Rajaeiyan, 2013). Then 0.3 mol $C_6H_8O_7$ dissolved in 40 mL of DW was added to the solution. Then the solution is continuously stirred at 40 ℃ for 15 min until colloidal solution is prepared. Next, the solution was placed on water bath at 80 ℃ to evaporate solvent and prepare gel. After 18 hr, the aerogel was placed on hot plate at 120 ℃ for 4hr then the obtained sol-gel precursor was heated in the oven for 3 hr at 200 ℃. Later the dried sol gel was grinded into powder and the powder was kept in the furnace for 2 hr. at 1000 ℃. Finally, the fine aluminum oxide was obtained as shown in Figure 5.4. To get the required amount of Al_2O_3, the same steps can be followed.

Raw materials used for synthesis of aluminum oxide are aluminum nitrate, citric acid, ethylene glycol, ethanol, Distilled water.



before stirring the solution

After stirring the solution for 15 minutes at 40℃

Evaporate solvent in water bath at 80℃



After aging for 18hr

Place on hot stirrer for 4hr at 120℃

After drying in oven at 200℃ for 3 hr


Grinding in the mortor

Calcinnation in furnace at 1000℃ for 2hr

Figure 5.4 Synthesis process of aluminum oxide nanoparticles.

5.11.2 Synthesis of Zinc Oxide Nanoparticles

ZnO Nanoparticles have been synthesized by precipitation method from Zinc nitrate precursor. Zinc nitrate, sodium hydroxide, deionized water, and ethanol are used to synthesis of zinc oxide nanoparticles. In this experiment, firstly, 0.5 M aqueous ethanol solution of zinc nitrate (Zn (NO3)2·6H2O) was dissolved for one hour under constant stirring using a magnetic stirrer. Then 0.9 M solution of $NaOH$ and ethanol was also prepared in the same way with stirring of one hour. Then add $NaOH$ a solution drop by drop touching the wall of the vessel by controlling PH at 10.5 into the aqueous solution of zinc nitrate under high-speed constant stirring. The reaction was allowed to proceed for 2 hours after the complete addition of sodium hydroxide and in this condition; the beaker is sealed for two hours. After that the solution was allowed to settle overnight and further, the supernatant solution was separated carefully. The remaining solution was centrifuged for 10 min, and the precipitate was removed. Thus, precipitated nanoparticles were washed three times with deionized water and two times with ethanol to remove the byproducts and then dried at about 80°C in oven. During drying, $Zn(OH)_2$ is completely converted into ZnO .Then finally kept in the furnace at 500℃ for three hours (Satyanarayana et al., 2012).

After dissolve ethanol and zinc nitrate for 1hr on magnetic stirrer

After dissolution of sodium hydro oxide for 1hr

After add sodium hydro oxide solution drop by drop into zinc nitrate

after aging the solution for 12 hr

Centrifuge the solution for 10 min

Drying in oven at 80℃

Grinding the powder in mortar

After calcination at 500℃ for 3 hr

Figure 5.5 Synthesis process of zinc oxide nanoparticles.

The ZnO nanoparticles diameter is calculated using Debye-Scherrer formula.

$$d = \frac{0.9\lambda}{\beta \cos\theta} \quad (5.38)$$

Where: 0.89 is Scherrer's constant, λ is the wavelength of X-rays, θ is the Bragg diffraction angle, and β is the full width at half-maximum (FWHM) of the diffraction peak corresponding to plane.

5.11.3 Volume Fraction of nanofluids

The concentration of the nanofluids in percent volume fraction can be estimated by Eq. (5.39) (Irwan and Satriananda, 2017).

$$\varphi = \frac{\frac{m_p}{\rho_p}}{\frac{m_p}{\rho_p}+\frac{m_f}{\rho_f}} \times 100\% \quad (5.39)$$

where: φ : Particles volume fraction, m_p: Mass of nanoparticles,ρ_p: Density of nanoparticles m_f: Mass of base fluids,ρ_f: Density of base fluids (Water)

The required amount of Al_2O_3 nanoparticles for prepare nanofluids is estimated using equation (5.39) is 0.8 g/l and similarly for ZnO is 1.14 g/l. (Taylor et al., 2012) compared a nano-fluid-based concentrating solar thermal system with a conventional one. Nano-fluids with volume fractions approximately to 0.001% or less could be beneficial.

5.12 Preparation of Nanofluids

The nano-fluids preparation is not just a simple process of mixing the nanoparticles with a base fluid. To get nano-fluids with homogeneously dispersed nanoparticles the proper mixing is required under certain environmental conditions. There are many methods used for the preparation of nano-fluids, which can be classified into two primary classes according to the number of steps involved during their preparation. These are the one-step method and the two-step method

5.12.1 One-Step Method

The one-step method consists of simultaneously making and dispersing the particles in the base fluid. In this method, agglomeration of nanoparticles is reduced, and the stability of fluids is increased (Li et al., 2009). One-step physical method cannot synthesize nano-fluids in large scale, and the cost is also high, so the one-step method is in developing. (Zhu et al., 2004).

5.12.2 Two-Step Method

To prepare nano-fluid two-step method is the most widely used method for preparing nano-fluids. In this method, first nanoparticles are synthesised by chemical or physical methods. Then, the nano-sized powder will be dispersed into a base fluid in the second processing step with the help of intensive magnetic force agitation, ultrasonic agitation, high-shear mixing, homogenizing, and ball milling. In this case ultrasonic cleaner is used to disperse nanoparticles into base fluid. Two-step method is the most economic method to prepare nano-fluids in large scale, because nano powder synthesis techniques have already been scaled up to industrial production levels. In this study the two-step method is used for prepare nano-fluid. fig 3.9 shows the two-step method to prepare nano-fluids.

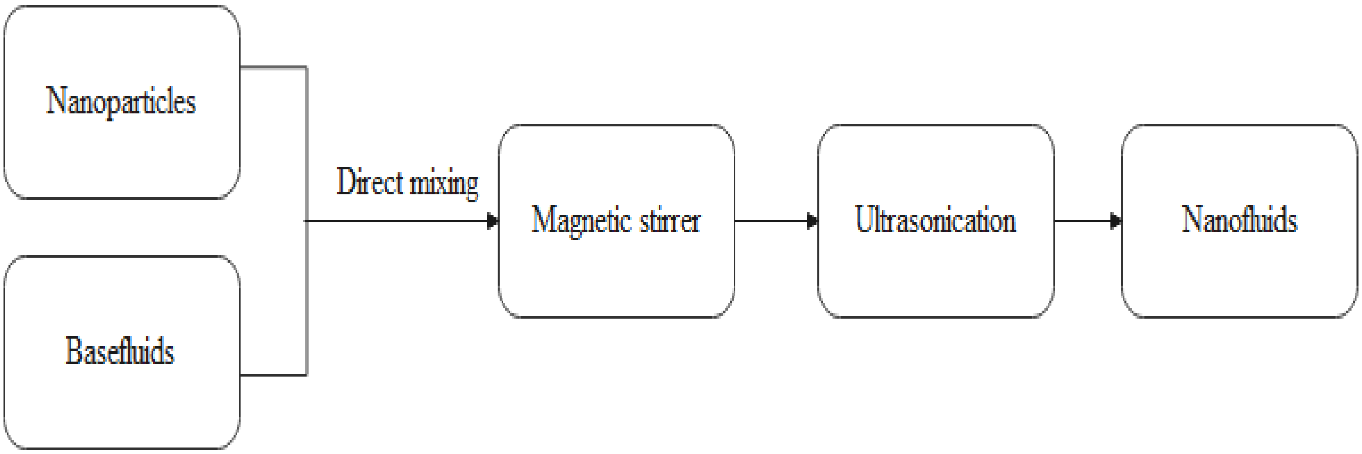

Figure 5.6 Two -step preparation of nanofluids

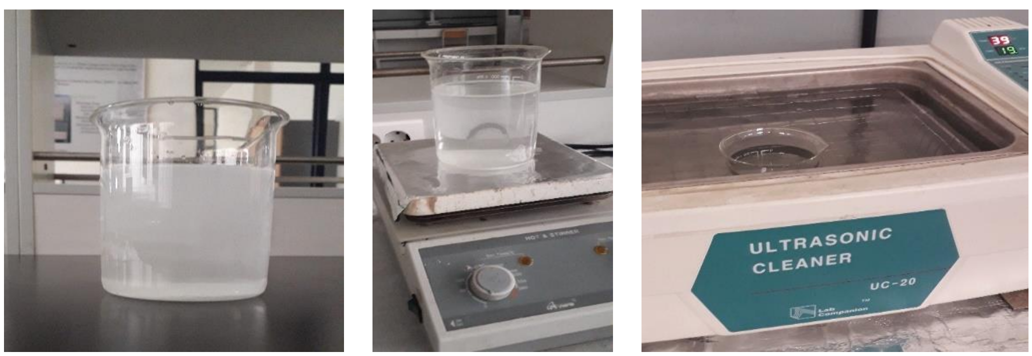

a) b) c)

Figure 5.7 Preparation of nanofluids a) Add nanoparticles in base fluid b) string by magnetic stirrer of 10min c) Sonication the fluid in ultrasonic cleaner.

In preparation of nanofluid sonication time has great roll in the stability of nanofluid. In this work different sonication duration. The nanofluid were sonicate for 30,60.90.120,150 and 180 min using ultrasonic machine. from the sonication result nanofluid after 180 min well disperse and stay for long time without sedimentation.

5.13 Selection of Phase Change Material (PCM)

To select an appropriate PCM for a specific solar application, the first criterion to be considered is the operational temperature range required by the cooking system and then its availability and cost. The operating temperature must match the transition temperature of the storage material. The PCM to be used in the design of thermal storage systems should achieve the following required thermophysical properties (Medved *et al*., 2010).

i. Melting temperature in the desired operating temperature range.

ii. High latent heat of fusion per unit volume so that the required volume of the container to store a given amount of energy is lesser.

iii. High specific heat to deliver for additional significant sensible heat storage.

iv. High thermal conductivity of both solid and liquid phases to support the charging and discharging of energy of the storage systems.

v. Small volume changes on phase transformation and small vapor pressure at operating temperatures to decrease the containment problem.

vi. Congruent melting of the PCM for a constant storage capacity of the material with each freezing/melting cycle

PCM selection for the present case is highly depend on availability in local market, melting point temperature range and cost. Among the available PCM, Magnesium chloride ($MgCl_2 6H_2O$) with melting point (Tm =118℃), latent heat of fusion 167 kJ/kg is selected to be used as the PCM in the indoor cooking unit of the present indirect solar cooking system. Magnesium chloride is available in Ethiopian local market and was purchased from Atomic Chemical Trading found in Cherkos, Addis Ababa (Ethiopia). Table 5.3 shows the physical property of magnesium chloride.

Table 5.3 Physical property of phase change material.

No.	Property	Value (Xie et al., 2017)
1	Melting temperature	391 K
2	Density	Solid (1570 $^{kg}/_{m^3}$), Liquid1450 ($^{kg}/_{m^3}$)
3	Specific heat capacity	Solid (1.201 kJ/kg K), Liquid (3.521kJ/kg K)
4	Latent heat fusion	167 kJ/kg

5.13.1 Sizing of Latent Heat Storage Unit

The size of latent heat storage unit was determined based on the amount of PCM in kilogram required to heat for late hour operation of the solar cooker with a load on it. The average daily useful energy requirement for cooking reportedly varies in the range of 1.7 –2.7 MJ/person/day (Sunil and Tera, 2018). Assuming 2.2MJ/day is required for an average person who needs a meal 3 times a day, 0.73 MJ/person/meal is required. The present solar cooker is intended to prepare about 80% of daily meal (i.e. other meals are considered as frying based meals out of most Ethiopian foods) for 5 persons. Thus 2.92MJ heat capacity is considered to determine the mass and storage volume of LHS unit. The storage volume of LHS unit can be determined from the mass of PCM by the expression (Joseph, 2012).

$$V_{PCM} = 1.5\left(\frac{\pi D^2}{4}\right)L \tag{5.40}$$

Where: V_{PCM} is the volume of PCM, D is diameter of PCM storage cylinder, L is length of PCM storage cylinder and Allowance factor 1.5 is induced accounting the thermal expansion of the PCM whenever phase change occurs.

$$Q_{pcm} = m_{pcm}[Cp_{pcm}(T_m - T_{in}) + L_{F\ pcm} \tag{5.41}$$

Then from equation (5.41) the required amount of PCM ($m_{PCM)}$) for cooking is 10 kg of $Mgcl_2$. $6H_2O$.

The volume of s PCM is calculated using equation (5.42)

$$V_{pcm} = \frac{m_{PCM}}{\rho_{PCM}} \tag{5.42}$$

5.14 Thermal Analysis of Thermal Energy Storage System

In the analysis of thermal energy storage system, it is well-meaning to mention some of the following the critical terms.

i. Charging and charging time

Charging is the process of storing heat energy in the latent heat storage material while it changes it phase from solid state to liquid state. Charging time indicates the total time it takes for the LHS material or PCM to completely melt in to liquid state. The LHS is said to be fully charged when the entire PCM is completely melted, i.e. when the melt fraction reaches a value of one.

ii. Discharging and discharging time

Discharging is the process of releasing heat energy in the latent heat storage material while it changes it phase from liquid state to solid state. Discharging time for LHS is defined with respect to the temperature decrease of the PCM. The LHS is said to be fully discharged when the entire PCM is solidified, i.e., the melt fraction becomes zero.

iii. Melt Fraction

Melt fraction (θ_f) is generally referred as the liquid fraction of the PCM when it exists in a 2-phase form. The highest temperature below which the material is completely in the solid state is called solidus temperature (T_S) and the lowest temperature above which the material is in the liquid state is called liquidus temperature (T_L). Melt fraction (θ_f) of the PCM was obtained from the relationship (Dawit, 2018).

$$\theta_f = \frac{T-T_S}{T_L-T_S} = \frac{T-T_m+\Delta T_m}{2\Delta T_m} = \begin{cases} 0 & for\, T < T_S \\ 0-1 & for\, T_S \leq T \leq T_L \\ 1 & for\, T > T_S \end{cases} \quad (5.43)$$

Where: T_m is the melting point of PCM

5.14.1 Energy Analysis of Latent Heat Storage System

Energy analysis of latent heat storage system applies the first law of thermodynamics for both charging and discharging modes of the PCM.

i. Energy Stored

The total heat stored in the LHS system ($ET.C$) consists of the sensible heat ($ES.C$) and the latent heat ($EL.C$). These can be obtained from the relationship (Niyas et al., 2017).

$$\mathrm{E_{S,C} = mC_p(T - T_{int})} \quad (5.44)$$

$$\mathrm{E_{L.C} = mL_F\theta} \quad (5.45)$$

$$\mathrm{E_{T,C} = m\left[C_p(T - T_{int})\right] + L_F\theta} \quad (5.46)$$

ii. Energy recovered

The total heat discharged from the LHS system ($ET.D$) consists of the sensible heat ($ES.D$) and the latent heat ($EL.D$). These are expressed as (Niyas *et al.*, 2017).

$$E_{S,D} = mC_p(T_{int} - T) \tag{5.47}$$

$$E_{L,D} = mL_F(1 - \theta) \tag{5.48}$$

$$E_{T.D} = m[C_p(T_{int} - T) + L_F(1 - \theta)] \tag{5.49}$$

5.14.2 Energy Efficiency of Latent Heat Storage System

The overall efficiency of the LHS also called the percentage of the energy recovered, is defined as the ratio of the net heat recovered during the discharging period to the net heat input during the charging period.

$$\eta_{LHS} = \frac{Q_{dis}}{Q_{ch}} \tag{5.50}$$

5.15 Design of Cooking Unit

The cooking chamber consists of PCM storage, HTF storage vessel and cooking pot were designed based on the amount PCM required, the amount of HTF required to be stored in the vessel and water utilized for cooking in the cooking pot. Amount of water were determined by considering the capacity of pot to perform an experimental test using the given standard and to prepare a meal for the required number of people. The amount of water required to prepare a meal for persons is estimated to be 2.5 l. Thus, volume of pot (V_{pot}) is found to be 0.005 m^3 whereas the volume of storage vessel (V_{vessel}) is 0.008 m^3.

5.16 Performance Parameters of the Cooker

The performance of solar cookers has generally been rated previously by test procedures that are dependent not on unique solar cooker properties but on climatic parameters, namely solar insolation, ambient temperature and local wind speeds and thus it is difficult to follow a unique standard for testing their performance (Ekechukwu and Ugwuoke, 2013). Different test standards have been proposed for evaluating the performance of solar cookers. Those are the American Society of Agricultural Engineers Standard ASAE S580, the European Committee on Solar Cooking Research (ECSCR) and the Bureau of Indian Standard for Testing (BIST). ASAE S580 uses single figure of merit which is the cooking Power(P) to measure the performance of the solar cooker. Although ASAE S580 provides a simple, yet meaningful and objective measure of cooker performance, it does not address issues other than strictly thermal performance of the cooker and it leaves out any direct measurement of heat losses (Shaw, 2002). The ECSCR provides a more subjective measure of cooker performance as it deals with observation of safety factors, ease of cooking pot access and estimated durability but it includes no means of normalization and is faced to errors and inaccuracies as it depends on measurement of some condition which depend on time (Shaw, 2002). BIST is mostly used test method which is first proposed by (Mullick et al., 1987) to evaluate the performance of solar cookers and provides a more technical framework using two figures of merit, calculated so as to be as independent of environmental conditions as possible. Thus, the present study uses both the ASAE S580 test standard and the two figures of merits of BIST as performance parameter.

5.16.1 Cooking Power

The cooking power(P) in watt of a solar cooker is found by using ASAE S580 test standard as follows;

$$P = m_w C_{p,water} \frac{T_t - T_{initial}}{\Delta t} \quad (5.51)$$

Where: $m_w is\ the\ mass\ of\ water\ in\ kg$,C_p= specific heat of water = 4.187$kJ/kg\ K$, $T_{initial}$ is the average initial temperature of tap water in Adama city , $T_t$is the water temperature after time t,Δt is the time it takes for $T_{initial}$ to reach T_t. From equation (5.51) energy required for cooking is 424 W.

The standardized form of cooking power (Ps) is also given by (Shaw, 2002).

$$P_s = P\left(\frac{700}{I_{tot,col}}\right) \quad (5.52)$$

Where: $I_{tot,col}$ = average of total insolation on the collector with in the test interval (W/m^2)

5.16.2 Thermal Figures of Merits

The two figures of merits based on BIST can serve as a performance criterion for a solar cooker.

i. **The first figure of merits (F1)** is estimate using equation (5.53).

$$F_1 = \frac{T_{max} - T_a}{H_s} \quad (5.53)$$

Where Hs is solar insolation on horizontal surface taken at stagnation time

ii. **The second figure of merits;** derived from the sensible heating of water is a measure of time required to raise the temperature of a known mass of water to its boiling temperature and is given as (Mullick et al., 1987).

$$F_2 = \frac{F_1(m_w C_{pw}}{A_{ap}.t} ln \left[\frac{1-\frac{1(T_{initial}-T_a}{F_1 \quad I_b}}{1-\frac{1(T_{final}-T_{amb})}{F_1 \quad I_b}} \right] \tag{5.54}$$

Where: T initial- initial tap water temperature, $Tfinal$-final water temperature (100°C) after time (t), A_{ap}- aperture area the collector, I_b= average horizontal insolation

5.17 Selection of Heat Transfer Fluid

Heat transfer fluid (HTF) plays great role in indirect solar collector heating system. HTF acts as a medium for transporting heat that is collected by the solar collectors to the actual water that is required to be heated up with the help of an HX. Selection criteria of HTF in view point of thermodynamic and heat transfer, such Coefficient of expansion, thermal conductivity, viscosity, specific heat, freezing point, boiling point. In thesis water and nanofluids is used as HTF to generate steam for indirect cooking. Table 5.4 shows a Physical property of nanofluids

Table 5.4 Physical property of aluminum oxide and zinc oxide nanofluids.

No.	Property	Al_2O_3 Nanofluid	ZnO Nanofluid
		Value	Value
1	Density (kg/m^3)	1057.6	1092
2	Thermal Conductivity (W/m K)	0.65	0.64
3	Specific heat capacity (kJ/kg K)	4.035	3.99

Physical property of water at STP.

Table 5.5 Physical property of water at STP.

No.	Property	Value
1.	Density	1000 kg/m^3
2.	Thermal conductivity	0.59 W/m K
3.	Specific heat capacity	4.187 kJ/kg K
4.	Boiling point	100°C
5.	Dynamic viscosity	0.000798 kg/m s

CHAPTER SIX

EXPERIMENTAL SETUP AND PROCEDURE

6.1 Introduction

This section presents the conceptual model, working principle, manufacturing process and the whole experimental setup and procedure followed while testing the prototype of indirect solar cooking system. The conceptual model of the system was developed using CATIA V5. The working principle of the system is elaborated in detail. The manufacturing process used for preparing the prototype is presented with descriptive photos of the whole process. The experimental setup and the measuring and testing devices used are also presented. Finally, procedures followed while measuring, testing and investigating of the various useful parameters of the system are discussed.

6.2 Conceptual Model of Indirect Solar Cooking System

Fig.6.1 shows the schematic diagram of indirect type solar cooker drawn using CATIA V5. The system consists of a Parabolic dish solar collector, Conical coil tube receiver LHS unit, cooking chamber, frame and support and closed loop piping network as connection for the whole system.

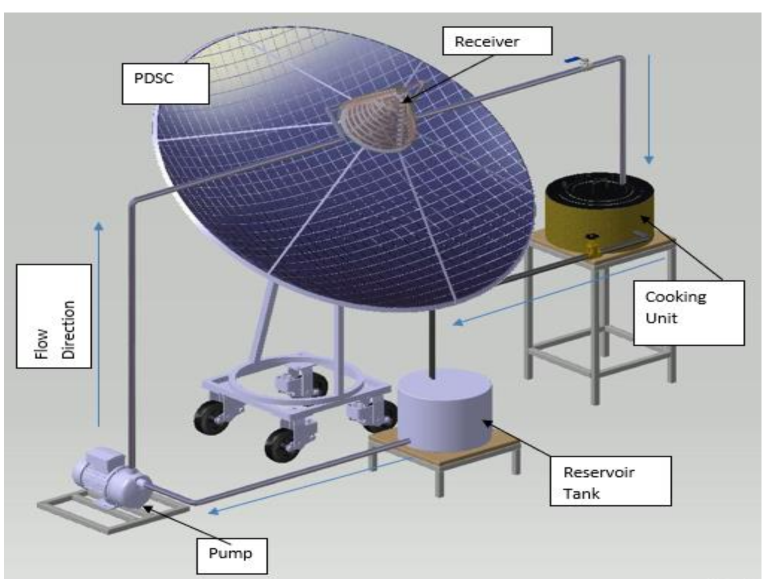

Figure 6.1 Conceptual schematic of a parabolic dish solar cooker.

Terminology

Pump – is a device that moves fluids by mechanical action, typically converted from electrical energy into hydraulic energy.

Reservoir tank – is defined as the space storage of fluids.

Parabolic dish solar collector – is a device collects solar radiation and converts into thermal energy.

Receiver – is a device absorbs the heat reflected from the collector and heats the fluids in the absorber.

6.3 Manufacturing of Parabolic Dish Solar Collector

For this work first, an unused parabolic dish metal plate was bought from the market and after that, the surface of the plate was cleaned. The dish contains 6 steel plates and it is assembled as shown in Figure 6.2. The aperture diameter of the dish is 1.8 m and the area is $2.54\,m^2$ The mirror is used because they have high reflectivity of about 95%. Then the mirror is cut into a small piece (3 mm×3 mm) to cover the surface of the dish. Totally 2822 pieces of mirror used to cover the surface of a dish. Then the piece of mirrors attached with CARMYFIX CM-43.

a

b

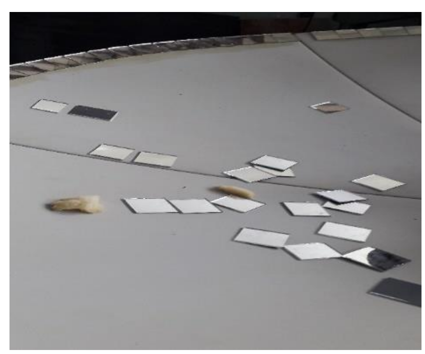

c

d e f

Figure 6.2 Manufacturing process of parabolic dish solar collector, a) Single plate of a dish b) Assembling the plate together c) Attaching the mirror on a dish d) After complete attaching a mirror e) Assemble a receiver on a dish f) Insulation the receiver with fiberglass.

6.4 Manufacturing of Receiver of collector

In this thesis, a cavity receiver is used due to its efficiency compared to other types of receivers. A conical cavity receiver is used in this work. To manufacture the receiver the material used were copper coil tube, Nipples, and metal plates. First, the geometry of the conical structure is manufactured with a 3 mm plate then a copper tube is rolled on the conical geometry as shown in figure 6.3 shows that the detailed manufacturing process of the receiver. Finally, the receiver was coved with fiberglass insulation material with a thickness of 50 mm.

Figure 6.3 Manufacturing process of conical cavity receiver, a) Structure of cone b) Rolling copper tube on structure c) Gas welding conical structure with copper tube d) Conical tube receiver.

6.5 Latent Heat Storage and Cooking Pot

The cooking chamber consists of PCM storage, HTF storage vessel and cooking pot were designed based on the amount PCM required, the amount of HTF required to be stored in the vessel and water utilized for cooking in the cooking pot. Three concentric cylindrical vessels with 380, 280 and 240 mm diameter and with a height of 155,130 and 110 mm were used for cooker respectively. The inner vessel is used as a cooking pot whereas the second vessel is used as a storage for storing HTF and the third cylinder was used to store the PCM. The second cylinder used as HTF storing and heat transfer passage to the cooking pot and PCM. The cooking pot was equipped with a cleaning pipe and cleaning valve. To reduce heat loss from the outer surface of storage it was insulated with insulation material. Three concentric cylindrical vessels are rived together and to facilitate the flow of HTF four holes were drilled two on the side and two on the top. The side holes are used to connect the vessel with the storage tank and one of the top hole was used to connect HTF storage with the tube from the receiver that circulates the fluid and the other on a top hole was to fill PCM.

Figure 6.4 Cooking pot and storage preparation for experimental test.

6.6 Overall System of Fabricated Parabolic Dish Solar Cooker Integrated with Phase Change Material

The overall systems include parabolic dish solar collector, thermal storage and cooking pot, Pump, HTF tank, and Connecting tube. The tubes are selected as they are easy to connect, available, corrosion-resistant, and resist high pressure and temperature. The cooking pot, receiver, and tubes are insulated with fiberglass to minimize heat loss.

Figure 6.5 Overall system of parabolic dish solar cooker.

6.7 Experimental Setup

For experimentally investigating the present indirect solar cooking system, the setup was installed in the test filed of ASTU, mechanical engineering department, Adama Ethiopia. The complete experimental setup of indirect solar cooker consists of parabolic dish solar collector, cooking chamber which consists of the cooking vessel and storage vessel and a closed loop pipe network having HTF (nanofluids and water) used as a connection for the whole system components. Figure 6.6 shows the photograph for the complete setup of indirect solar cooker. In the setup the heat source for the cooker is obtained from the parabolic dish solar collector using nanofluids and water as HTF which is circulated with the help of pump connected between the collector and the storage tank unit. The working fluid is pumped using centrifugal pump in the system then the fluid is heated at the focal point of the collector then heated fluid flow into cooking unit. In cooking unit heat transfer takes place from storage to the cooking pot then fluid return to a tank and the fluid circulate in the system.

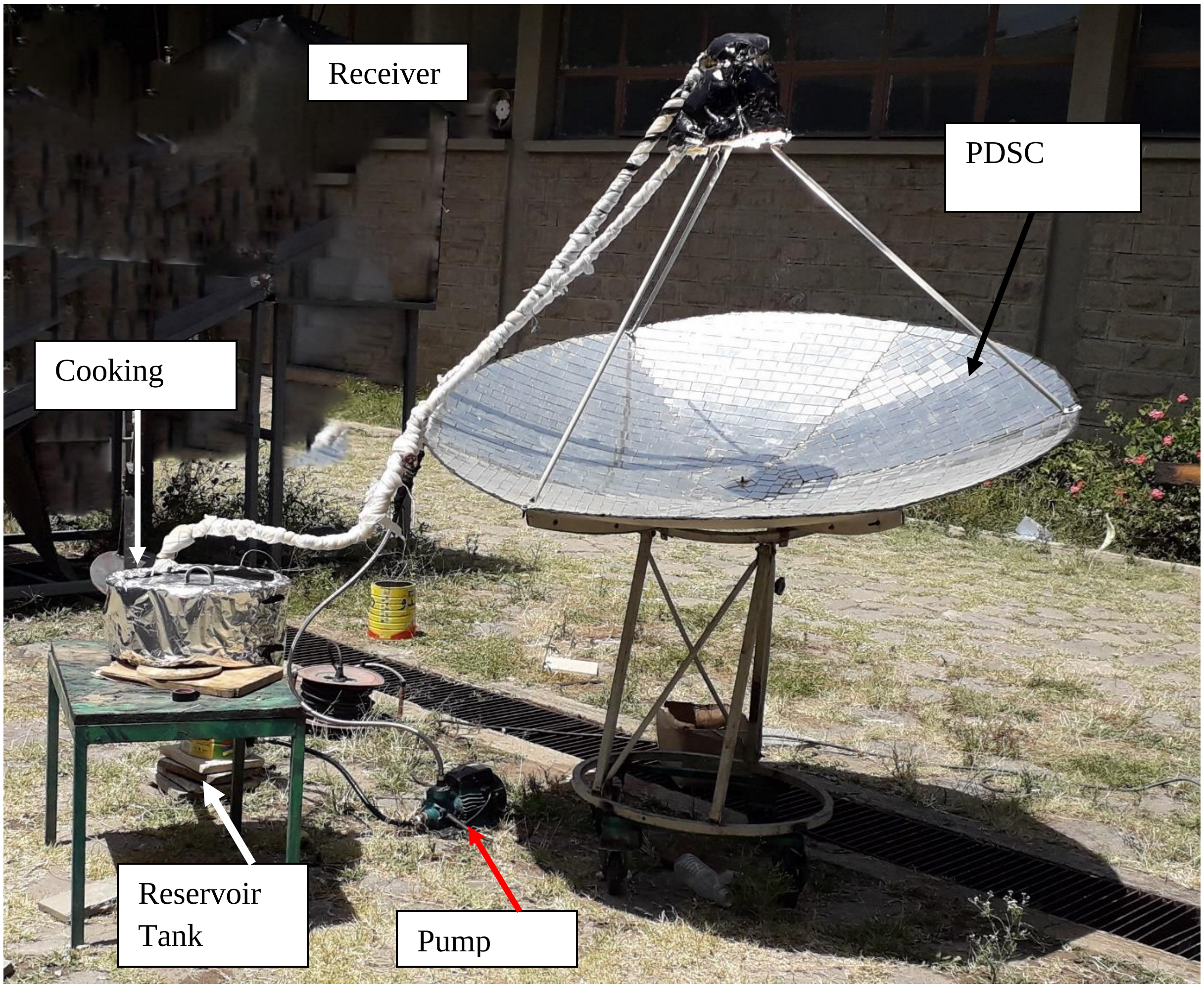

Figure 6.6 Experimental setup of the system.

CHAPTER SEVEN

RESULTS AND DISCUSSIONS

7.1 Introduction

This chapter presents the result obtained from the experimental analysis of the Parabolic Dish Solar Collector, LHS unit and cooking unit under different conditions. This section presents the experimental investigations made on each component of the indirect solar cooker. The results of no-load, boiling, cooking and performance tests performed on the cooking chamber is also presented and discussed.

7.2 Solar Radiation

The amount of solar radiation received affects the performance of the system, since the receiver temperature, HTF fluid temperature, and others are directly related to solar radiation. Thus, as solar radiation increases the temperature also increase proportionally. The solar radiation increases and reach to a maximum value at noontime and starts to decline in the afternoon. From figure 7.1 at 9:00 am, the solar intensity is 557.69 W/m^2, and as time passes, the intensity starts to rise until reaching the peak with a value of 903.2 W/m^2 around 12:00 pm. After that time, the intensity decreases to approximately 351.8 W/m^2 at 16:00 pm.

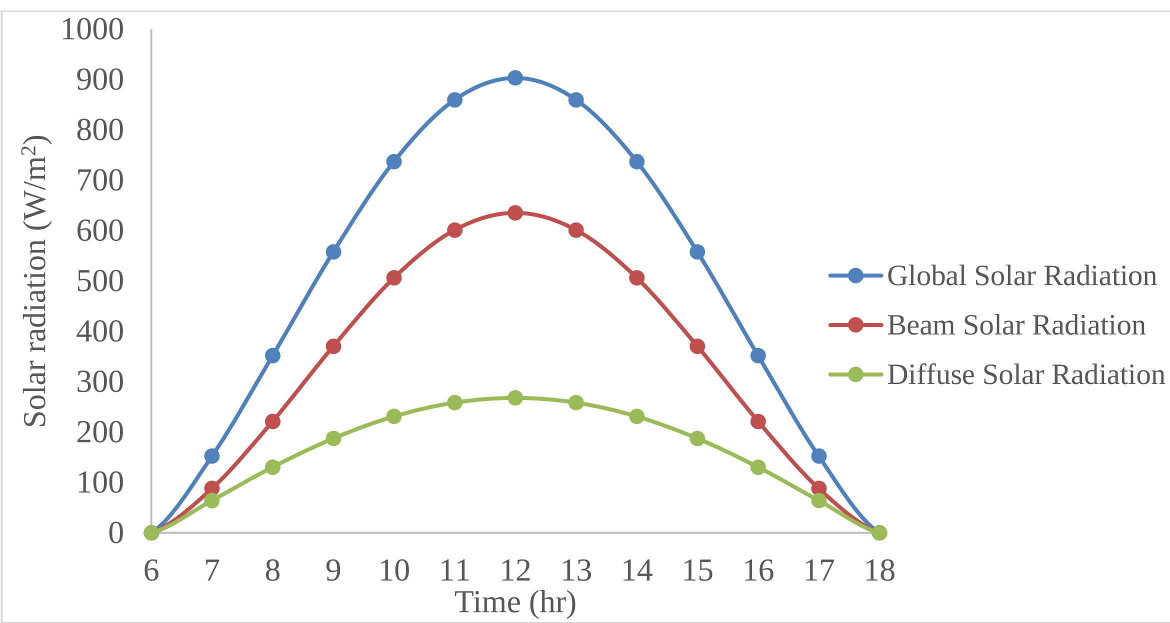

Figure 7.1 Estimation of solar radiation of Adama city.

7.3 Analytical Results of Thermo-Physical Properties

7.3.1 Thermal Conductivity

The thermal conductivity of nanofluids are calculated by using Maxwell Equation (2.1) which can be applied to the homogeneous and low volume fraction liquid-solid suspensions. It was found that by using the theoretical model the thermal conductivity of nanofluids highly increases with rise in volume fraction as shown in Figure 7.2. The result achieved was similar to the experiment result found by (Mariappan, 2012).

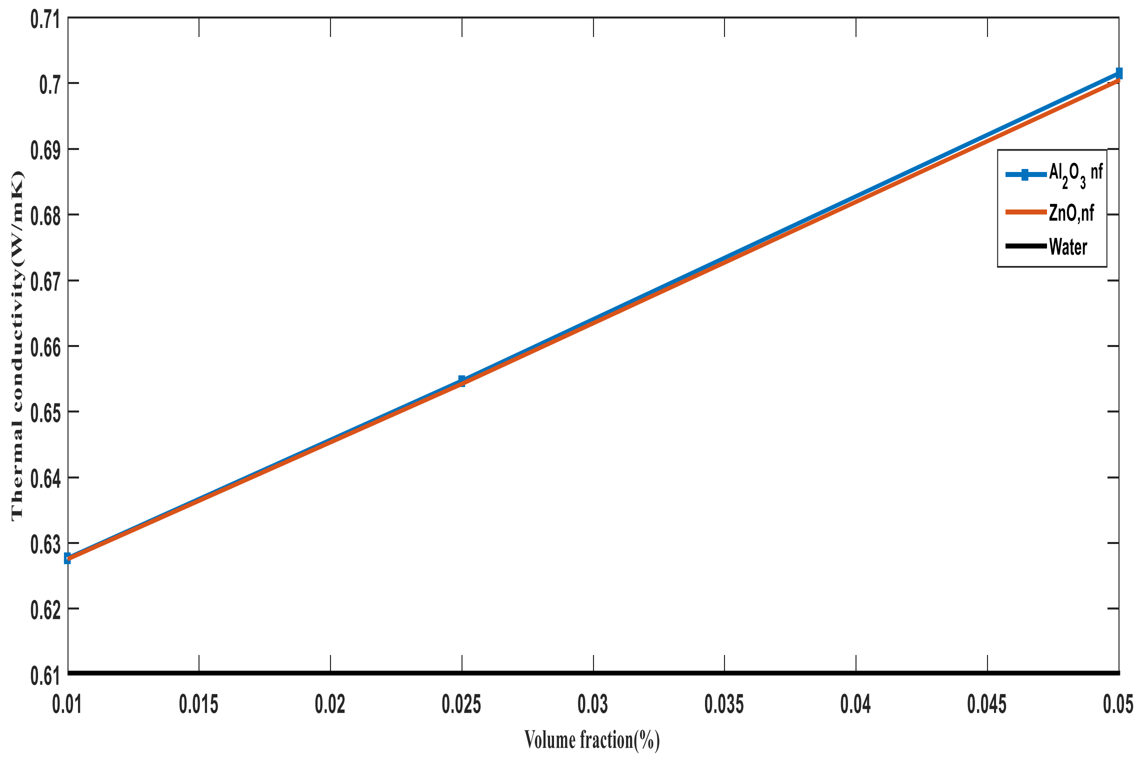

Figure 7.2 Thermal conductivity of nanofluids.

7.3.2 Density of nanofluids

Before the investigation of nanofluids on parabolic dish solar collector performance carried out analytical analyses have been done on two types of metal oxides nanofluids namely: Al_2O_3, and ZnO to made basis in theoretical comparison with the experimental investigation in literature. Density is an important thermo-physical property of working fluid and must be considered. As shown in the Fig.7.3 the theoretical density of nanofluids is calculated from equation (2.5) and greater than that of water in all cases. As shown in the figure density rises linearly as volume concentration increases.

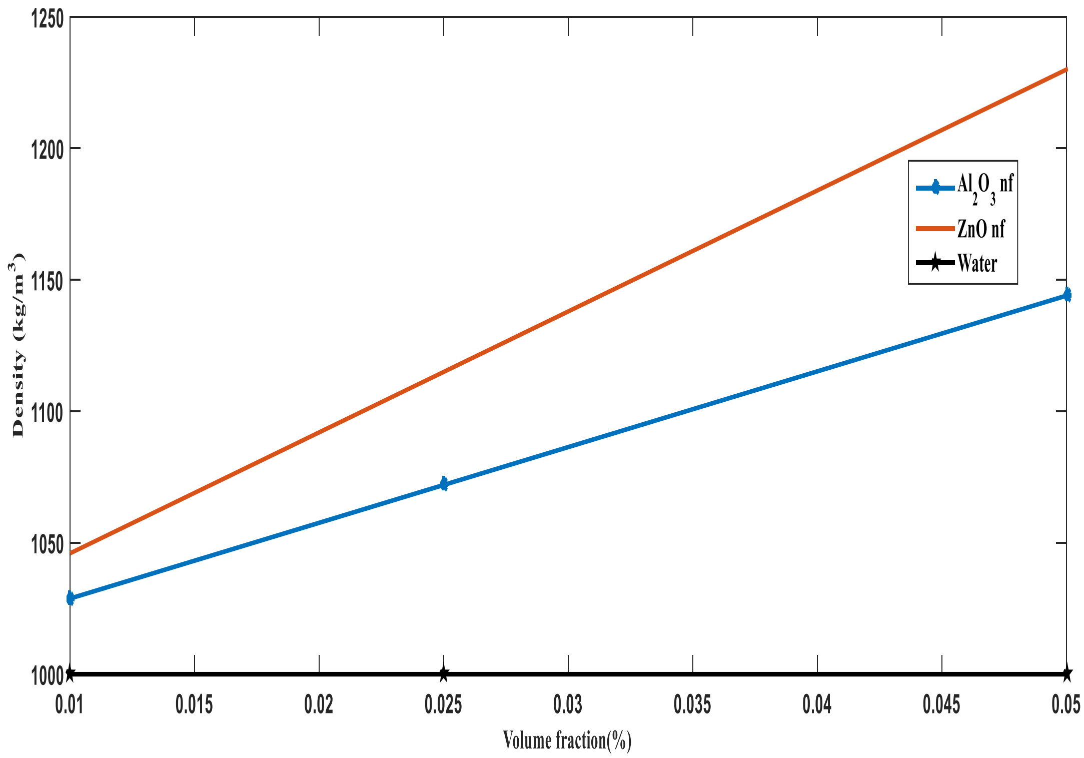

Figure 7.3 Density of nanofluids

7.3.3 Specific Heat

The specific heat of nanofluids is necessary to evaluate the performance of parabolic dish solar collector using nanofluids. It is the amount of energy that must be added, in the form of heat, to one unit of mass of the substance in order to cause an increase of one unit in its temperature. The specific heat of nanofluids are inversely proportional to the volume concentration of nanoparticles as shown in Fig.6.4 and this result is related to that of (Madhu & Rajasekhar, 2017). According to the literature CuO nanofluids has least specific heat and water has highest specific heats. Liquid water has one of the highest specific heats among common substances, about 4187 J/K/kg. The smaller specific heats directing to smaller amount of energy needed to raise temperature of nanofluids.

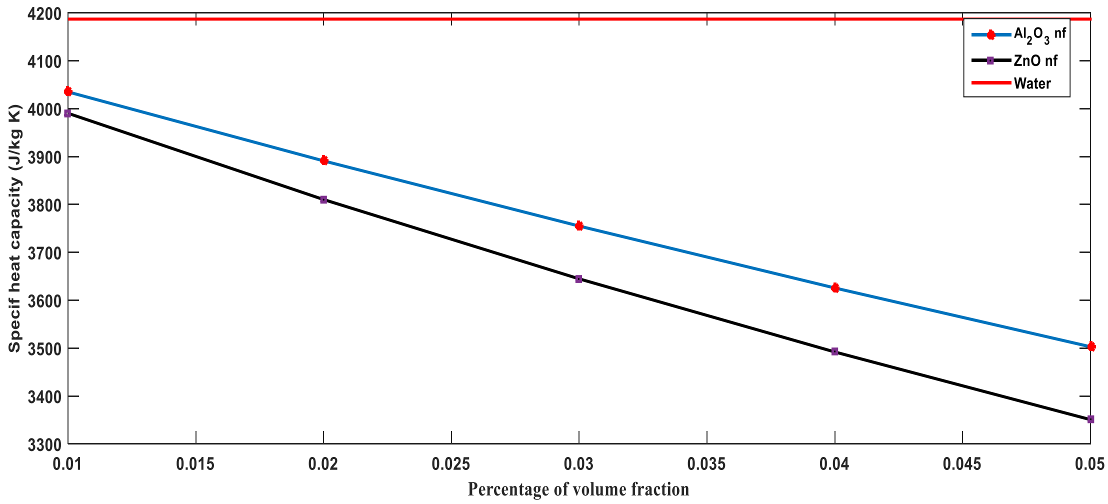

Figure 7.4 The effects of different volume concentration of nanoparticles on specific heats.

7.4 The XRD Results of Nanoparticles

7.4.1 The X-Ray Diffractometer (XRD) result of ZnO Nanoparticles

Shimadzu-700 X-ray diffractor is an instrument used for the characterization of nanoparticles. Figure 7.5 shows the Xray diffraction pattern of ZnO nano powder. The characterization of nanoparticles carried out in materials science and engineering laboratory (ASTU). Definite line broadening of the XRD peaks indicates that the prepared material consists of particles in nanoscale range. The average crystalline size of zinc oxide obtained using Debye-Scherrer formula equation s 21.33 nm. The XRD result obtained is very similar with that of (Talam et al., 2012) in which the nano particles sizes found to be as stated in literature.

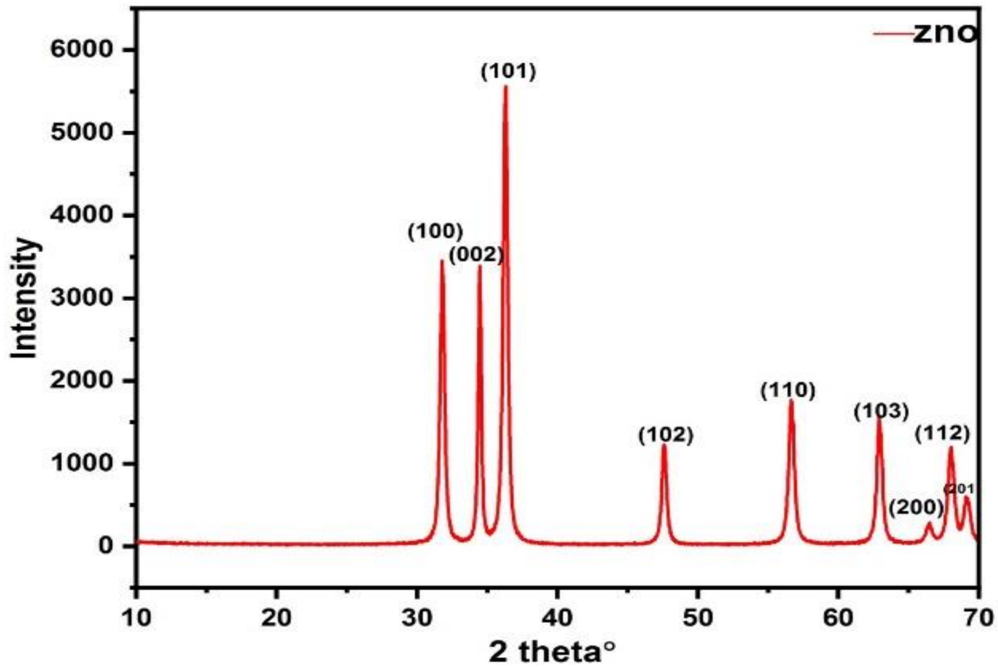

Figure 7.5 XRD result of zinc oxide nanoparticles.

7.4.2 The X-Ray Diffractometer (XRD) Result of Al_2O_3 Nanoparticles

The instrument used is Shimadzu XRD -700 X-ray diffractometer. The XRD results shows that the high and sharp intensity of Al_2O_3 as shown in Figure 7.6. This XRD result of Al_2O_3 is almost similar with that of (Vijaya et al., 2018) in which the particles sizes found to be 25 nm as stated in literature. The XRD result is plotted on Origin software 2 theta vs intensity as shown in figure 7.6.

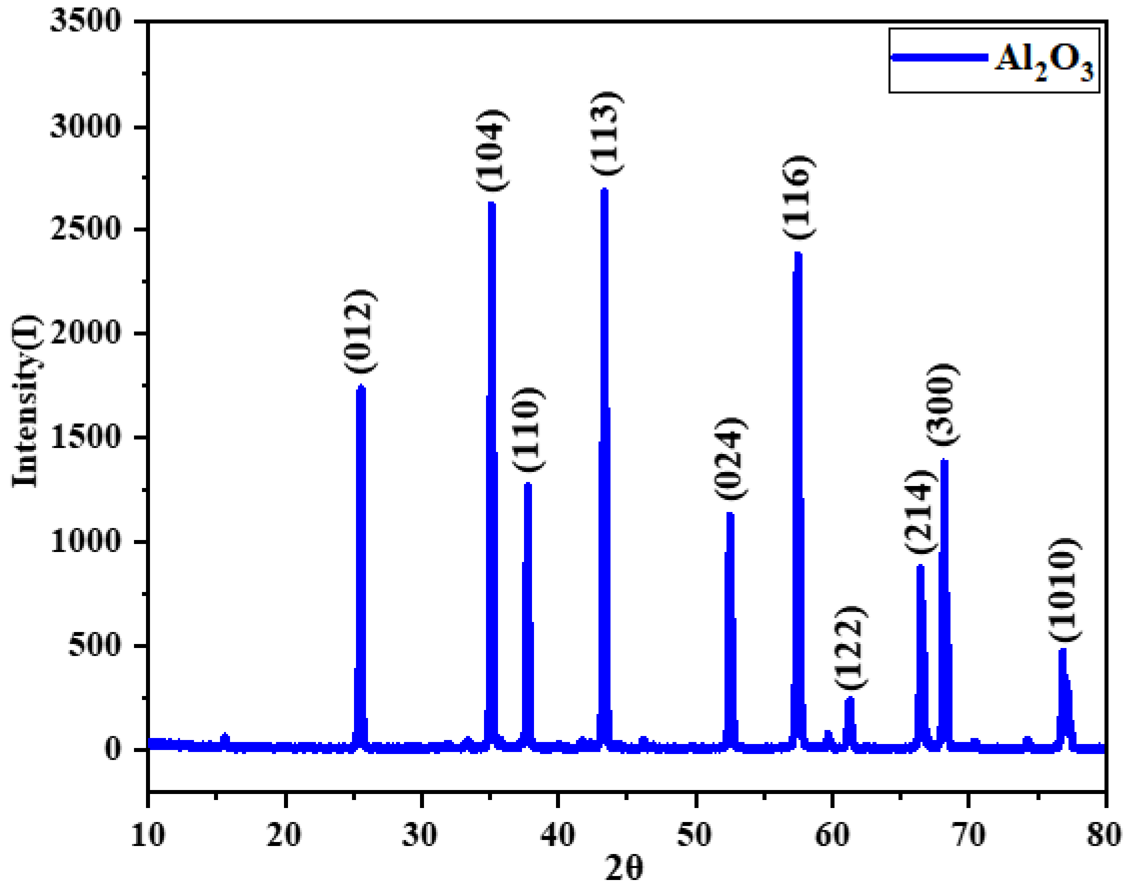

Figure 7.6 XRD result of aluminum oxide nanoparticles.

7.5 Ambient Temperature during Experimental Test

The ambient temperature of Adama city measured during the experimental test period were presented in the figure 7.7. The ambient temperature is reaching the maximum value at noontime and starts to decrease in the afternoon. The variation of ambient temperature with time of the day was given in figure 7.7. The maximum ambient temperature measured between 11:30 am to 13:30 pm was 306 K. The minimum temperature measured on the same day was 298 K, at 9:00.

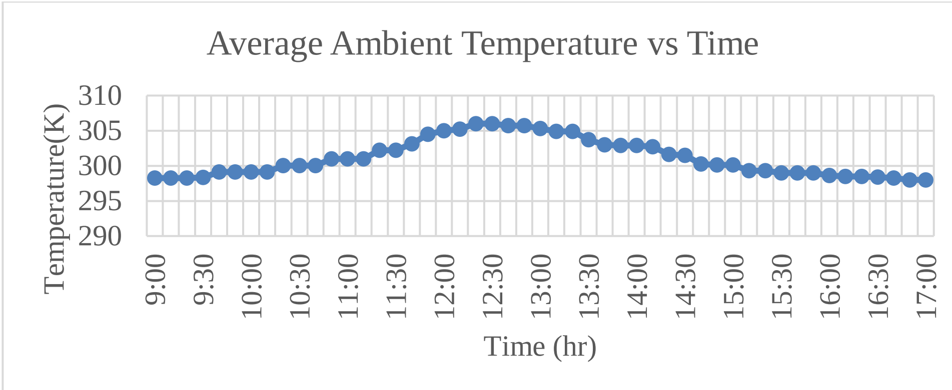

Figure 7.7 Average ambient temperature of Adama city during experimental test.

7.6 Experimental Results of the PDSC

7.6.1 Temperature Distribution of Receiver

Figure 7.8 shows that absorber wall temperature, ambient temperature, beam solar intensity throughout the day for each single hour are calculated by using Microsoft excel software. The solar beam insolation showed a parabolic path with the peak value attaining the mid-day which later decreasing. The temperature distribution over the wall of solar absorber had a fluctuated value due to the weather condition (cloud, wind). The maximum average wall temperature of conical cavity absorber reaches 305 ℃ at the mid-day, 12:30 am. Similar work from the literature review has been validated, the result of the study was the maximum temperature of the absorber was 300.3 ℃ has obtained (Seyoum, 2020).

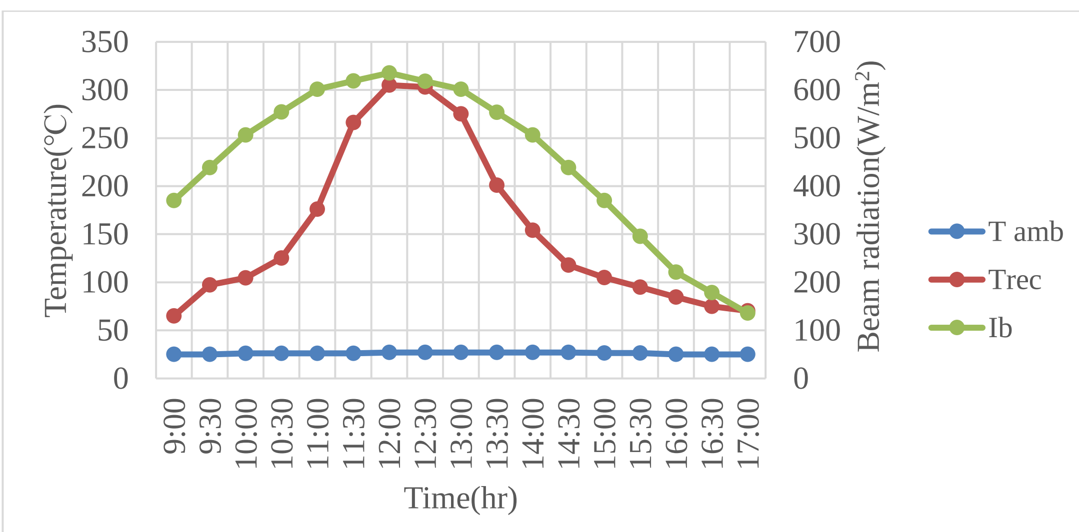

Figure 7.8 Variation of Average surface temperature of receiver and solar beam radiation.

7.6.2 Variation of Temperature of Receiver and outlet fluid temperature

Figure 7.9 shows that temperature varation of receiver temperature,oulet temperature and ambient temperature during experimental test. The temperature the maximum at noon due high solar intensity the decrease when sun radiation is reduced.

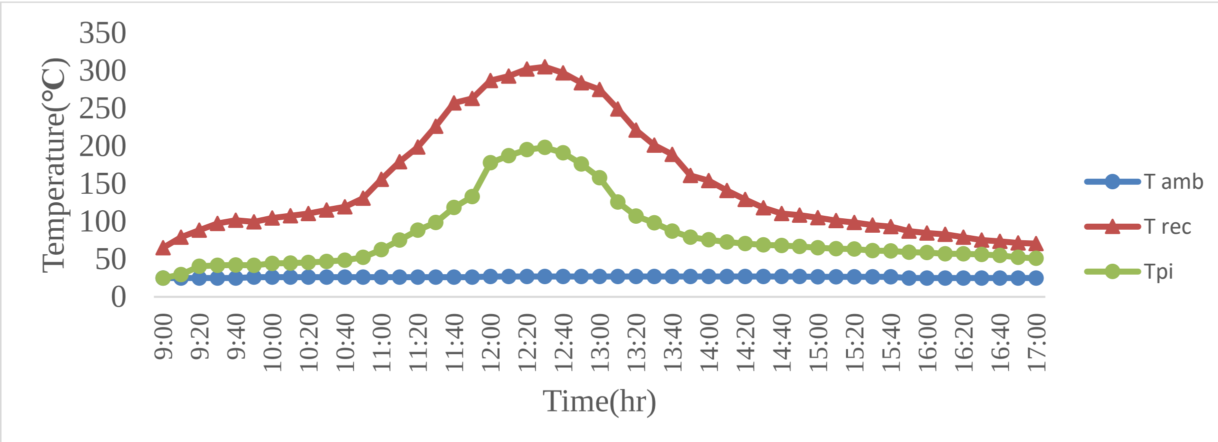

Figure 7.9 Variation of temperature of receiver and outlet of temperature of fluid.

7.6.3 Comparison of outlet temperature of fluid with and without nanofluids

As shown in figure 7.10 The outlet temperature of nanofluids as HTF is higher as compared with water as working fluid. As we can see from figure 6.9 the outlet temperature of aluminum oxide nanofluid higher compared with ZnO nanofluid and water. The temperature fluid reach maximum at noontime. The maximum average outlet temperature recorded with volume fraction of 1% for Aluminum oxide nanofluid and Zinc oxide nanofluid is,456.4, 452K respectively were as for volume fraction of 2 % is 459.6 K and 454.7 K for aluminum oxide and zinc oxide nanofluids respectively. The maximum average temperature recorded water as working fluid is 439.5 K

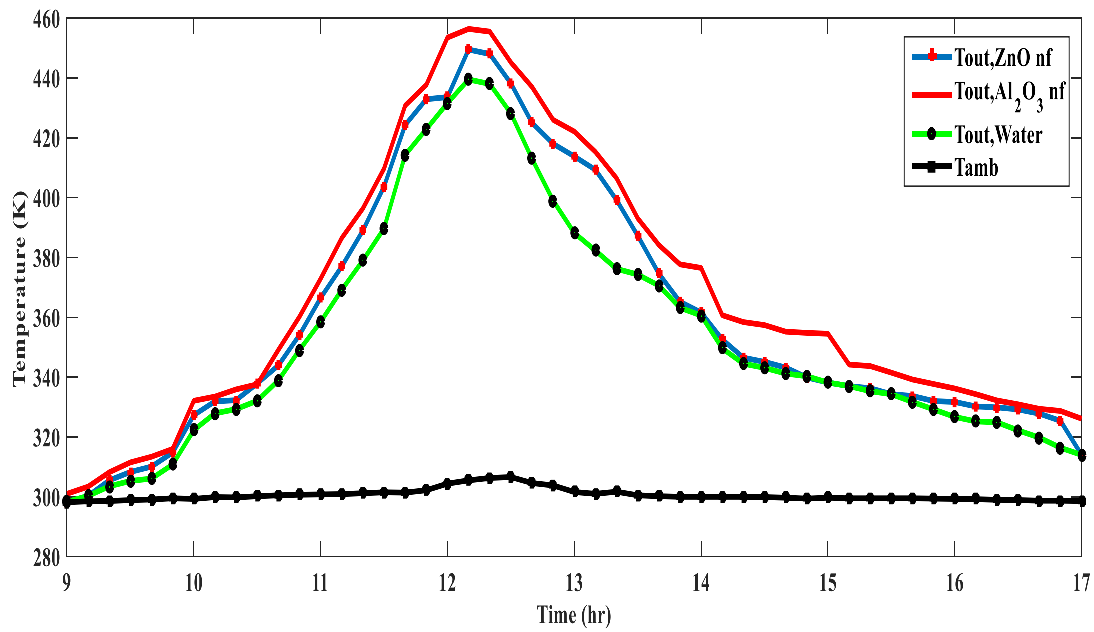

a

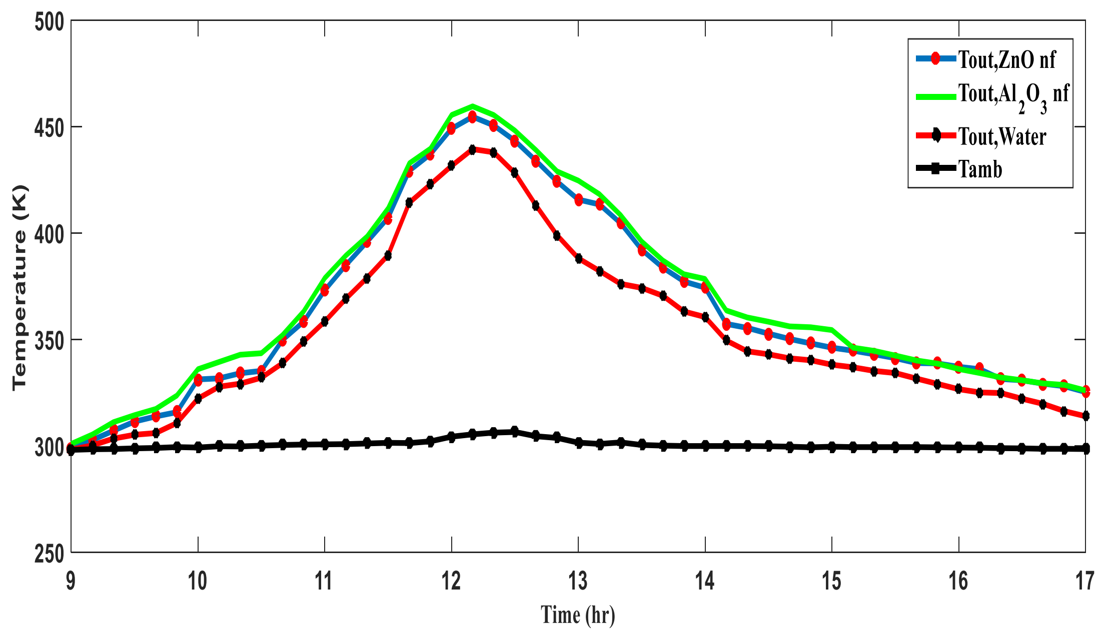

b)

Figure 7.10 Comparison of outlets temperature of water and nanofluids. a) Outlet temperature nanofluids with volume fraction of 1 % and b) Outlet temperature of nanofluids with volume fraction of 2 %.

7.6.4 Comparison of Efficiency of Parabolic Dish Solar Collector with and without Nanofluid as Working Fluid

From the experimental result, the efficiency of the solar collector is calculated using equation 5.32 with water and nanofluid as working fluids. From the experimental result, the maximum efficiency of solar collector obtained with aluminum oxide nanofluid and zinc oxide nanofluid as HTF with volume fraction of nanoparticles 1% was 69.13 and 65.5 % respectively, as shown in figure 7.11(a). For 2 % volume fraction of aluminum oxide and zinc oxide nanofluids the average efficiency of collector was 71.63 and 67.99% respectively. The efficiency of parabolic dish solar collector using water as working fluid was obtained 61.6%. Therefore, from the results use of aluminum oxide nanofluid increment the efficiency of parabolic dish solar collector by 7.53 and 10.03% for volume fraction of 1 and 2% respectively, compared with water and similarly 3.63 and 6.39 % increment for zinc oxide nanofluid with a volume fraction of 1and 2% respectively. This is due to the nanofluids have higher thermal conductivity compared with water.

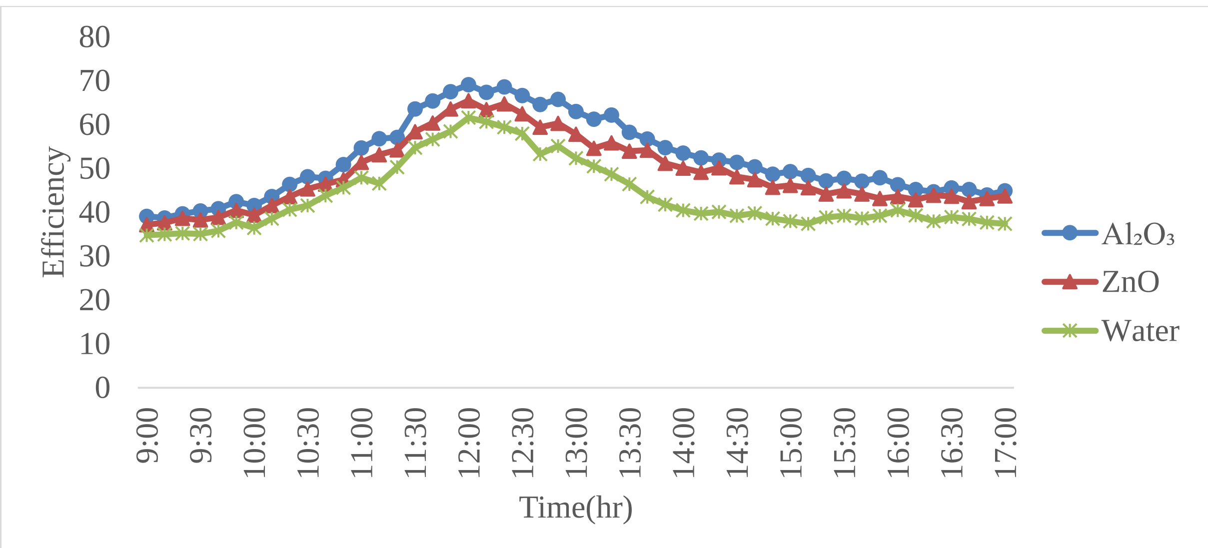

a).

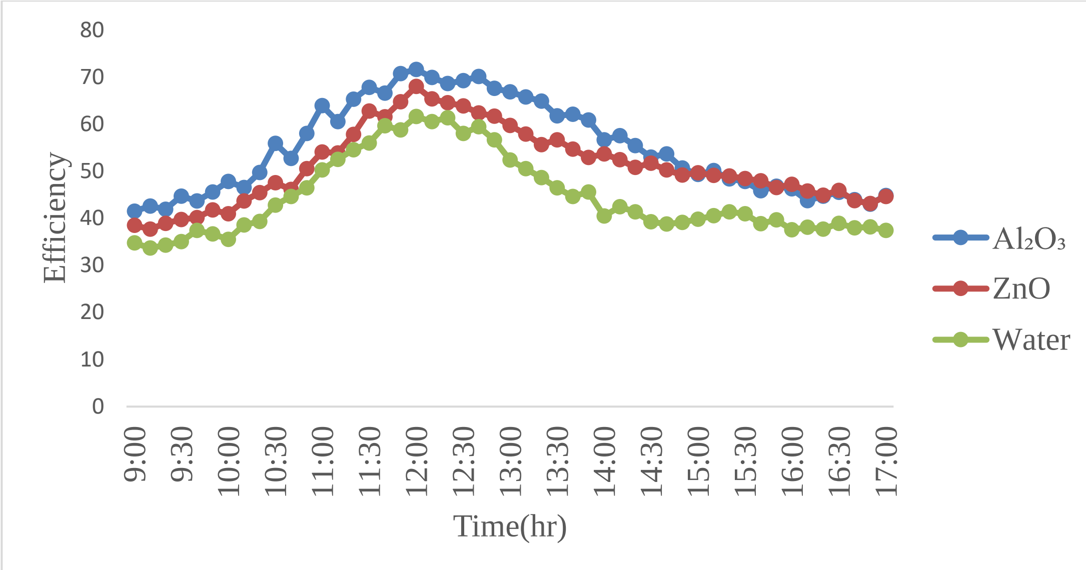

b).

Figure 7.11 Variation efficiency of PDSC with different HTF. a) Efficiency of parabolic dish solar collector with volume fraction nanoparticles 1% b) Efficiency of solar collector with volume fraction of nanoparticles 2%.

7.6.5 Useful Heat Energy of Parabolic Dish Solar Collector

The useful heat gain is calculated from the measurements of the inlet and outlet HTF temperatures and mass flow rate as established in equation (5.30). Figures 7.12 show the useful heat gain of Aluminum oxide, Zinc oxide, and water as HTF. The experiments were carried out from 9:00 am to 17:00 pm for several days. However, the useful heat gains first increase, reach a peak value around noon, and then decrease. This is due to the fact that the useful heat gain is strongly influenced by the incident beam solar radiation and change of temperature.

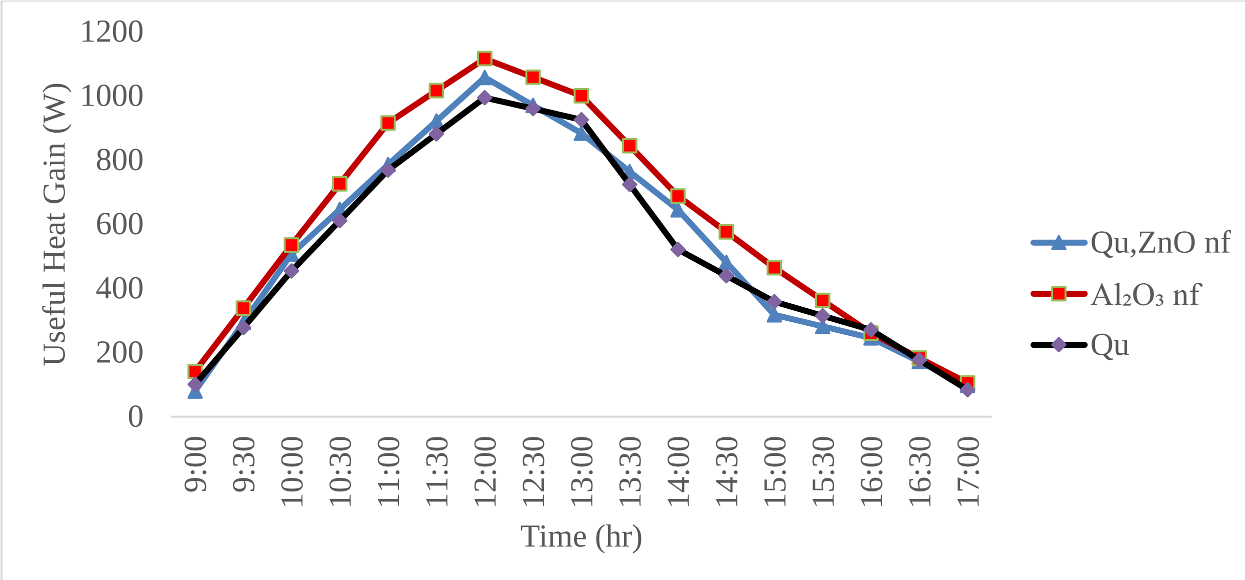

Figure 7.12 Useful heat gain with different HTF as a function of time

7.7 Experimental Result of Latent Heat Storage System

In this section the results and their implication obtained from experimental investigation of LHS unit during charging/discharging processes are discussed.

7.7.1 Stored/Released During Charging/Discharging Processes

Initially, when the PCM is in the solid-state during charging, heat gets stored in the form of sensible heat only. Once the PCM reaches near the phase change temperature (391 K), heat gets stored in the form of latent heat. Similarly, after melting of the PCM, further increment in temperature of PCM results heat to be stored in the form of sensible heat again. When the magnesium chloride reaches to its melting point during charging process the fluid temperature reaches 391 K. the amount of sensible, latent and total energy stored in the PCM were 1.92, 1.436 and 3.35 MJ respectively. During discharging process on the other hand, the PCM is initially in liquid state (398.6 K) then heat gets released inform of sensible heat until it reaches to its melting point 391 K. then the PCM starts to release its latent heat as the phase change occurs. The amount of sensible, latent and total energy released during discharging process was 1.57, 1.35 and 2.92 MJ respectively.

7.7.2 PCM Temperature Variation

Figure 7.13 shows the temperature variation of PCM with time. As shown in figure the PCM temperature reach maximum at noon and then temperature drop as solar radiation also decreased.

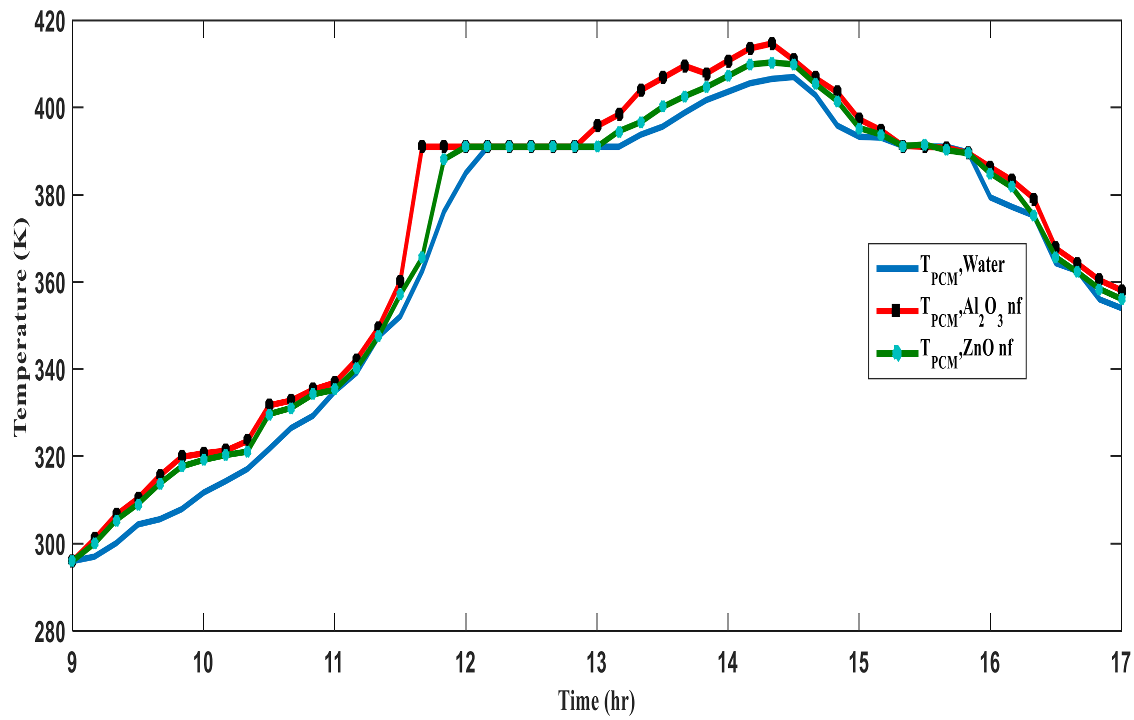

Figure 7.13 Variation of temperature of PCM with different working fluid

7.7.3 Charging and Discharging Time of PCM

Melt fraction is the most important factor that influences the performance of any latent heat storage system during the melting/solidification process. The average melt percentage of the PCM various between 0 and 1. Figure 7.14 indicates the changes in average melt fraction during the charging/discharging process with time. The graph was plot using equation (5.43) from experimental result record during test. The rise/fall of the average melt fraction of LHS during charging/discharging is faster at the beginning due to the presence of a higher heat transfer rate between the HTF and PCM, as shown in figure 7.14 (a) and (b). Due to the low heat transfer rate between the HTF and the PCM, this becomes slower over a specific amount of time. The charging/discharging period for the magnesium chloride -filled LHS system was 125 and 161 min, respectively.

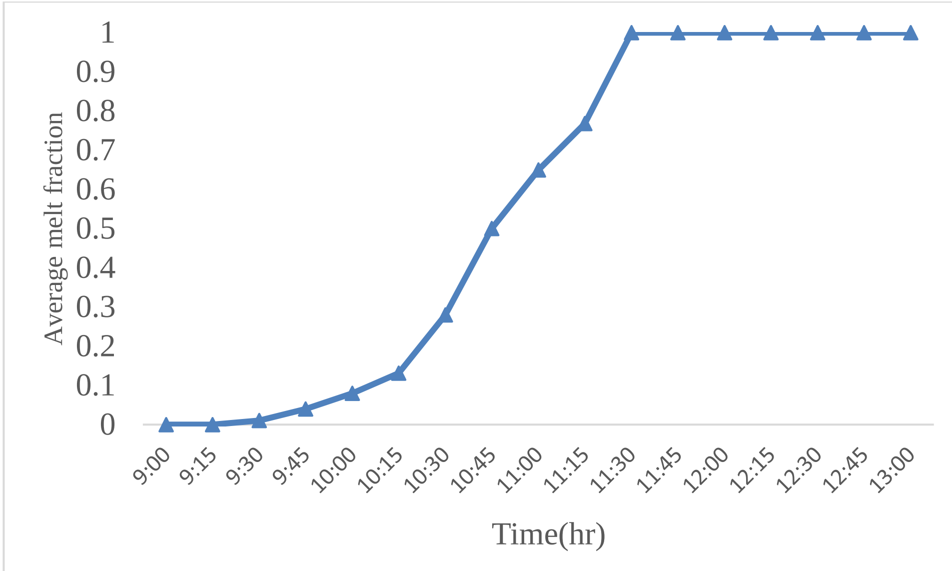

a) Charging

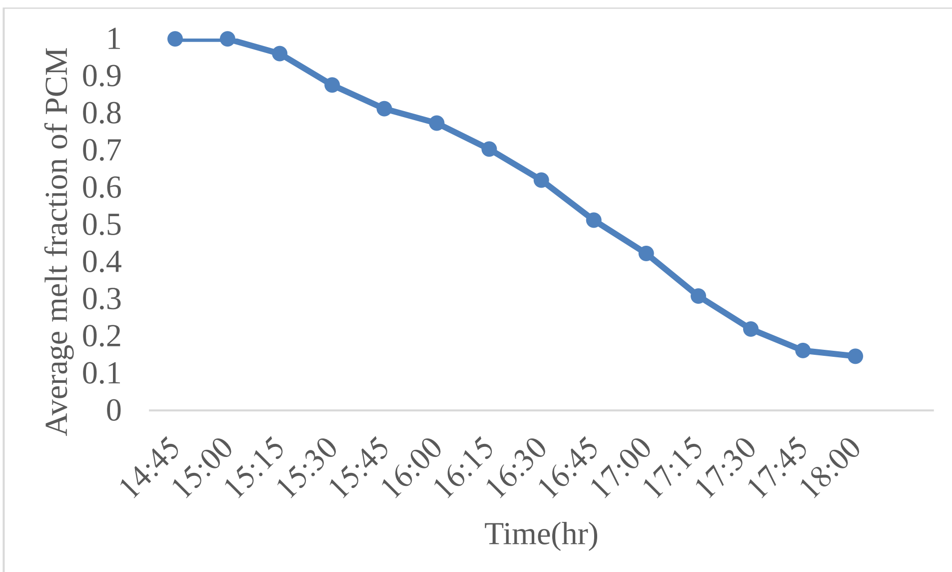

b) Discharging

Figure 7.14 Charging and discharging time of PCM. a). Charging time b). Discharging time

7.8.4 Average Temperature Distribution of PCM During Charging and Discharging

Figure 7.15 a and b shows the temperature profile during charging and discharging the PCM.

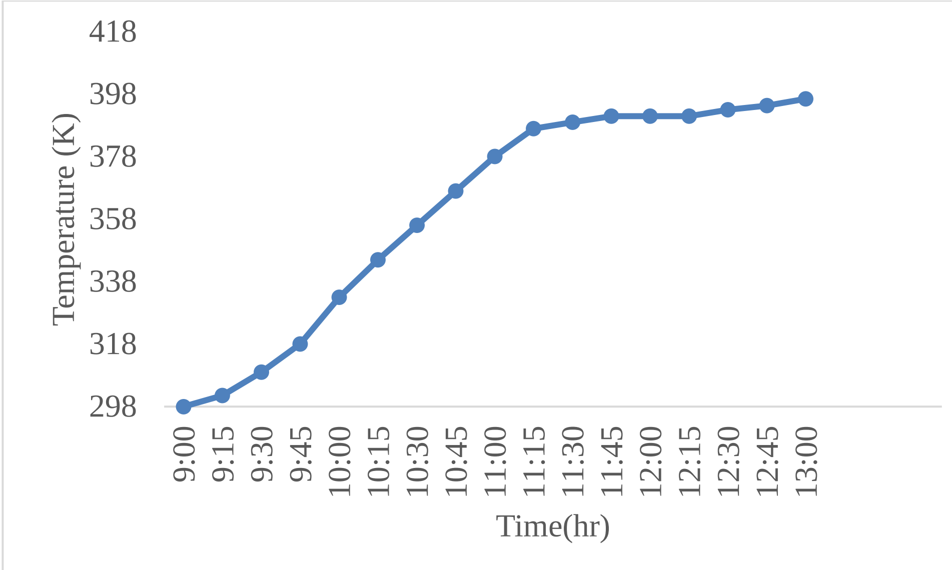

a) Charging

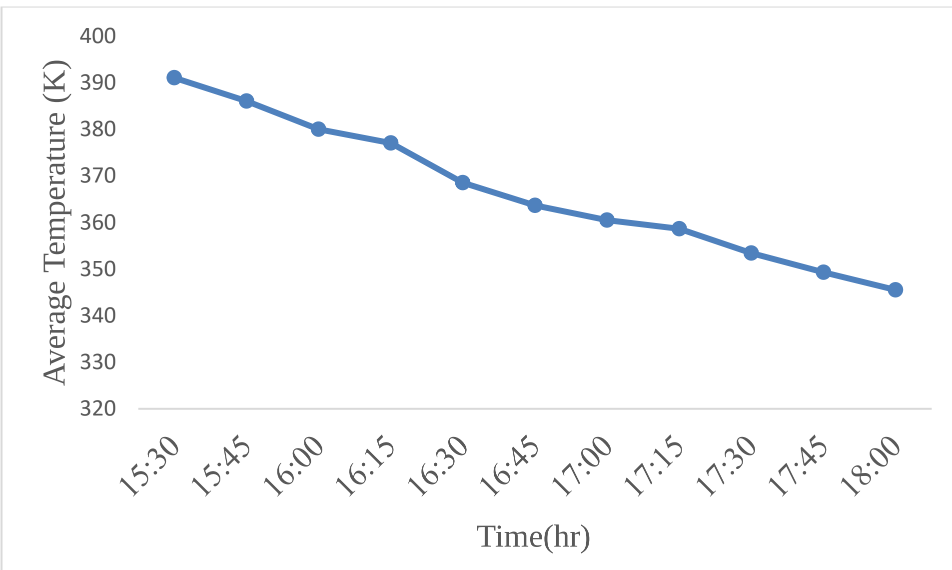

b) Discharging

Figure 7.15 Temperature distribution of PCM during charging and discharging, a) Charging, b) Discharging

7.8 Cooking Tests

To check the performance of the cooker under various conditions, different types of test were performed on the cooker. (i) Experiment without loading the cooking pot of the solar cooker. This set of experiment was conducted to investigate the effectiveness of the cooker and to investigate its thermal capability of the integrated PCM storage unit for cooking. (ii) Experiment with water as a cooking load this set of experiment were performed to conform the results of the first experiment without a load of high heat capacity and to calculate the cooking power of the cooker at different cooking time. (iii) Experiment with actual cooking load. This experiment is also performed to investigate the cooker capability to cook actual food items based on the result of the second experiment.

7.8.1 No-Load Test

The behavior of HTF, charging and discharging processes as well as the general analysis of the system when it was not performing any cooking, were determined using a no-load experiment in which the water was just heated, with no cooking load added to the system. This test was used to predict the time it takes the system to cook various food items. A no-load test was conducted with a full setup of the experiment. To start the experiment, the system pipelines were filled with nanofluids water as HTF. At 12:50 maximum temperature of 435.4 and 402.1 K was achieved in the storage vessel and the cooking pot surface was, respectively. The result of the no-load test implies that the load test can be performed as the temperature achieved is enough to boil water at the peak hour of the day (11:30-15:30) in the selected site (Adama latitude =8.54 ° longitude =39.28 °E altitude = 1648 m). To see the effect of the LHS system, the no-load test was performed. Figure 7.16 shows the temperature variation of water in the storage vessel, PCM and cooking pot during the no-load discharging process.

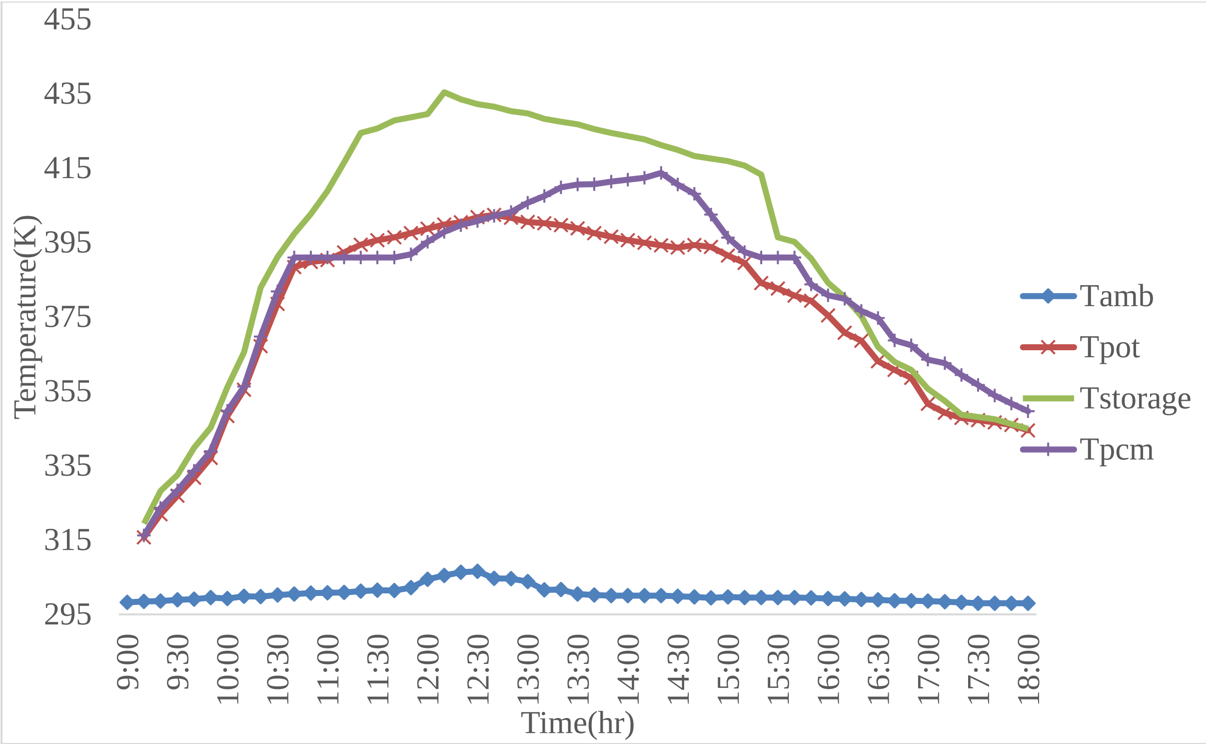

Figure 7.15 The average temperature of PCM. Cooking pot, working fluids and ambient temperature during no load test.

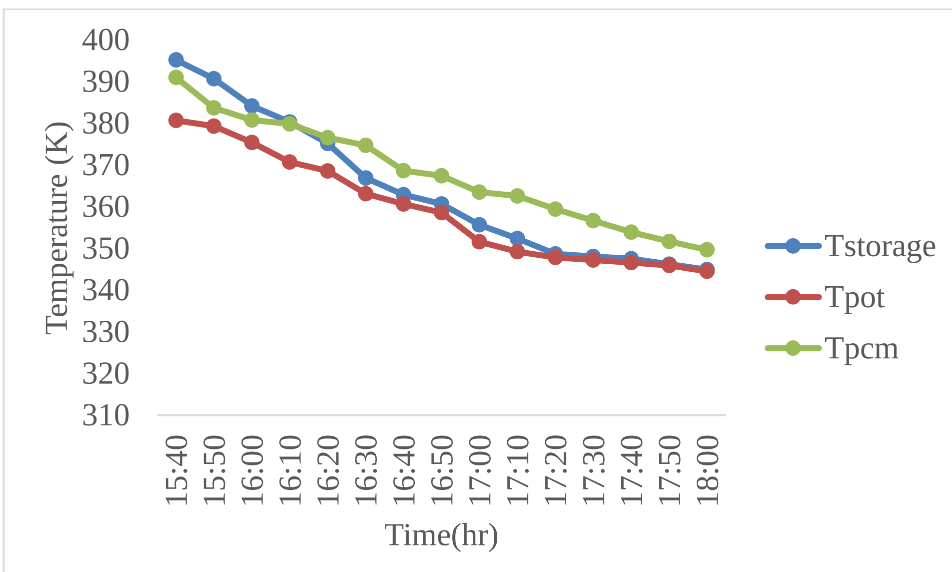

Figure 7.16 Variation of temperature during Discharging with no load test

7.8.2 Boiling Test

Experimental results from boiling water with solar cookers are often the basis on which the cookers' performance can be measured. Since almost all food items involve heating water, it is of the utmost importance that the behavior of this solar cooker be checked during water boiling. A serious of water boiling experiment was performed on 19th October 2021 from 11:30 - 12:30. Those boiling experiment were done using 3.5 kg of water. Highly conductive cooking pot (Aluminum pot) filled with water is bathed in the hot water and hot nanofluids of the storage vessel. Indirect conduction heat transfer occurring between hot fluids and the cooking pot makes the water in the pot to rise its temperature. The initial temperature of loaded water was 27 ℃. In the first test water starts to form bubble with in 10min after it had been placed in the cooker and starts boiling after 25min at 94.5 ℃ (caused by the Altitude of Adama city). After water in the first experiment is poured out from the pot, the second boiling test starts. Starting from 27 ℃, the water in the second test took 28 min to reach 94 ℃. The last experiment was performed after unloading the water in from the second experiment. Similarly, to boils water it takes 40 min in third test. From the boiling test it can be seen that for the test period from 11:30 to 15:30 the cooker can be used for cooking any kind of boiling type meals.

7.8.3 Load Test with Food Item

Based on the results of the boiling test, a final set of experiments has been conducted on the cooker with the actual cooking load on 20th October 2021. The load was loaded at different solar radiation intensities. The first cooking test was at 12:00 with 500g of pasta using 1.5 kg of water. Then after 33 min, the pasta was cooked well. To see the effect of LHS storage in heating and warming of food for a specific period of time, the second cooking test was started at 16:00 after the solar intensity is low enough for the PCM to operate. Then past was taken 50 min to cook after 16:00. Maintaining the pasta in the pot for 50 min it was found that the cooker was able to cook it even if it takes more minute. Different photographs taken during the load test is presented in appendix C.

7.9 Thermal Figures of Merit

First figure of merits for the cooker with and without nanofluids as HTF were determined from no load test results of ambient temperature, average solar radiation and mean temperature of absorber using equation (5.53). The maximum amount of F1 obtained was 0.31Km^2/W. The minimum possible value of F1 to cook any meal using solar cooker is 0.1 Km^2/W (Ekechukwu and Ugwuoke, 2002). Second figure of merits was estimated using equation (5.54) evaluated from water boiling test and found to be 0.42 Km^2/W.

7.10 Economic Analysis of the Solar Cooking System

In the utilization of solar thermal application, the main thing that arose in customers mind is its economical point of view. Generally, solar processes are characterized by high first cost and low operating costs. Thus, the basic economic problem is comparing an initial known investment with estimated future operating costs. Among the economical evaluation methods, life cycle saving method is mostly used evaluation tool and thus, it was selected for the present study.

7.10.1 Total Cost of the Present Indirect Solar Cooker

The total initial investment cost of the present cooker includes the cost of the collector, storage system, cooking units and connecting units of the system. Appendix B summarizes the details of all the costs associated with the present solar cooker.

7.10.2 Investment Cost

Investment cost is related with the buying and installing costs of the solar system which includes all the cost of collector, thermal storage cooking unit and other connecting and related costs. Installed cost of a solar system is the sum of cost related with collector area and cost independent of collector area (Dagim, 2016).

$$\mathrm{CI} = \text{Cost of collector} + \text{Cost components other than collector} \tag{7.1}$$

Thus, CI = 5200.00-birr +11600.00 birr = 16800.00 birr

7.10.3 Life Cycle Cost (LCC)

LCC is the sum of all costs associated with an energy delivery system including all of the items of hardware and labor that are involved in installing the equipment plus the operating expenses over a selected period of analysis or over its useful operating lifetime. LCC of a solar system can be determined from the investment cost and present value of maintenance and pumping cost over its life time using a relation given by (Addisu, 2007);

$$\mathrm{LCC} = \mathrm{CI} + \mathrm{C_m}\,\frac{1}{\mathrm{i}}\left(1 - \left(\frac{1}{(1+\mathrm{i})^{\mathrm{n}}}\right)\right) \tag{7.2}$$

Where; CI is investment cost

$C_m$is annual maintenance and pumping cost

n is operating life time in years

in the present economic analysis, interest rate, inflation rate, salvage rate and discount rate were assumed to be 10% and the life cycle cost of the solar cooker for 7 years of operation can be determined as;

$$\mathrm{LCC} = 16800 + 1680\,\frac{1}{0.1}\left(1 - \left(\frac{1}{(1+0.1)^7}\right)\right) = 24978.86\ \mathrm{Birr}$$

7.10.4 Life Cycle Saving of Energy

The life cycle saving (LCS) of solar cooker is the total energy cost saved due to replacement of electricity by alternative solar energy in the present worth (Duffie and Beckman, 1991).

LCS of energy (KWh)can be determined by;

$$\mathrm{LCS} = \mathrm{P_e E_s}\left(\frac{1+\mathrm{i_e}}{1-\mathrm{i_e}}\right)[1 - (\frac{1+\mathrm{i_e}}{1+\mathrm{i}})^{\mathrm{n}}] \tag{7.3}$$

Where;P_e unit price of solar energy

E_S annual energy saving for a solar system

i - is the annual market discount rate.

i_e-is the annual market rate of energy escalation is assumed to be 15% for 2019G.C

The unit price of solar energy system can be determined when the life cycle cost of the system is equal to the life cycle energy savings of the solar cooking system during its life time.

When LCC = LCS

$$\mathrm{CI} + \mathrm{C_m}\,\frac{1}{\mathrm{i}}(1 - \left(\frac{1}{(1+\mathrm{i})^{\mathrm{n}}}\right) = \mathrm{P_e E_s}(\frac{1+\mathrm{i_e}}{1-\mathrm{i_e}})[1 - (\frac{1+\mathrm{i_e}}{1+\mathrm{i}})^{\mathrm{n}}$$

$$\mathrm{P_e} = \frac{\mathrm{CI}+\mathrm{C_m}\frac{1}{\mathrm{i}}(1-(\frac{1}{(1+\mathrm{i})^{\mathrm{n}}})}{\mathrm{E_s}\left(\frac{1+\mathrm{i_e}}{1-\mathrm{i_e}}\right)[1-(\frac{1+\mathrm{i_e}}{1+\mathrm{i}})^{\mathrm{n}}} \tag{7.4}$$

For the present case annual energy saving (Es) by the solar cooker was estimated from the average daily useful energy requirement of cooking which reportedly varies in the range of 1.7 –2.7 MJ/person/day (Sunil and Tera, 2018). Thus, the average annual energy saving by the present solar cooker which is intended to prepare 80% of daily meal (i.e. other meals are considered as frying based foods for most of Ethiopian foods) for 5 persons can be estimated as follows;

Daily energy requirement for average person is 2.2MJ*80% /day≅ 1.76MJ/day

Daily energy requirement for 5 persons is 11 MJ/day ≅ 7.35kw

Annual energy requirement for 5 persons is 4015MJ/year = 2682.75kw

Therefore; annual energy saving by the solar cooker Es= 3098.57 birr

7.10.5 Payback Period of the Indirect Solar Cooking System

Payback period is defined as the time needed for the cumulative energy savings to equal the total initial investment, that is, how long it takes to get an investment back by savings in electricity or fuel.

Neglecting the maintenance cost, the payback period of solar cooker is evaluated when;

$$\boldsymbol{LCCS = CI@\, n = N_p};$$

$$C_f E_s \left(\frac{1+i_e}{1-i_e}\right)[1-\left(\frac{1+i_e}{1+i}\right)^n = CI$$

$$N_P = \frac{\ln\,(1+\frac{CI(\frac{i_e-i}{1+i_e})}{C_f E_s}}{\ln\,(\frac{1+i_e}{1+i})} \qquad (7.5)$$

Where LCCS is the life cycle saving of electric cost [Birr]

Cf is the unit cost of electricity for the first year of analysis (Birr/KWh)

Therefore; the payback of the present indirect solar cooker is 3.39 years.

8. CONCLUSIONS AND RECOMMENDATIONS

8.1 Conclusions

In this thesis, the performance of parabolic dish solar collector for cooking using aluminum oxide, zinc oxide nanofluids and water as HTF was studied. To conduct the experiment design, sizing, manufacturing of components, Synthesis of nanoparticles, characterization of nanoparticles and nanofluids preparation are carried out. Different experimental investigations and tests were conducted to evaluate the performance of system components. A closed-loop experiment was conducted on the developed prototype of PDSC to investigate various performance parameters. Good agreement was obtained between the literature and experimental results. To store the energy for cooking during off peak sunshine Magnesium chloride hydrate ($MgCl_2.6H_2O$) was used to store the latent heat. The solar radiation of Adama city was estimated and during the experimental test the monthly average maximum Global, Diffuse and beam solar radiation is 903.2 ,267.85 ,635.35 W/m^2 respectively.

From the experimental, the following results are obtained.

- During the experimental test the maximum average outlet temperature for aluminum oxide nanofluid for 1 and 2 % volume fraction was 456 and 459.6 K respectively.
- The maximum average outlet temperature of ZnO nanofluid for 1 and 2 % volume fraction was 452 and 454.7 K respectively.
- The average maximum outlet temperature of the water was 439.4 K
- The average maximum efficiency of PDSC Aluminum oxide nanofluid as HTF for the volume fraction of 1 and 2 % was 69.13 and 71.63 % respectively.
- The average maximum efficiency of PDSC zinc oxide nanofluid as HTF for 1 and 2 % volume fraction was 65.5 and 67.99 % respectively.
- The average maximum efficiency of parabolic dish solar collector using water as working fluid was obtained 61.6%.
- The maximum outlet temperature and maximum efficiency were obtained when 2% of volume fraction was used.
- From experimental results as volume fraction nanoparticles increased the temperature and efficiency also increased.

- From the experimental result obtained that when Al_2O_3 nanofluid used as HTF improve the efficiency of the system compared with ZnO nanofluid and water.

In general, from the experimental result using a PDSC with nanofluid as HTF increase the efficiency of the collector compared with water as a working fluid.

8.2 Recommendations

Solar cooking system provides a solution to reduce consumption of electricity and fuels. For sure operation of solar cooker in large scale application I recommend auxiliary heating source to be included in the system in addition to thermal energy storage system to control the heating process in manageable manner. The present study addressed the experimental performance analysis of parabolic dish solar collector using nanofluids as HTF. The following points are recommended for future work.

- In this study the tracking system is manual another researcher to work on automatic tracking system is recommended.
- The Life of nanofluids is not studied in this thesis it is open area to other researcher study on it.
- In this study the Conical cavity receiver was used as absorber its open area for other researcher to study with different types of receivers.

REFERENCES

Abid, T. A. (2016). " Performance assessment of parabolic dish and Parabolic trough solar thermal power plant using nanofluids and molten salts". *International Journal of Energy Research*, 550-563.

Addisu. B. (2007). Large Scale Application of Solar Water Heating System in Ethiopia. *"Masters thesis in addis ababa university"*.

Asfafaw H. Tesfay, M. B. (2015). Solar cookers with latent heat storage for intensive cooking application. *International Solar Energy Society Conference Proceedings*.

Azzouzi D, B. B. (2017). "Experimental and analytical thermal analysis of cylindrical cavity receiver for solar dish". *Renewable Energy* , 111–121.

Batchelor. (1977). "The effect of Brownian motion on the bulk stress in a suspension of spherical particles ". *J. Fluid Mech*, 97-117.

Brinkman, H. (1952). "The viscosity of concentrated suspensions and solutions". *J Chem Phys*, 571-581.

Chandraprabu Venkatachalam, S. G. (2019). "Dataset of solar energy potential assessment for Adama city (Ethiopia)". *Data in brief 24*.

Cengel, A. G. (2014). "Heat and mass transfer". *Fundamentals and applications, 5th ed McGraw-Hill Education*.

Choi. (1995). "Enhance Thermal Conductivity of fluids with nanoparticles". *ASME FED*, 99-103.

Chopkar, S. I. (2008). Effect of particle size on thermal conductivity of nanofluid, 1535-1542.

Chopra, P. (2006). "Synthesis and characterization of nanofluid for advaced heat transfer application". *scriptal material*, 549-552.

Dascomb, J. (2009). Low-Cost Concentrating Solar Collector for Steam Generation. *Electronic Theses, Treatises and Dissertations*.

Dawit, G. (2018). "Thermal Analysis of Solar Flat Plate Collector Coupled with Heat Storage" . *Doctoral dissertation): http://gyan.iitg.ernet.in/handle/123456789/1263*.

Duffie, J. B. (2013). "Solar Engineering of Thermal Processes, 4th ed".

Einstein. (1956). " Investigation on the theory of brownian motion". *Dover*.

El Ouederni1, M. B. (2009). Experimental study of a parabolic solar concentrator. pp. 395 – 404.

Eswaramoorthy1, S. A. (2013). "Experimental Study on Solar Parabolic Dish Thermoelectric Generator". *International Journal of Energy Engineering (IJIRAE),*, 62-66.

Evangelos Bellos, C. T. (2018). "The use of nanofluids in solar concentrating technologies" . *A comprehensive review, Journal of Cleaner Production*.

Fan, L. W. (2011). Review of heat conduction in nanofluids, 40-801.

Fareed. M. Mohamed, A. Y. (2012). Design and Study of Portable Solar Dish Concentrator Fareed. pp. 52-61.

Geyeer, W. B. (2001). "power from the Sun". 42.

Gleiter. (1989). "Nanocrystalline materials". *Prog. Mater. Sci.*, 223 – 315.

International , E. A. (2011). "Solar Energy Perspectives". *Renewable energy*.

Irwan Nurdin, a. S. (2017). "The effect of particle volume fraction and temperature on the enhancement of thermal conductivity of maghemite (γ–Fe2O3) water based nanofluids". *AIP Conference Proceedings*.

Jayachandraiah, H. P. (2016). "Evaluation of hermal performance of cone shaped helical coil heat exchanger by using CFD analysis". *Anveshana's International Journal of Research in Engineering and Applied Sciences*, 45-51.

Jayesh Novel pakhare, H. p. (2017). "Experimental performance evaluation of parabolic solar dish collector with nanofluid". *Concentrated solar thermal energy technology*, 115-123.

Jonathan K. Swanepoel, W. G. (2020). "Helically coiled solar cavity receiver for micro-scale direct steam generation". *Applied Thermal Engineering*.

Junyu Ji, W. L. (2020). "Overview on the Preparation and Heat Transfer Enhancement of Nanofluids". *Journal of Physics Conference Series*.

Kantole, J. B. (2012). "Modelling and design of a latent heat thermal storage system with reference to solar absorption refrigeration". *Doctoral dissertation, University of Johannesburg*.

Karimi R, G. T. (2018). "A detailed mathematical model for thermalperformance analysis of a cylindrical cavity receiver in a solar parabolic dish collector system ". *Renewable Energy 2018*, 768-782.

Kebede, D. (2020). "Computational Modeling and Performance Analysis of Solar Thermal Storage Integrated with Parabolic Solar Concentrator for Cooking Application". *Addis Ababa Institute of Technology*.

Khanafer, K. V. (2011). A critical synthesis of thermophysical characteristics of nanofluids, 4410–4428.

Kimoto K., K. N. (1963). An electron microscope study on fine metal particles prepared by evaporation in argon gas at low pressure. p. 702.

Lee, S. L. (2010). A review of thermal conductivity data, 269–322.

Li, J. Z. (2009). "A review on development of nanofluid preparation and characterization". *Powder Technol*, 89–101.

Loni R, K. A.-A. (2016). "Optimizing the efficiency of a solar receiver with tubular cylindrical cavity for a solar-powered organic Rankinecycle". *Energy* , 1259-1272.

Loos, M. (2015). Carbon nanotube reinforced composites. *Science direct*.

Madhu, P. &. (2017). "Measurement of Density and Specific Heat Capacity of Different Nanofluids". *International Journal of Advance Research, Ideas and Innovations in Technology*, 69.

Manav Sharma, J. N. (2015). “Design, fabrication and analysis of helical coil receiver with varying pitch for solar parabolic dish concentrator”. *International Journal on Theoretical and Applied Research in Mechanical Engineering (IJTARME),*, 4.

Mawire A, T. S. (2014). " Experimental energy and exergy performance of a solar receiver for a domestic parabolic dish concentrator for teaching purposes". *EnergySustainable Dev*, 162-169.

Maxwell, J. (1881). "A Treatise on electricity and magnetism, second ed". *Clarendon Press,Oxford*.

Medved, D. M. (2010). "Latent heat storage systems". *Appendixes*.

Mekhilef, R. S. (2011). "A review on solar energy use in industries". *Renew Sustain. Energy Rev*, 1777–1790.

Mohammed, I. L. (2012). "Design and development of a parabolic dish solar water heater". *International Journal of Engineering Research and Applications (IJERA)*, 822-830.

Mohammed, I. L. (2013). "Design and Development of a Parabolic Dish Solar Thermal Cooker". *International Journal of Engineering Research and Applications (IJERA)*, 1179-1186.

Muthusivagami RM, V. R. (2010). "Solar cookers with and without thermal storage". *A review. Renew Sust Energy Rev*, 691–701.

Niyas, H. R. (2017). Performance investigation of a lab-scale latent heat storage prototype–experimental results. *Solar Energy*, 971-984.

Özerinç, S. A. (2010). "Enhanced Thermal Conductivity of Nanofluids". *A State-of-the-Art Review, Microfluid. Nanofluid*, 145-170.

Pak, Y. C. (1998). "Hydrodynamic and heat transfer study of dispersed fluids with submicron metallic oxide particles". *Exp. Heat Transfer*, 151-170.

Parthipan1, B. N. (2015). Experimental performance study of parabolic dish concentrator with cylindrical cavity receiver by variable mass flow rate of water, 203-207.

Panwar NL, K. S. (2011). "Role of renewable energy sources in environmental protection". *A review. Renew Sust Energy Rev*, 1513–1524.

Rajendran, E. G. (2018). "Experimental Studies on the Effect of Enhanced Thermal Conductivity of SiC+Water Nanofluid in the Performance of Small Scale Solar Parabolic Dish Receiver" . *Int. J. Nanosci.* .

Ramesh, N. P. (2011). Review of thermo-physical properties, wetting and heat transfer characteristics of nanofluids and their applicability in industrial quench heat treatment. p. 334.

Sabbagh, A. S.-S. (1977). Estimation of the total solar radiation from meteorological data. *Solar Energy*, 307-311.

Salimpour, M. R. (2008). "Heat Transfer Characteristics of a Temperature-Dependent-Property Fluid in Shell and Coiled Tube Heat Exchangers". *International Communications in Heat and Mass Transfer*, 1190-1195.

Saravanakumar, S. A. (2017). "A review on the classification,characterisation,synthesis of nanoparticles and their application". *IOP Conference Series Materials Science and Engineering*.

Satyanarayana Talam, S. R. (2012). "Synthesis Characterization, and Spectroscopic Properties of ZnO Nanoparticles". *International Scholarly Research Notices*.

Sharma, A. (2011). "A comprehensive study of solar power in India and World". *Renew. Sustain Energy Rev*, 1767–1776.

Shubham Shinde, R. S. (2017). "Steam Generation by Using Solar Dish Collector". *International Research Journal of Engineering and Technology (IRJET)*, 430-433.

Sina Eterafi, S. G. (2021). Effect of covering aperture of conical cavity receiver on thermal performance of parabolic dish collector:Experimental and numerical investigation. *Journal of renewable energy and enviroment*, 29-41.

Siti Nur Syakirah Mohamad1, N. M. (2019). "Synthesis of alumina nanoparticles by sol-gel method and their applications in the removal of copper ions (Cu2+) from the solution, IOP Conference Series". *Materials Science and Engineering*, 701.

SohelMurshed, K. (2005). "Enhanced thermal conductivity of TiO2-water Base Nanofluids". *International Journal of Thermal sciences*, 376-373.

Soltani S, B. M. (2019). "A novel optical-thermal modeling of a parabolic dish collector with a helically baffled cylindrical cavity receiver". *Energy*, 88-98.

Stine, G. M. (1989). "Cavity receiver convection heat loss". *Proceedings of the International Solar Energy Society – Solar World Congress (SWC)*.

Thirugnanasambandam, S. I. (2010). A review of solar thermal technologies, 312–322.

Tiwari, A. T. (2016). Handbook of Solar Energy Theory, Analysis and Application. *Springer Science+Business Media Singapore*.

Trisaksri, S. W. (2007). "Critical review of heat transfer characteristics of nanofluids". *Renew. Sustain. Energy Rev*, 512–523.

Vajjha, D. D. (2012). "A review and analysis on influence of temperature and concentration of nanofluids on thermophysical properties". *Int. J. Heat Mass Transfer*.

Vanita Thakkar, A. D. (2015). "Performance Analysis Methodology for Parabolic Dish Solar Concentrators for Process Heating Using Thermic Fluid". *Journal of Mechanical and Civil Engineering (IOSR-JMCE)*, 101-114.

Vijaya Pandurang Dhawale, V. K. (2018). Synthesis and Characterization of Aluminium Oxide (Al2O3) Nanoparticles and its Application in Azodye Decolourisation. *International Journal of Environmental Chemistry*, 10-17.

Vinayak Sakhare, V. (2014). "Experimental Analysis of Parabolic Solar Dish with Copper Helical coil Receiver". *International Journal of Innovative Research in Advanced Engineering (IJIRAE)*,.

Wang, A. M. (2007). "Heat transfer characteristics of nanofluids". *A review, Int. J Therm. Sci*, 1-19.

Wang F, L. R. (2013). "Optical efficiency analysis of cylindrical cavityreceiver with bottom surface convex ". *Solar Energy*, 195-204.

Wang, X. a. (1999). "Thermal conductivity of nanoparticle-fluid mixture". *Thermophys.heat transfer*, 474-480.

Woldeyohannes, A. T. (2013). " Effect of Particle Size on Effective Thermal Conductivity of Nanofluids". *Asian Journal of Scientific Research*, 339-345.

Xuan, W. R. (2000). "Conceptions for heat transfer correlation of nanofluids ". *International Journal of Heat and Mass Transfer*, .3701-3707.

Yaseen. H. Mahmood, M. K. (2015). Design of Solar dish concentration by using MATLAB program and Calculation of geometrical concentration parameters and heat transfer. *Tikrit Journal of Pure Science*, 101-106.

Yettou, B. A. (2014). Solar cooker realizations in actual use: An overview. *Renewable and Sustainable Energy Reviews*, 288-306.

Zhu, Y. S. (2004). "A novel one-step chemical method for preparation of copper nanofluids". *Journal of Colloid and Interface Science*, 100-103.

Zou C, Z. Y. (2017). "Design and optimization of a high-temperature cavity receiver for a solar energy cascade utilization system". *Renewable Energy 2017;103:478–89*, 478-489.

APPENDIX A:

Thermocouple Calibration

Thermocouple is device used for measure the temperature which consisting of two wires of different metals joined at each end. The most popular thermocouple is the type K, which is high sensitive for measuring temperature with a measurement temperature range of –200 to +1260°C. Calibration of thermometers can be carried out using a reference thermometer in a temperature calibration test by comparing both measurement values of a reference thermometer and other thermometers. Calibration test for four channel digital k-type thermocouple was conducted in Adama Science and Technology University Chemical Engineering Department with thermometer by using 0.4 kg of water boiling for 21 min.

Thermocouple specification

K-type thermocouple specifications

- Serial Number: 2019002867
- Temperature range: -50 to 1350 ℃
- Power supply: 9 V
- Weight: approx. 230 g

Figure A.1 Calibration of thermocouple

Table A.1 Measured temperature vs corrected temperature

Time(min)	Tw1 (k type Thermocouple) (℃)	Tw2(Thermometer) (℃)	Uncertainty (%) [(Tw1−Tw2)Tw2⁄]×100
1	29.9	29.7	0.66
3	34.6	34.4	0.57
5	41.3	40.9	0.96
7	49.7	49.4	0.6
9	56.2	55.8	0.71
11	62.1	61.8	0.48
13	70.8	70.3	0.7
15	77.4	76.9	0.64
17	84.2	83.7	0.59
19	90.1	89.6	0.55
21	96.9	96.2	0.72
Average Uncertainty			0.68

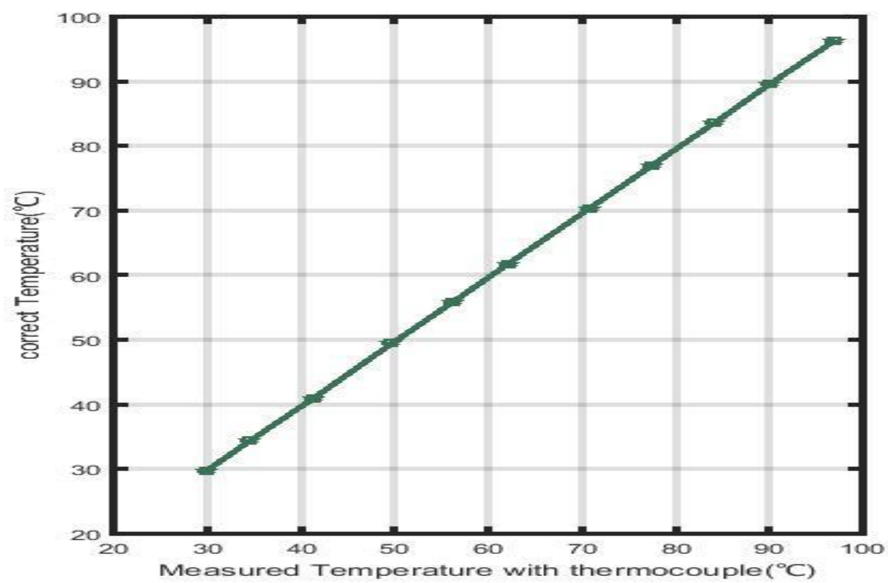

Figure A.2 Graph of measured temperature vs corrected temperature.

APPENDIX B

Total Cost of Indirect Solar Cooking System

Table B.1 List of components costs.

No.	Item	Specification	Quantity	Unit Price	Total Price
1	PDSC				
1.1	Dish	Area,2.54m^2	1	1800.00	1800.00
1.2	Mirror	Area 2.6	1	2500.00	2500.00
1.3	CARMYFIX CM-43	3Kg	3	300.00	900.00
	Subtota1				5200.00
2	Cooking Unit				
2.1	Cooking pot	D=24cm, H=11cm	1	250.00	250.00
2.2	HTF Storage	D=28cm, H=13cm	1	350.00	350.00
	Subtotal				600.00
3	Thermal Storage System				
3.1	PCM Storage	D=38cm,H=15.5cm	1	800.00	800.00
3.2	$MgCl_2.6H_2O$	10Kg	10	240.00	2400.00
	Sub total				3200.00
4	Nanofluids Preparation				
4.1	$Al(NO_3)_3.9H_2O$	500g	1	500.00	500.00
4.2	$Zn(NO_3)_2$	5000g	1	750.00	750.00
4.3	Citric Acid	500g	1	400.00	400.00
4.4	Ethylene glycol	1/2L	1/2	500.00	500.00
4.5	Ethanol	3L	3	230.00	690.00
4.6	Subtotal				2840.00
5	Connecting pipe and other miscellaneous costs				

5.1	Copper tube	5m	1	1000.00	1000.00
5.2	Connecting hose	1.2m	4	`180.00	720.00
5.3	Reducer	1/2''	4	35.00	140.00
5.4	Nipples	½''	2	40.00	80.00
5.5	Valves	½''	2	130.00	260.00
	Sub total				2200.00
	Total				13440.00
6	Manufacturing, labor and assembly cost	25% material cost			3360.00
7	Operating(power), maintenance and replacement cost	10% of investment cost			1344.00
	Grand Total				18144.00

APPENDIX C

Photos taken during experimental test of cooker

Figure C.1 Photographs taken from cooking test.

APPENDIX D

The photos of chemicals used to synthesis nanoparticles and PCM

Specification of Aluminum Nitrate ($Al(NO_3)_3$

M.W. 375.13

Minimum assay	98.0%
Chloride (Cl)	Max.0.005%
Sodium (Na)	Max.0.01%
Iron (Fe)	Max.0.005%
Potassium (K)	Max.0.01%
Sulfate (SO_4)	Max. 0.01%

Figure D.1 Aluminum Nitrate

Specification of Zinc Nitrate

Zn $(NO_3)_2.6H_2O$] Assay	99%
PH value	3.5
Insoluble matter in water	0.005%
Chloride	0.001%
Sulfate	0.002%

Iron	0.0003%
Lead	0.005%
Ammonium sulfide	0.10

Figure D.2 Zinc Nitrate

Phase change material (PCM)

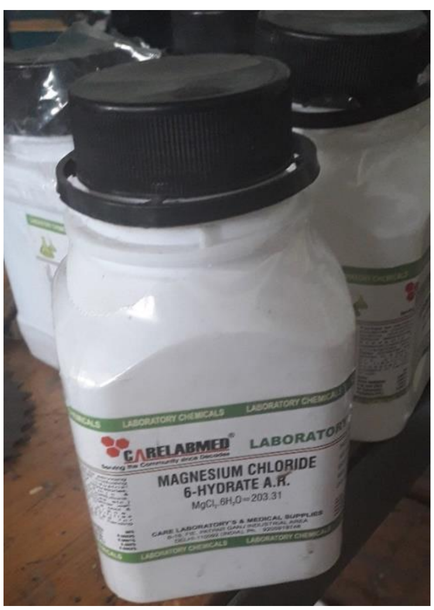

Figure D.3 Magnesium chloride hydrate